

https://dspace.org/

Synthesis, testing and characterization of porous biocompatible porous bioactive glasses for clinical use

Erasmus, Erika Pombili-Ipawa

2017

https://hdl.handle.net/10539/24960

Erasmus, Erika Pombili-ipawa (2017) Synthesis testing and characterization of biocompatible porous bioactive glasses for clinical use, University of the Witwatersrand, Johannesburg, <http://hdl.handle.net/10539/24960>

Downloaded from a DSpace repository. https://dspace.org/

SYNTHESIS, TESTING AND CHARACTERIZATION OF POROUS BIOCOMPATIBLE POROUS BIOACTIVE GLASSES FOR CLINICAL USE

Prepared by:

Erika Pombili-Ipawa Erasmus

A dissertation submitted to the Faculty of Engineering and the Built Environment, University of the Witwatersrand, Johannesburg, in fulfillment of the requirements for the degree of Master of Science in Engineering.

Johannesburg 2017

DECLARATION

I declare that this dissertation is my own unaided work. It is being submitted for the degree of Master of Science in Engineering to the University of the Witwatersrand, Johannesburg. It has not been submitted before for any degree or examination to any other university.

……...

Erika Pombili-Ipawa, ERASMUS

……. Day of …….. Year ……

ABSTRACT

The quest for the processing of glass scaffolds that remains amorphous upon sintering while maintaining a fast dissolution and conversion to hydroxyapatite rate is growing. Therefore; glasses within the borosilicate borophosphate and phosphate family were sintered into 3 dimensional (3D) porous scaffolds using 60 and 70 vol. % $NH_4(HCO_3)$ as a foaming agent. In this work the sintering ability of (borosilicate S53B50), borophosphate (P40B10) and phosphate (Sr) bioactive glasses was investigated. The glass powders were crushed and sintered in air at a heating rate of 10°C/min for 2 hours at sintering temperatures between 480°C-600°C. The density of the samples was found to decrease when the temperature was increased up to 580°C. To process highly porous scaffolds with porosity required for scaffold applicable to tissue engineering, the powders were further mixed with 60 vol. % and 70 vol. % of NH_4 (HCO_3) foaming agent. Meanwhile, the density of the samples sintered with NH_4 (HCO_3) was found to decrease with an increase in NH_4 (HCO_3) content. This indicates an increase in porosity of the samples. The glass compositions reached an open porosity of more than 60% at the addition of 70 vol. % NH_4 (HCO_3). The *in vitro* properties of the scaffolds investigated in SBF showed that Upon immersion; the pH of the solution containing the borosilicate scaffolds increased due to the typical non-congruent dissolution of theses glass family leading to large Na+/H+ exchange and large alkaline and alkaline earth release. Borophosphate as well as phosphate scaffolds induced a decrease in pH upon dissolution attributed to the congruent dissolution of those materials and therefore; the large release of phosphorus within the media. The as prepared scaffolds showed a compressive strength of 1.29 ± 0.21, 1.56 ± 0.63, 3.63 ± 0.69 MPa for the samples borosilicate borophosphate and phosphate sintered with 60 vol. % NH_4 (HCO_3), respectively. From SEM/EDS, XRD and ICP-OES analysis a clear precipitation of hydroxyapatite was reported on the borosilicate glass scaffolds. The borophosphate scaffold was found to be stable and to react at a slow rate. The crystallized phosphate glass; however was found to release very large amount of phosphate; compared to the amorphous glass; indicating preferential leaching of the phosphate rich crystal phase. Except for the borophosphate scaffolds; the mechanical properties dropped with increasing immersion time.

ACKNOWLEDGEMENTS

Lord, Our Father, thank you for guiding me through this time until I successfully accomplished my project, I believe this was one of the plans you had for me and I owe my success to you.

After almost two years of intense lab work, I finally get to sit down and write a note of thanks as I round off my work. I have to say this was an intense learning period for me, not only on an academic level but also on a personal level. Therefore, I would like to give my profound appreciation and reflect on the people who have supported and stood by me throughout this period.

I would first like to thank **Prof. I. Sigalas** for granting me this opportunity to do my Masters under his supervision. Thank you for your moral support, mentorship, encouragement and for always steering me in the right direction whenever I ran into a sticky situation. It was indeed a pleasure working with you.

Dr. O. Johnson: You have always seen my potential being my undergrad supervisor and now postgrad. Thank you for giving me an opportunity to reach my full potential. You have indeed groomed me into a well-established academia. I will forever be grateful.

Dr. J. Massera: Thank you for the wonderful collaboration. I have to say, Finland was an experience for me. I would also like to thank you for your expertise on the project, your positive feedback, prompt responds on my work and your willingness to always help me. I truly did enjoy working with you.

I would also like to thank my parents and siblings for their wise counsel, support, and patience and for always being there for me and keeping me in your prayers and my boyfriend for his encouragement. To my friends, thank you for always creating a platform to not always talk about our research work but most importantly for giving support and always ready to give a solution when I have problems on my findings.

Lastly, I would like to thank African Material Science and Engineering Network (AMSEN) for your financial support, this project wouldn't be a success without your aid.

TABLE OF CONTENTS

DECLARATION ..... **ii**

ABSTRACT ..... **iii**

ACKNOWLEDGEMENTS ..... **iv**

LIST OF FIGURES ..... **viii**

LIST OF TABLES ..... **xii**

CHAPTER 1: INTRODUCTION **1**

1.1 Motivation 1
1.2 Problem statement 2
1.3 Aim and Objectives 3
1.4 Scope of research 3
1.5 Structure of the dissertation 3

CHAPTER 2: LITERATURE REVIEW **5**

2.1 Discovery of Bioactive glasses 5
2.1.1 Glass structure of bioactive glasses 6
2.1.2 Synthesis of Bioactive glass 7
2.1.3 Surface reactivity of bioactive glasses 9
2.2 Properties of Biomaterials 11
2.2.1 Biocompatibility 11
2.2.2 Bioactivity 12
2.2.3 Types of Bioceramics-tissue attachment 14
2.3 Porous Bioceramics 15
2.3.1 Porous bioactive scaffolds 16
2.3.2 Selection of biomaterials for scaffold fabrication 23
2.3.2.1 Bioceramics and bioactive glasses 23
2.3.2.1.1 Hydroxyapatite (HA) and Tri-calcium phosphate (TCP) 23
2.3.2.1.2 Silicate bioactive glasses 24
2.3.2.1.3 Borate bioactive glasses 27
2.3.2.1.4 Phosphate bioactive glasses 28

2.3.2.2 Synthetic and Natural polymers 31
2.4 Fabrication techniques for porous scaffolds 16
2.4.1 Direct foaming 17
2.4.2 Foam replication 18
2.4.3 Sol gel process 19
2.4.4 Thermally bonding of particles or fibres 21
2.5 Mechanical properties of scaffolds for tissue engineering 31
2.6 Clinical Applications of Bioceramics 34

CHAPTER 3: METHODOLOGY 38

3.1 Materials and chemicals 38
3.2 Glass and powder preparation 39
3.2.1 Synthesis 39
3.2.2 Milling 40
3.2.3 Drying and sieving powder 40
3.2.4 Mixing and Compaction of powders 41
3.3 Sintering 41
3.3.1 Sintering with and without $NH_4(HCO_3)$ 41
3.4 In vitro bioactivity 41
3.5 Characterization techniques 43
3.5.1 Particle size measurements 43
3.5.2 Thermal Properties 43
3.5.3 Density measurements 43
3.5.3.1 Density of samples sintered with $NH_4(HCO_3)$ 43
3.5.3.2 Density of samples sintered without $NH_4(HCO_3)$ 44
3.5.4 Cutting the sintered samples 45
3.5.5 XRD analysis of powder and sintered samples 45
3.5.6 SEM analysis of powder and sintered samples 45
3.6.7 ICP analysis 46
3.5.8 Analysis of the porous scaffolds 46
3.5.8.1 Mercury Porosimetry Intrusion 46
3.5.8.2 X-ray micro computed tomography 47
3.6 Mechanical properties 48

CHAPTER 4: EXPERIMENTAL RESULTS 49

4.1 Preparation of glass powders 49
4.2 Thermal properties of the glasses 52
4.3 Sintering of glass powder 53

4.3.1 Samples sintered without $NH_4(HCO_3)$ 53
4.3.2 Samples sintered with $NH_4(HCO_3)$ 58
4.4 Analysis of the porous scaffolds 62
4.5 In vitro properties 69
4.5.1 Variation of pH 69
4.5.2 Variation of mass 71
4.5.3 ICP analysis 74
4.5.4 Phase and Microstructural analysis 76
4.5.4.1 XRD analysis 76
4.5.4.2 SEM images 79
4.6 Mechanical properties 85

CHAPTER 5: DISCUSSION 88

5.1 Densification and Microstructure of sintered glasses 88
5.1.1 Effects of particle size on crystallization 88
5.1.2 Effect of sintering temperature on crystallization 89
5.2 In vitro properties of the scaffolds 94
5.2.1 Variation of pH 94
5.2.2 Variation of mass 96
5.2.3 ICP analysis 96
5.2.4 Phase and Microstructural analysis 97
5.2.4.1 XRD analysis 97
5.2.4.2 SEM analysis 97
5.3 Mechanical properties 100

CHAPTER 6: CONCLUSIONS and FUTURE WORK 104

REFERENCES 106

Appended papers

I. Erasmus, E.P., Johnson, O.T., Sigalas, I. & Massera, J. (2017) "Effects of Sintering Temperature on Crystallization and Fabrication of Porous Bioactive Glass Scaffolds for Bone Regeneration". *Sci.Reports*. **7**.

II. E.P Erasmus, R. Sule, O.T. Johnson, I. Sigalas and J. Massera (2017) "In vitro Evaluation of Porous Bioactive Glasses (S53B50, P40B10 and Sr) Scaffolds fabricated using Foaming Agent for Bone Regeneration". To be submitted

LIST OF FIGURES

Figure 2-1: Structure of (a) Crystalline and (b) vitreous silica (only three oxygen atoms are shown per SiO_4 tetrahedron; with the fourth lying above or below the image plane).....7
Figure 2-2: Flow diagram of the process for sol-gel bioactive glass synthesis 8
Figure 2-3: Compositional diagram for bone-bonding. Note regions A, B, C, and D. Region S is a region of class A bioactivity where bioactive glass bond to both bone and soft tissues and are gene activating 12
Figure 2-4: A ternary diagram showing I_B as a function of composition A: bonding at 30 days or less; B: no bonding, reactivity too low; C: no bonding; reactivity too high; D: no bonding, no glass formation 12
Figure 2-5: SEM image showing the pore microstructure of a bioglass® scaffold fabricated by the foam replica method.....19
Figure 2-6: A flow chart of the sol-gel foam process 20
Figure 2-7: Microstructure of a bioactive glass foam scaffold produced through the sol-gel process.....20
Figure 2-8: Tetrahedral unit of a silicate.....54
Figure 2-9: Tetrahedral unit of a phosphate.....29
Figure 2-10: Compressive strength as a function of porosity.....34
Figure 3-1: Milling mechanism if the planetary ball mill.....40
Figure 3-2: Principle components of a MicroCT scanner.....47
Figure 4-1: X-ray diffraction patterns of S53B50, P40B10 and Sr bioactive glasses after milling presented in Table 4-1.....50
Figure 4-2: X-ray diffraction patterns of S53B50; P40B10 and Sr bioactive glasses after milling presented in Table 4-2…….50
Figure 4-3: SEM images of (a) S53B50 (b) P40B10 and (c) Sr bioactive glass powder showing the particle size and shape prepared without $NH_4(HCO_3)$ 51
Figure 4-4: SEM images of (a) S53B50 (b) P40B10 and (c) Sr bioactive glass powder showing the particle size and shaped prepared with $NH_4(HCO_3)$……..51
Figure 4-5: DTA thermographs of (a) S53B50 (b) P40B10 and (c) Sr 52
Figure 4-6: XRD pattern for glass S53B50 as a function of temperature.....55
Figure 4-7: XRD patterns for glass P40B10 as a function of temperature 55

Figure 4-8: XRD patterns for glass Sr as a function of temperature 56
Figure 4-9: SEM micrographs of the cross section of glass S53B50 samples sintered at (a) 580°C and (b) 600°C 57
Figure 4-10: SEM micrographs of the cross section of glass P40B10 sintered at (a) 580°C and (b) 600°C..... 57
Figure 4-11: SEM micrographs of the cross section of glass Sr samples sintered at (a) 580°C and (b) 600°C..... 57
Figure 4-12: SEM micrographs of the cross section of glass samples sintered at 600°C for glass (a) P40B10 (b) S53B50 and (c) Sr 58
Figure 4-13: XRD patterns of the as prepared porous glass scaffolds for S53B50, P40B10 and Sr 60
Figure 4-14: SEM micrographs of porous S53B50; P40B10 and Sr bioactive scaffolds mixed with (a),(c) and (e) 60 vol. % $NH_4(HCO_3)$ and (b), (d) and (f) 70 vol. % $NH_4(HCO_3)$, sintered at 540°C and 500°C for 1 hour, respectively 61
Figure 4-15: High magnification SEM micrographs of porous S53B50, P40B10 and Sr bioactive glasses mixed with (a); (b) and (c) 70 vol. % $NH_4(HCO_3)$, respectively 62
Figure 4-16: Pore size distribution of S53B50 glass scaffolds at different $NH_4(HCO_3)$ content; obtained from mercury intrusion porosimetry 63
Figure 4-17: Pore size distribution of P40B10 scaffolds at different $NH_4(HCO_3)$ content; obtained from mercury intrusion porosimetry 64
Figure 4-18: Pore size distribution of Sr glass scaffolds at different $NH_4(HCO_3)$ content; obtained from mercury intrusion porosimetry 65
Figure 4-19: An X-ray micro tomography (µCT) image of S53B50 glass scaffold mixed with (a) 60 vol. % $NH_4(HCO_3)$ (b) 70 vol. % $NH_4(HCO_3)$ 66
Figure 4-20: An X-ray micro tomography (µUT) image of P40B10 glass scaffold mixed with (a) 60 vol. % $NH_4(HCO_3)$ and (b) 70 vol. % $NH_4(HCO_3)$ 66
Figure 4-21: An X-ray micro tomography (µUT) image of Sr glass scaffold mixed with (a) 60 vol. % $NH_4(HCO_3)$ and (b) 70 vol. % $NH_4(HCO_3)$ 67
Figure 4-22: pH of SBF as a function of immersion time for glass S53B50 scaffolds 69
Figure 4-23: pH of SBF as a function of immersion time for glass P40B10 scaffolds 70
Figure 4-24: pH of SBF as a function of immersion time for glass Sr scaffolds..... 71
Figure 4-25: Weight loss (%) as a function of immersion time for glass S53B50 scaffolds 72

Figure 4-26: Weight loss (%) as a function of immersion time for glass P40B10 scaffolds 73
Figure 4-27: Weight loss (%) as a function of immersion time for glass Sr scaffolds 73
Figure 4-28: Ion concentration in the immersion solution of S53B50 for (a) B , (b) Ca , (c) P and (d) Si as a function of time 74
Figure 4-29: Ion concentration in the immersion solution of P40B10 for (a) B, (b) Ca, (c) P and (d) Sr as a function of time 75
Figure 4-30: Ion concentration in the immersion solution of Sr for (a) Ca, (b) P and (c) Sr as a function of time 76
Figure 4-31: XRD traces of S53B50-60 vol. % $NH_4(HCO_3)$ immersed in SBF for 24; 48;72 and 168 hours……78
Figure 4-32: XRD traces of S53B50-70 vol. % NH_4 (HCO_3) immersed in SBF for 24, 48, 72 and 168 hours……79
Figure 4-33: XRD traces of P40B10 mixed with 60 and 70 vol. % NH_4 (HCO_3) immersed in SBF for 168 hours……...80
Figure 4-34: XRD traces of Sr mixed with 60 and 70 vol. % NH_4 (HCO_3) immersed in SBF for 168 hours……80
Figure 4-35: SEM images of the surface of S53B50-60 vol. % NH_4 (HCO_3) bioactive glass scaffolds after immersion in SBF for (a) 24, (b) 48 , (c) 72 and (d) 168 hours……81
Figure 4-36: SEM images of the surface of S53B50-70 vol. % NH_4 (HCO_3) bioactive glass scaffolds after immersion in SBF for (a) 24, (b) 48, (c) 72 and (d) 168 hours……82
Figure 4-37: EDS spot analysis of as-formed HA particles on glass S53B50-70 vol. % NH_4 (HCO_3) after immersion in SBF for 24 hours……...83
Figure 4-38: SEM images of the surface of P40B10-60 vol. % NH_4 (HCO_3) bioactive glass scaffolds after immersion in SBF for (a) 24, (b) 48, (c) 72 and (d) 168 hours……84
Figure 4-39: SEM images of the surface of Sr-60 vol. % NH_4 (HCO_3) bioactive glass scaffolds after immersion in SBF for (a) 24, (b) 48, (c) 72 and (d) 168 hours……84
Figure 4-40: EDS spot analysis of the as-formed HA particles on glass P40B10-70 vol. % NH_4 (HCO_3) after immersion in SBF for 168 hours……85
Figure 4-41: EDS spot analysis of the as-formed HA particles on glass Sr-60 vol. % NH_4 (HCO_3) after immersion in SBF for 24 hours……...86

Figure 4-42: Compressive strength of scaffolds as a function of immersion time in SBF at 60 vol. % content……87
Figure 4-43: Compressive strength of scaffolds as a function of immersion time in SBF at 70 vol. % content……88
Figure 5-1: Crystallization temperature as a function of particle size 89
Figure 5-2: Effect of glass stability range (ΔT) on viscous flow sintering.....90
Figure 5-3: Relative density of S53B50, P40B10 and Sr bioactive glasses as a function of temperature sintered without $NH_4(HCO_3)$.....91
Figure 5-4: Schematic diagram on the fabrication of highly porous scaffolds during sintering.....93
Figure 5-5: Initial ion dissolution mechanism of conversion of glass S53B50 to HA 95
Figure 5-6: Initial ion dissolution mechanism of conversion of glass (a) P40B10 and (b) Sr to HA 95
Figure 5-7:SEM images of the surface of S53B50-70 vol. % $NH_4(HCO_3)$ bioactive glass scaffolds after immersion in SBF for 24 hours……98
Figure 5-8: Final mechanism of conversion of glass (a) S53B50, (b) P40B10 and Sr to HA in SBF.....99
Figure 5-9: Typical stress/extension curve for S53B50 prepared with 70 vol. % $NH_4(HCO_3)$ immersed in SBF for 168 hours.....102
Figure 5-10: Typical stress/extension curve for P40B10 prepared with 60 vol. % NH_4 103

LIST OF TABLES

Table 2-1: Sequence of interfacial reactions involved in forming a bond between bone and a bioactive glass 9
Table 2-2: I_B values for various Bioceramics 13
Table 2-3: Comparison of the ion concentrations of SBF K9 with those of blood plasma 13
Table 2-4: Types of Bioceramics-tissue attachment 14
Table 2-5: Types of bioceramic tissue attachment and bioceramic classification 14
Table 2-6: Scaffold requirements for bone tissue engineering 22
Table 2-7: Compositions of various bioactive glasses 26
Table 2-8: Methods used to create bioactive glass scaffolds; and characteristics of the fabricated scaffolds 17
Table 2-9: Mechanical properties of human bone 32
Table 2-10: Parameters of scaffolds 33
Table 2-11: Current uses of Bioceramics in various clinical applications 36
Table 3-1: Supplier of all glass materials used in this project 38
Table 3-2: Supplier of all chemicals used in this project 38
Table 3-3: Composition of S53B50, P40B10 and Sr glasses presented in (mol. %) 39
Table 3-4: Comparison of the ion concentration of SBF K9 with those of blood plasma 42
Table 4-1: Results obtained from the particle size analysis after milling for samples sintered without $NH_4(HCO_3)$ 49
Table 4-2: Results obtained from the particle size analysis after milling for samples sintered with $NH_4(HCO_3)$ 49
Table 4-3: Glass transition temperature (T_g), onset of crystallization temperature (T_x) and working range (ΔT) of S53B50, P40B10 and Sr bioactive glasses; as determined by differential thermal analysis (DTA) 53
Table 4-4: Composition, Temperature, Time, Density, Open porosity and Relative density 54
Table 4-5: Composition, Density and Open porosity of sintered scaffolds 59
Table 4-6: Composition; Average pore diameter and % Porosity of scaffolds 68
Table 5-1: List of sample compositions 94

LIST OF SYMBOLS

3D	Three dimensions
BO	Bridging oxygen
NBO	Non-bridging oxygen
DTA	Differential thermal analysis
HA	Hydroxyapatite
SBF	Simulated body fluid
XRD	X-ray diffraction
SEM	Scanning electron microscopy
µCT	micro computed tomography
$NH_4(HCO_3)$	Ammonium bicarbonate
T_g	Glass transition temperature
T_x	Temperature at onset of crystallization
I_B	Bioactivity index
NC	Network connectivity
Vol. %	Volume percent
MPa	MegaPascal
Mol. %	Mole percent
°C	degree Celsius
B50	S53B50
B10	P40B10

CHAPTER 1: INTRODUCTION

1.1 Motivation

The repair and regeneration of large bone defects from disease or trauma remains a significant clinical challenge. Tissue engineering and regenerative medicine aims to replace diseased or restore damaged tissue using combinations of functional cells and biodegradable scaffolds made from engineered biomaterials (Chen *et al.*, 2008). At present, autografts and allografts are mainly used in the repair of defected bones. These grafts offered all the desired properties required for bone repair and regeneration, which are osteoconductivity, osteogenesis, and osteoinductivity. However, bone grafts are associated with high operating costs for harvesting the graft, limited availability, donor site morbidity and complications including infection, pain, and hematoma ((Burg *et al.*, 2000),(Laurencin *et al.*, 2006),(Hutmacher, 2000), (Tomford, 1995)) . On the other hand, allografts are subject to cleaning and preparation processes designed to remove cells to minimize immune response. In addition, these process techniques potentially reduce the osteoinductivity, osteoconductivity, and mechanical strength of the graft To overcome these limitations, significant effort has been devoted to the development of biomaterials as bone-graft substitute that can augment or regenerate bone, (Burg *et al.*, 2000). This has led to the investigation of using bioactive glasses as the substitute biomaterial in bone regeneration.

Porous bioactive glass scaffolds are of particular interest, if not critical, to bone tissue engineering. These scaffolds are designed to have features that provide the promotion of tissue ingrowth and transportation of nutrients (Hutmacher, 2000). With this said, an ideal scaffold should therefore possess the following characteristics (i) a highly porous structure with a good degree of interconnected pore network; (ii) biocompatibility and bioresorbability with controllable degradation and resorption rates to match cell/tissue growth in vitro and/or in vivo; (iii) suitable surface chemistry for cell attachment; proliferation and differentiation; (iv) mechanical properties to match those of the tissues at the site of implantation (Hutmacher, 2000).

1.2 Problem statement

One major challenge in today's bone tissue engineering application is the development of a scaffolding material that is mechanically strong and yet biodegradable. To engineer bone tissue which is hard and functions to support the body, the scaffold material must be strong and tough. Ideally the scaffold material needs to be biodegradable as the biodegradation would help avoid the detrimental effects of a persisting foreign substance and allow its gradual replacement with the new bone, (Chen *et al.*, 2012).

Unfortunately, it is known that mechanical strength and biodegradability contradict each other. In general, mechanically strong materials (e.g., crystalline hydroxyapatite, titanium (Ti) alloys and crystalline polymers) are virtually inert and remain part of the repaired bone, while biodegradable materials (e.g. amorphous hydroxyapatite and glasses) tend to be mechanically fragile (Chen *et al.*, 2012). In addition; glass is not the only material that is mechanically fragile but, in all cases, when creating a porous structure (regardless of the material) the mechanical properties will be decreased. Mechanical strength is limited by the largest defect. This forms the greatest challenge in the design of bioceramics for bone engineering at load bearing sites, but there are processing approaches such as sintering of 45S5 bioglass® , (Rezwan *et al.*, 2006). During sintering; the 45S5 bioglass® particles fuse together through viscous flow resulting in a well densified compact which often increases the strength of the sintered material without loss of bioactivity.

Another problem associated with bioactive glasses is the tendency to crystallize during freezing after melting which makes it difficult to create porous amorphous bioglass. Processing approaches such as sintering of 45S5 bioglass® have been developed (Chen and Boccaccini, 2006a). However, in all cases it was seen that the sintering led to partially or fully crystallized forms. The presence of the crystalline phases tends to retard the formation of the hydroxyapatite layer, hence, glass becomes less bioactive in simulated body fluid, (Filho *et al.*, 1996).

1.3 Aim and Objectives

The primary aim of this research work is to synthesize, test and characterize biocompatible glass using borophosphate, borosilicate and phosphate glasses for clinical use as a scaffold material. The objectives are to:

1. Determine the time-temperature conditions at which the glasses can be sintered without or with minor crystallization
2. Fabricate porous scaffolds with $NH_4(HCO_3)$ foaming agent
3. Test for bioactivity (simulated body fluid (SBF), layer formation, pH change) and mechanical and cell testing.

The outcome of this research will provide information on the temperature at which sintering can take place without interfering with crystallization, the glass composition suitable for sintering will be established, the bioactivity of these glass composition as well as the mechanical properties will be determined.

1.4 Scope of research

This research involved the characterization of the crushed and milled glasses using particle size distribution (PSD), X-Ray Diffraction (XRD) and Scanning Electron Microscopy-Energy Dispersive Spectroscopy (SEM-EDS). The glasses were first sintered without the luminescent additives; the resulting sintered materials, were then characterized by density, XRD, Hg-Porosimetry, SEM-EDS and micro-computed tomography (μCT). If the experiments were successful, samples were prepared for biocompatibility testing at Technical University of Tampere (TUT), Finland. These tests would include: Bioactivity Testing (SBF, layer formation, pH change) and mechanical tests after immersion in simulated body fluid.

1.5 Structure of the dissertation

The outline of the dissertation is as follows:

Chapter 2 presents a review on the background information on bioactive glasses, which includes the structure, synthesis, properties and applications of bioactive glasses. This section also includes previously published results for a wide range of bioactive glasses such as silicate, borate and phosphate glasses.

Chapter 3 gives a detailed discussion of the experimental equipment's and techniques used to prepare and determine the physical and chemical properties of the starting as well as the sintered materials.

All the results obtained on the preparation and sintering of the material with and without $NH_4(HCO_3)$ as well as the in vitro bioactivity of the porous scaffolds in SBF are listed and discussed in **Chapter 4** and **Chapter 5**, respectively.

Chapter 6 includes the conclusions drawn from the work and future work.

CHAPTER 2: LITERATURE REVIEW

In this chapter, glass is discussed based on its structure, synthesis, properties and applications as well as bioceramics and techniques used to fabricate porous scaffolds. The glasses of interest in this project are found in the SiO_2-CaO-Na_2O-P_2O_5 and P_2O_5-CaO-Na_2O systems with the incorporation of B_2O_3 and SrO to partially and fully substitute SiO_2 and CaO, respectively. Although these glasses have similar structures, they all offer different properties that are desirable for various applications in tissue engineering (T.E). This section also includes previously published results for a wide range on bioactive glasses such as silicate, borate and phosphate glasses. Among the applications listed in the review, no porous bioglass devices have found clinical use to date, hence the need for new glass materials which can be processed into amorphous porous scaffolds.

2.1 Discovery of Bioactive glasses

The findings by Hench *et al*., (1971) in the early 1970s that some SiO_2-CaO-Na_2O-P_2O_5 glasses induce no formation of fibrous tissue on contact with living tissue but rather bond chemically to it, aroused much interest in the development of bioactive glasses and glass ceramics, and their use as biomedical materials. Bio ceramics and bioactive glasses are a subset of biomaterials which are used in medical applications as scaffolds to repair and regenerate damaged bone tissue due to their similar chemical and structural properties as that of the body's own bone mineral, hence they are biocompatible.

According to Arstila *et al*., (2008), the main idea was that an implant made of bioactive glass would be quickly and firmly fixed with tissue, before encapsulation takes place and consequently would not necessarily require mechanical means of fixation nor a porous surface. This kind of fixation is possible due to kinetic modification of the glass surface that occurs upon implantation. The surface forms a biologically active hydroxycarbonate apatite (HCA) layer which provides a bonding interface for tissues. The HCA phase that forms on implants is chemically and structurally equivalent to the mineral phase in bone, (Arstila *et al*, 2008). It is this equivalence which is responsible for interfacial bonding, which is superior to that attained with for example, metal implants (Hench, 1991). The interface between the bioactive glass and bone is often so strong that removal of an implant necessitates

breaking the surrounding bone or in some cases, the implant, but not the interface (Rawlings, 1993).

2.1.1 Glass structure of bioactive glasses

There are three different components that exist within the glass structure; this includes the network formers (for example SiO_2, P_2O_5 and B_2O_3); network modifiers (for example Na_2O, CaO and SrO) and the intermediate oxides which can act as a network former or modifier (for example Al_2O_3, PbO). The network former is the essential component of the glass and is the oxide of an element with high valence, that is, able to form a three-dimensional (3D) glass structure (Vallet-regí and Balas, 2008). According to Zachariasen, (1932) an oxide glass may be formed (1) if the sample contains a high percentage of cations which are surrounded by oxygen in tetrahedral coordination or by oxygen triangles; (2) if these tetrahedrals or triangles share only corners with each other and (3) if some oxygen atoms are linked to only two such cations and do not form further bonds with any other cations. This basically means that the glass must contain appreciable amounts of the cations which can form vitreous oxides or of other cations which are able to replace any of the former isomorphously. Some of the glass forming cations include B^{+3}, Si^{+4} , P^{+3} , P^{+5} , As^{+3} , As^{+5}, Ge^{+4}, (Zachariasen, 1932). When adding modifiers to a glass network it is important that the cations must be large and carry a small charge because small and highly charged cations like Ti^{+4}, Mg^{+2} tend to produce detrivification, (Zachariasen, 1932). Modifiers such as Na^{+}, K^{+}, Ca^{+2} are known to have large cations and relatively small charges.

The biological behaviour of glasses, glass ceramics and ceramics has been reported by Karlsson and Ylanen, (1998) to depend on the relative proportion of the bridging oxygen to non-bridging bonds in the phases of the material. The most important structural parameter which affects the dissolution of a glass is the network connectivity, (Hill, 1996). The network connectivity (NC) is defined as the average number of bridging oxygen (BO) atoms bound to a network-forming cation, where a BO atom is defined as an oxygen atom which is chemically bonded to two network polyhedra. Oxygen atoms which do not connect two network polyhedra are called non-bridging (NBO) atoms. The NC depends critically on composition because the inclusion of network-modifying cations such as sodium or calcium typically breaks T-O-T bonds (where T is a network former), causing the formation of NBO and

decreasing the network connectivity, (Tilocca, 2009). High values of NC typically indicate a well-connected glass network which is not prone to dissolution and is not bioactive. Whereas lower values indicate a fragmented, disconnected network which has many reactive sites and is prone to dissolution and typically demonstrate bioactivity, (Jamieson *et al.*, 2016).

Glasses both bioactive and the conventional silica glass have two distinctive features, these include: their amorphous structure and their temperature behaviour, which shows a glass transition range (T_g), which is the temperature interval where a system transforms from a supercooled liquid to a solid glass (Brauer, 2015). The atomic arrangement of glass is characterized by an extended three-dimensional network which lacks symmetry and periodicity in contrast to crystalline solids (Figure 2.1a) (Zachariasen, 1932).

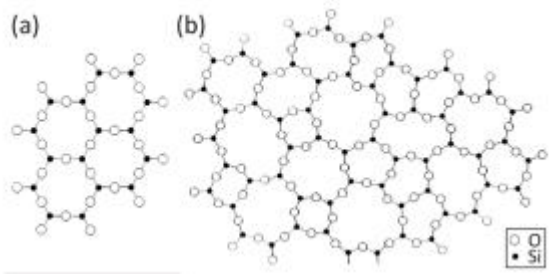

Figure 2-1: Structure of (a) Crystalline and (b) vitreous silica (only three oxygen atoms are shown per SiO_4 tetrahedron; with the fourth lying above or below the image plane) (Zachariasen, 1932)

2.1.2 Synthesis of Bioactive glass

Bioactive glasses have been synthesized by the melt or sol gel processes (Jones *et al.*, 2010).The original bioactive glass was melt derived (46.1 mol.%, SiO_2, 24.4 mol.%, Na_2O, 26.9 mol.%, CaO, 2.6 mol.%, P_2O_5) and was named bioglass® 45S5 (Hench, 1973). Melt derived silicate glasses are made by melting oxide components in a crucible at temperatures above 1100°C (where exact temperature depends on the glass composition) and pouring into a mould (casting a shape) or quenching into water (making a frit or powder).

On the other hand, sol-gel derived glasses are synthesized by the hydrolysis of alkoxides to form a sol, which is a colloidal silica solution (Hench *et al.*, 1990),(Sepulveda *et al.*, 2002). This process is presented in Figure 2.2. A commonly used silica precursor is tetraethylorthosilicate (TEOS). Triethylphosphate is used to add phosphate and the salt calcium nitrate is usually used to introduce calcium. The silica species in the sol then undergo polycondensation to form a network of silica (Si-O-Si bridging bonds) and is termed a gel. The gel is then heat treated to drive off the condensation by products of water and ethanol and to remove the nitrates (Brinker *et al.*, 1990). Sol-gel-derived bioactive glasses tend to be more bioactive and degrade more rapidly than melt-derived glasses of similar composition due to their mesoporous texture (pore diameters in the range 2 – 50 nm) which is inherent to the sol gel process (Sepulveda *et al.*, 2002). In addition, this textural porosity also increases the specific surface area by two orders of magnitude as compared to a melt derived glass.

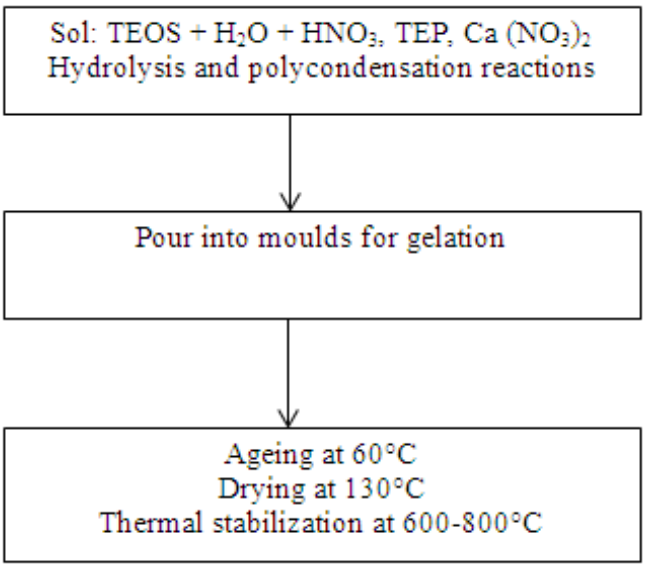

Figure 2-2: Flow diagram of the process for sol-gel bioactive glass synthesis (Jones, 2007a)

The difference between these two processes lies in the SiO_2 content. Melt-derived glasses often contain 60 mol.% or less SiO_2 in order to be able to bond to bone, while sol-gel processed glasses can contain up to 100 mol.% SiO_2 and still be bioactive (Jones , 2007a).

2.1.3 Surface reactivity of bioactive glasses

When bioactive glasses are immersed in any physiological environment (e.g. body fluids), their unique surface reactivity leads to the formation of a hydroxycarbonate apatite layer. This is the result of the release of soluble ions when the glass starts to dissolve. Among the ions which are released Si, Ca, P and Na are included. These ions have been found to induce favorable intracellular and extracellular responses leading to rapid bone formation (Xynos *et al.*, 2000). The various surface reactions which occur at the bioactive glass surface upon immersion in the body fluid have been described extensively by Larry Hench and are described in Table 2.1 (Hench, 1974) , (Hench, 1993)

Table 2-1: Sequence of interfacial reactions involved in forming a bond between bone and a bioactive glass (Hench, 1974)**,**(Hench, 1998)

Increasing time (hours)	Surface reaction stages	Reactions
	12	Proliferation and growth of bone
	11	Crystallization of matrix
	10	Generation of matrix
	9	Differentiation of stem cells
	8	Attachment of stem cells
	7	Action of macrophages
	6	Biochemical adsorption of growth factors on HCA layer
	5	Crystallization of the HCA layer
	4	Chemisorption of amorphous Ca + PO4 + CO3
	3	Silica-gel polymerization: SiOH + SiOH → Si-O-Si

Log t	2	Network dissolution and formation of silanol (SiOH) bonds
	1	Exchange of alkali ions with hydrogen ions from body fluids
	0	Surface of bioactive glass

The five important reaction stages which lead to the rapid release of soluble ionic species and formation of the HCA layer are further elaborated below:

Stage 1: Rapid exchange of Na^+ and Ca^{2+} with H^+ or H_3O^+ from solution causing hydrolysis of the silica groups, which creates silanols (Si-OH), e.g:

$$Si\text{-}O\text{-}Na^+ + H^+ + OH^- \longrightarrow Si\text{-}OH^- + Na^+_{(aq)} + OH^- \qquad 2.1$$

Ion exchange diffusion is controlled with a $t^{1/2}$ dependence. The pH of the solution increases as a result of the H^+ ions in the solution being replaced by cations.

Stage 2: Stage 1 increases the hydroxyl concentration of the solution, which leads to attack of the silica glass network. Soluble silica is lost in the form of Si (OH_4) to the solution, resulting from the breaking of Si-O-Si bonds and the continued formation of Si-OH (silanols) at the glass-solution interface:

$$Si\text{-}O\text{-}Si + H_2O \longrightarrow Si\text{-}OH^- + OH^-\text{-}Si \qquad 2.2$$

Stage 3-5: Condensation and repolymerization of the Si-OH groups then occurs, leaving a silica-rich layer. The surface is, therefore depleted in alkalis and alkali-earth cations (Stage 3). Ca^{2+} and PO_4^{3-} groups then migrate to the surface through the silica-rich layer and from the surrounding fluid, forming film rich in $CaO\text{-}P_2O_5$ on top of the silica-rich layer (Stage 4). The $CaO\text{-}P_2O_5$ film crystallizes as it incorporates OH^- and CO_3^{2-} anions from solution to form a mixed HCA layer.

The formation of such a bioactive apatite layer is the common characteristic of all known bioactive inorganic materials used for bone replacement, orthopaedic implants and bone tissue engineering scaffolds (Hench, 2002), (Gerhardt and Boccaccini 2010).

2.2 Properties of Biomaterials

2.2.1 Biocompatibility

One of the most critical properties of any biomaterial is its biocompatibility, which according to Williams, (1989) is 'the ability of a material to perform with an appropriate host response in a specific application'. The range of biocompatibility of biomaterials is based on their chemical reactivity with the physiological environment. This range includes oxides which are bioinert, bioactive and bioresorbable. Bioinert refers to any material which does not elicit any response or interact with the surrounding tissues when placed in a biological environment, common examples include Al_2O_3 and ZrO_2, (Yamamuro, 2004); whereas bioresorbable are materials which dissolve upon implantation and slowly degrade as the new tissues are being formed; examples include $Ca(PO_4)_2$ and PLGA copolymers. In addition to that, the bioactivity of biomaterials in the SiO_2-CaO-Na_2O-P_2O_5 system differs depending on their specific composition. It should be noted that, there is a close relationship between the bioactivity and biocompatibility of a material. The ternary system shown in Figure 2.3 shows the different classes in which biomaterials can exist. Bioactivity index (I_B), on the other hand, is defined as the time taken for more than half of a material's interface to bond to bone. Materials with an I_B value greater than 8 (see Figure 2.4) are considered to be Class A. These materials are expected to bond to soft tissues. Bioglass® is a typical known Class A bioactive material. Meanwhile materials exhibiting an I_B less than 8 but greater than 0 are considered Class B bioactive materials, e.g synthetic hydroxyapatite (sHA), which will only bond to hard tissue, (Jones, 2007a). The difference between the two classes is that Class A bioactive materials are both osteogenic and osteoconductive while class B bioactive materials exhibit only osteoconductivity (Chen *et al.*, 2008).

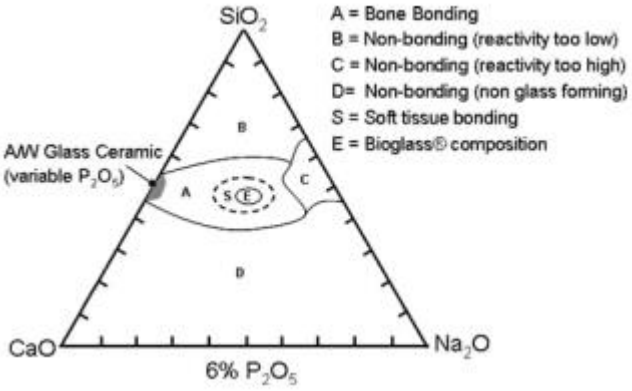

Figure 2-3: Compositional diagram for bone-bonding. Note regions A, B, C, and D. Region S is a region of class A bioactivity where bioactive glass bond to both bone and soft tissues and are gene activating (Hench, 2006)

2.2.2 Bioactivity

To assess the bioactivity of a material, Hench proposed an *in vivo* bioactivity index I_B (Figure 4), which is defined as $I_B = 100/t_{50bb}$ is the time required for more than 50% of the interface to be bonded (Hench, 1991)

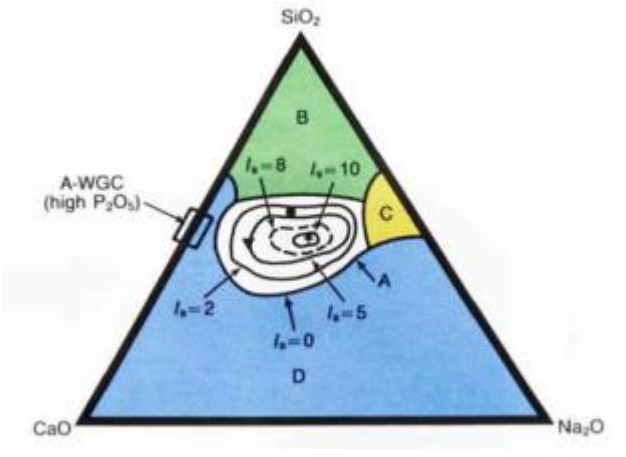

Figure 2-4: A ternary diagram showing I_B as a function of composition A: bonding at 30 days or less; B: no bonding, reactivity too low; C: no bonding; reactivity too high; D: no bonding, no glass formation (Hench, 1991)

According to Huang, Best *et al.*, (2007), the rate of bone bonding to implant and the strength and stability of the bond vary with the composition and microstructure of the bioactive materials. They further stated that bioactive glasses with 42-53% SiO_2 form

a bond to bone very rapidly, within days, and also form an adherent bond with soft tissues. Whereas, bioactive glasses with 54-60% of SiO_2 require 2-4 weeks to bond with bone, but do not bond with soft tissues. Generally, the higher the value of the bioactivity index of the material, the faster the rate of apatite formation on its surface and the better bonding with bone. Table 2.2 shows I_B values for various Bioceramics.

Table 2-2: I_B values for various Bioceramics

Bioceramic	**I_B ($100/t_{50bb}$)**
45S5	12.5
Ceravital	5.6
55S4.3	3.7
HA	3.1
Ceravital KGX, KGX'	2.3
316 S.S. Si_3N_4	0

In order to study the behaviour of a material *in vitro*, various kinds of buffers have been introduced to deionised water to maintain the pH of the solution in the physiological range (7.2 - 7.4) and form physiological solution or pseudo-extracellular fluids (Huang and Best *et al.*, 2007). Kokubo developed and named the solutions as simulated body fluid (SBF) K1 to K9 in ascending order of ion content and concentration (Kokubo *et al.*, 1990). SBF K1 is equivalent to the tris buffer solution, containing no physiological cations, SBF K2 is physiological saline. However, it was suggested that SBF K9 was a suitable medium for initial *in vitro* study, as its ion concentration is close to those of human blood plasma (Table 2.3).

Table 2-3: Comparison of the ion concentrations of SBF K9 with those of blood plasma (Kokubo *et al.*, 1990)

	Concentration mM	
	SBF K9	**Blood Plasma**
Na^+	142.0	142.0
K^+	5.0	5.0
Mg^{2+}	1.5	1.5
Ca^{2+}	2.5	2.5
Cl^-	147.8	103.0
$(HCO_3)^-$	4.2	27.0
$(HPO_4)^{2-}$	1.0	1.0
SO_4^{2-}	0.5	0.5

Kokubo *et al.*, (1990) further stated that the presence of Ca and P ions in SBF accelerated the repolymerization of silica on the glass, the formation of an amorphous Ca, P layer and the crystallization to hydroxycarbonate apatite (HCA). However, Mg ions in SBF were found to slow down both the formation of the amorphous Ca, P phase and the crystallization of HCA.

2.2.3 Types of Bioceramics-tissue attachment

The survivability of a bioceramic requires formation of a stable interface with living host tissue (Hench, 1998). The mechanism of tissue attachment is directly related to the type of response at the implant interface (Gross *et al.*, 1988). No material implanted in living tissues is inert; all materials elicit response from living cells. There are four types of response shown in Table 2.4 that allow different means of achieving attachment of prostheses to the musculo-skeletal system, whereas Table 2.5 summarises the attachment mechanisms

Table 2-4: Types of Bioceramics-tissue attachment

If the material is toxic, the surrounding tissue dies.
If the material is nontoxic and biologically inactive (almost inert), a fibrous tissue of variable thickness forms.
If the material is nontoxic and biologically active (bioactive), an interfacial bond forms.
If the material is nontoxic and dissolves, the surrounding tissue replaces it.

Table 2-5: Types of bioceramic tissue attachment and bioceramic classification

Type of attachment	**Type of bioceramic**
Dense, nonporous, almost inert ceramics attach by bone growth into surface irregularities by cementing the devices into the tissue, or by press-fitting into a defect (morphological fixation).	Al_2O_3, ZrO_2

For porous implant, bone ingrowth occur which mechanically attaches the bone to the material (biological fixation)	Porous hydroxyapatite HA-coated porous metals
Surface-reactive ceramics, glasses, and glass ceramics Attach directly by chemical bonding with the bone (bioactive fixation).	Bioactive glasses Bioactive glass-ceramics Dense HA
Resorable ceramics and glasses in bulk or powder form Designed to be slowly replaced by bone.	Bioactive glasses Tri-Calcium Phosphate Calcium Phosphate salts Calcium Sulfate (Plaster of Paris)

2.3 Porous Bioceramics

The concept of porous bioceramic is driven by the need for ingrowth of tissues into pores on the surface and throughout the implant (Hench, 1998). This was originated by Hulbert *et al.*, (1987) many years ago. These porous structures provide an increased interfacial area between the implant and the tissues which results in an increased resistance to movement of the device in the tissue. The interface is established by the living tissue in the pores. This type of attachment is referred to as biological fixation. Biological fixation is capable of withstanding more-complex stress states than implants that achieve only morphological fixation. However, the limitation associated with porous implants is that, for the tissue to remain viable and healthy, pores must be >100-150 µm in diameter. Such large pores are required to provide a blood supply to the ingrown connective tissue and allow cell migration (Hench, 1991). Vascular tissue which is required to circulate body fluids does not appear in pores that are <100 µm. It is also important to note that, if micromovement occurs at the interface of a porous implant the surrounding tissue may be damaged. In

turn this will cut off the blood supply leading to tissue necrosis, inflammation, and loss of interfacial stability (Hench, 1998).

2.4 Fabrication techniques for porous scaffolds

For a given bioactive glass scaffold, the porosity, pore size and pore interconnectivity are critical parameters. Generally, an ideal bone tissue scaffold should possess an interconnected porous structure (it should be highly permeable), with porosity >90% and pore diameters in the range of 10- 500 µm for cell seeding, tissue ingrowth and vascularization, as well as for nutrient delivery and waste removal (Chen *et al.*, 2006b); (Yang *et al.*, 2001); (Karageorgiou *et al.*, 2005). Locs *et al.*, (2013) studied the preparation of porous ceramics by viscous slurry foaming using hydroxyapatite powder and ammonium hydrogen carbonate as the foaming agent for the generation of pores in the glycerol-based viscous ceramic slurry. Open and total porosity were found to increase from 25 to 69% and from 32 to 73% when NH_4 (HCO_3) was varied from 0 to 2.75 wt. %. The sintered ceramics were found to have well-connected and irregularly shaped pores.

Meanwhile (Kazutaka *et al.*, 2009) produced highly porous alumina based ceramics by incorporating polymethymethacrylate (PMMA) microspheres with different diameters as a template and MgO or SiC powder as a sintering aid and subsequent calcinations at 1600°C. The sintered ceramics formed spherical pores which correlated to the morphology of the PMMA microspheres. Highly porous and mechanically strong alumina-based ceramics having an open porosity of 62%; a connected space size of 1.3µm, and a compressive strength of 147.6 MPa were fabricated by incorporating PMMA microspheres with a mean particle size of 22.6µm and an appropriate amount of SiC.

A large number of techniques have been developed to fabricate scaffolds with the desired properties. Some of the techniques include thermal bonding of particles or fibres, direct foaming, foam replication, gel-casting, sol gel or sacrificial porogens which are known for producing scaffolds with large interconnected pores. Table 2.8 shows some of the methods used to create bioactive glass scaffolds. This section summarizes the potential of these techniques as well as their draw backs.

Table 2-6: Methods used to create bioactive glass scaffolds, and characteristics of the fabricated scaffolds. (Rahaman *et al.*, 2011)

Method	**Glass**	**Porosity (%)**	**Pore size (µm)**	**Strength *(MPa)**
Thermal bonding of				
Particles	13-95	40-45	100-300	22 ± 1
Short fibers	13-93	45-50	>100	5
Polymer foam replication	45S5	89-92	510-720	0.4 ± 0.1
	13-93	75-85	100-500	11 ± 1
	13-93B3	80-85	100-500	5 ± 0.5
Sol-gel foam	70S30C	82	500(100)*	2.4
Unidirectional freezing of suspension	13-93	53-57	90-110	25 ± 3
	13-93	50-55	60-120	27 ± 8
	13-93	50	50-150	47 ± 5
Solid freeform fabrication				
Selective laser sintering	13-93	58-60	700-1000	15 ± 1
Freezing extrusion fabrication	13-93	50	300	140 ± 70
Robocasting	6P53B	60	500	136 ± 22

2.4.1 Direct foaming

Direct foaming involves the incorporation of air or gas into a suspension or liquid media in order to keep the structure of the air bubbles created and dried. The consolidated foams are then sintered at high temperatures to obtain high-strength porous ceramics (Studart *et al.*, 2006); (Ohji *et al.*, 2012). This technique allows low-cost and easy production of highly porous ceramic materials, up to more than 95% porosity (Ohji et al., 2012). Additionally, porous ceramics with unidirectional channels have been developed recently by using continuous bubble formation in ceramic slurry (Song *et al.*, 2008); (Banno *et al.*, 2009). The total porosity of directly foamed samples is proportional to the amount of gas incorporated into the suspension or liquid medium during the foaming process. The pore size, on the other hand, is

determined by the stability of the wet foam before setting takes place (Studart *et al.*, 2006). However, wet foams are thermodynamically instable systems which can undergo Ostwald ripening and coalescence in order to reduce the Gibbs free energy of the system resulting in large pores in the final porous bodies (Studart *et al.*, 2006); (Ohji *et al.*, 2012).

The most critical issue on direct foaming methods is the approach used to stabilize the air bubble incorporated within the initial suspension or liquid media. To overcome the problem associated with the unstable nature of the wet foams, surfactants such as lipid and proteins have been introduced into the suspension. This surfactant slows down the coalescence and disproportionation of bubbles by adsorbing at the air bubble interface and reducing the air-water interfacial energy. Despite the efforts, the low adsorption energy of the surfactants at the gas-liquid interface cannot prevent the long-term destabilization of foams. This is because wet foams stabilized with long-chain surfactants collapse within a few minutes after foaming, whereas those stabilized by proteins exhibit bubble disproportionation within few hours. Therefore, direct foaming based on surfactants require a setting agent to consolidate the foam microstructure before extensive coalescence and disproportionation take place (Studart *et al.*, 2006).

2.4.2 Foam replication

The replica technique is based on the immersion of a cellular structure or foam in a ceramic suspension or precursor solution in order to produce a macro porous ceramic exhibiting the same morphology as the original porous material (Studart *et al.*, 2006). Various synthetic and natural cellular structures can be used as templates. In addition, the templates need to have adequate flexibility, shape recovery ability and homogenous open cell structure. The most frequently used synthetic template includes porous polymeric sponge such as polyurethane (Ohji *et al.*, 2012). In the case were the suspension is produced from bioactive glass particles (e.g. bioglass®), the polymer is immersed in the suspension, which subsequently infiltrates the structure leading to a homogenous coating of bioglass® particles on the surface of the polymer substrate. After drying, the polymer is slowly burned out at high temperature (>450°C) in order to minimise microstructure damage (i.e. micro cracking) of the porous bioglass® coating (Chen *et al.*, 2008). The glass is then sintered at high temperature for densification to occur.

Scaffolds derived through this method have one advantage over all the other fabrication methods which is the high porosity with large pore diameters. Various scaffolds 45S5, 13-93, 13-93B3 and 70S30C (Chen *et al.*, 2006b), (Fu *et al.*, 2010); (Fu *et al.*, 2008), (Jones *et al.*, 2006) have been prepared using this method and porosities in the range of 75 – 92 % (Table 8) have been achieved. Additionally, (Chen *et al.*, 2008) stated that porosity higher than 90% can be obtained with pore sizes ranging from 500 to 700 µm. Figure 2.5 shows the macroscopic pore structure of a Bioglass®-based glass ceramic scaffold fabricated by this technique. The pores are interconnected, which allows fluid to pass through the foams with relatively low pressure drop. However, due to cracking the struts during the pyrolysis, the mechanical properties of ceramic reticulated foams are generally poor (Ohji *et al.*, 2012).

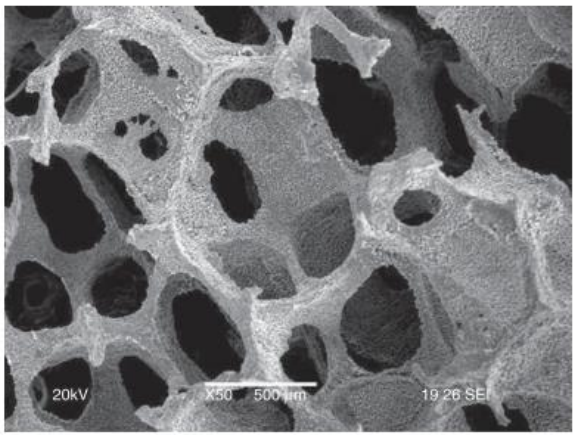

Figure 2-5: SEM image showing the pore microstructure of a bioglass® scaffold fabricated by the foam replica method (Chatzistavrou and Boccaccini, 2011)

2.4.3 Sol gel process

Porous bioactive glass scaffolds can be produced by adding a foaming step to the sol-gel process. The hydrolysed sol can be foamed by the vigorous agitation in air with the aid of a surfactant. The surfactant lowers the surface tension and temporarily stabilizes the foam (Jones *et al*, 2009). This followed by condensation and gelation reactions. The sol gel foam process is shown in Figure 2.6, this process was used to produce porous scaffolds for glass 58S and 70S30C (see Figure 2.7) (Jones *et al.*, 2007b), (Jones and Hench, 2003), (Elizabeth *et al.*, 2004). The gel is then subjected to aging and sintering to increase the strength and obtain the three-strengthen dimensional structure of the scaffolds; respectively.

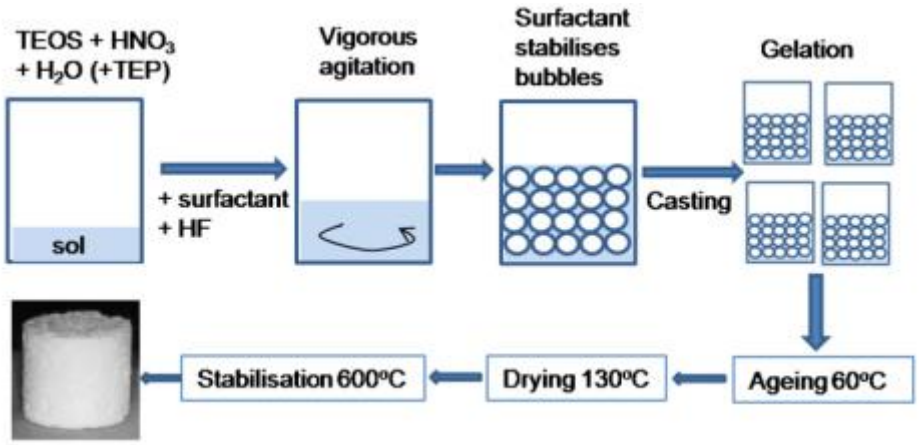

Figure 2-6: A flow chart of the sol-gel foam process (Jones *et al.*, 2009)

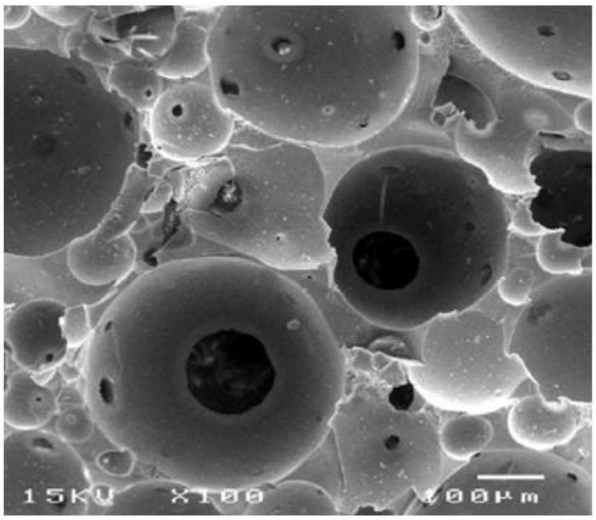

Figure 2-7: Microstructure of a bioactive glass foam scaffold produced through the sol-gel process (Jones *et al.*, 2009)

Scaffolds with a hierarchical structure consisting of mesopores (2 – 50 nm) for enhanced bioactivity and cell attachment and an interconnected array of macropores (10 – 500 µm) for tissue ingrowth can be achieved (Chen *et al.*, 2008). This hierarchical pore architecture is considered to be beneficial for stimulating the response of the scaffolds to cells, because it mimics the hierarchical structure of

natural tissues and more closely stimulates a physiological environment (Fu *et al.*, 2011).

Due to the inherent porosity that results from the sol-gel process, scaffolds derived from this process often have high surface area (100-200 m^2/g); as a result, these scaffolds degrade and convert faster to HA than scaffolds obtained from melt-derived glass with the same composition. However, these sol-gel derived scaffolds have low strength (0.3 – 2.3 MPa) (Jones *et al.*, 2006) and consequently they are suitable for substituting defects in low-load sites only (Fu *et al.*, 2011).

2.4.4 Thermally bonding of particles or fibres

This is one of the simplest methods for forming a scaffold. In this process the scaffold is formed by thermally bonding a loose, random packing of particles or short fibres in a mold with the desired geometry (Brovarone *et al.*, 2004); (Brovarone *et al.*, 2006), (Fu *et al.*, 2007). Bioactive glass scaffolds of 13-93 with porosity between 40 – 50% have been produced through this method. On the other hand, in order to increase the pore size and porosity of the scaffolds, the bioactive glass particles are often mixed with porogens (such as NaCl, or starch) which are removed by leaching or decomposition after forming the scaffold but prior to sintering. The major concern with this method is the poor pore connectivity between neighbouring pores.

2.3.1 Porous bioactive scaffolds

Bioactive scaffolds, which are important component in tissue engineering, are porous structures that act as substrate, upon which cells adhere and grow and organise into normal healthy bone as the scaffold degrades. The scaffold provides structural and mechanical support as well as the surface for cell growth. Its presence allows cells to generate the biological structural component of the extracellular matrix (ECM) in culture conditions (Sabree *et al.*, 2015). On the other hand, scaffolds for bone tissue engineering are also subjected to many interlinked and often opposing biological and structural requirements, which are summarised in Table 2.6.

Table 2-7: Scaffold requirements for bone tissue engineering (Ma, 2004), (Salgado *et al.*, 2004) , (Hench, 1991)

---

1. **Ability to deliver cells**

The material should not only be biocompatible (i.e. harmless), but also foster cell attachment, differentiation and proliferation.

2. **Osteoconductivity**

It would be best if the material encourages osteoconduction with host bone. Osteoconductivity does not only eliminate the formation of tissue encapsulation but it also brings about a strong bond between the scaffold and host bone.

3. **Biodegradability**

The composition of the material, combined with the porous structure of the scaffold, should lead biodegradation *in vivo* at rates appropriate to tissue regeneration.

4. **Mechanical properties**

The mechanical strength of the scaffold, which is determined by both the properties of the biomaterial and the porous structure, should be sufficient to provide mechanical stability to constructs in load bearing sites prior to synthesis of new extracellular matrix by cells.

5. **Porous structure**

The scaffold should have an interconnected porous structure with porosity >60% and diameters >100 µm for cell penetration, tissue ingrowth and vascularisation, and nutrient delivery.

6. **Fabrication**

The material should possess desired fabrication capability, e.g., being readily produced into irregular shapes of scaffolds that match the defects in bone of individual patients.

7. **Commercialisation potential**

The synthesis of the material and fabrication of the scaffold should be suitable for commercialisation.

One major drawback in the design of tissue engineering scaffolds is that most materials are not simultaneously mechanically competent and bioresorbable, i.e., mechanically strong materials are usually bioinert, while degradable materials tend to be mechanically weak (Karageorgiou *et al.*, 2005). Hence, the fabrication of composites comprising biodegradable polymers and bioactive glass becomes a suitable option to fulfil the requirement of bioactivity, degradability and mechanical competence (Chen *et al.*, 2008).

2.3.2 Selection of biomaterials for scaffold fabrication

As mentioned earlier, one of the requirements of a scaffold is biocompatibility; hence, the materials used for the applications in bone regeneration must be compatible with the natural bone. Natural bone is composed of organic collagen and hydroxyapatite, therefore it is vital to mimic the bone components by using biomaterials that possess similar characteristics. Typically ceramics, synthetic and natural polymers are the preferred materials.

2.3.2.1 Bioceramics and bioactive glasses

2.3.2.1.1 Hydroxyapatite (HA) and Tri-calcium phosphate (TCP)

Due to their similarities in composition to bone ceramic scaffolds such as hydroxyapatite (HA) and tri-calcium phosphate (TCP) have been considered as scaffolds in bone regeneration applications. These scaffolds are typically characterized by high mechanical stiffness (Young's Modulus), very low elasticity and a hard brittle surface. From a bone perspective, they exhibit excellent biocompatibility due to their chemical and structural similarity to the mineral phase of native bone (O'Brien, 2011). The interactions of osteogenic cells with ceramics are important for bone regeneration as ceramics are known to enhance osteoblast differentiation and proliferation (Hench, 1998); (Ambrosio *et al.*, 2001). Unfortunately, the close similarity of hydroxyapatite to the mineral component of bone, which is stable in the body, results in lack of biodegradation of HA in the body,

which is generally an undesirable feature for tissue engineering scaffold materials (Chen *et al.*, 2008).

Bioactive glasses and glass-ceramics have also been used in bone repair applications and are being developed for tissue engineering application (Hench and Wilson, 1984); (Yamamuro *et al.*, 1990); (Hench, 1998),(Rahaman *et al.*, 2006). Bioactive glasses have an amorphous structure, whereas glass-ceramics are crystallized glasses consisting of a composite of a crystalline phase and a residual glassy phase (Rahaman *et al.*, 2011).

2.3.2.1.2 Silicate bioactive glasses

The bioactive glass designated 45S5 was the first original bioactive silicate glass discovered by Hench, (1973) which could bond to both hard and soft tissues. This glass is composed of oxides in the SiO_2-Na_2O-CaO-P_2O_5 system. A silicate glass is based on the three dimensional (3D) glass-forming SiO_2 network in which Si is fourfold coordinated to O (Figure 2.8).

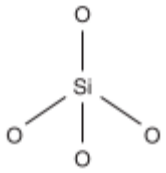

Figure 2-8: Tetrahedral unit of a silicate

They key compositional features that are responsible for the bioactivity of 45S5 glass are its low SiO_2 content (when compared to more chemically durable silicate glasses), high Na_2O and CaO (glass network modifiers) content and high CaO/P_2O_5 ratio.

Furthermore, silicate glasses with compositions in the system SiO_2-Na_2O-CaO-P_2O_5 offer remarkable advantages due to their high bioactivity index (Class A), and their ability to bond to both soft and hard tissues (Hench, 1998). Class A materials are osteogenic and osteoconductive while Class B bioactive materials (such as HA) exhibit only osteoconductivity. Despite their excellent properties, glasses in this system, particularly bioglass® 45S5, has been found to crystallize rapidly during thermal treatment. This behaviour is caused by the small processing window between

its glass transition and the onset of crystallization temperature which prevents sintering by viscous flow of particles, which often results in the glass network not reaching its optimum densification. In order to sinter a glass by viscous flow sintering, the temperature must be well above T_g but below T_c onset. Bioactive glasses strongly exhibit surface nucleation crystallization and viscous flow sintering will be dramatically reduced if the glass crystallizes (Massera *et al.*, 2012); (Fagerlund *et al.*, 2012a). This often leads to scaffolds with a low strength (Chen *et al.*, 2006b). Additionally this makes it quite difficult to process 45S5 glass into porous 3D scaffolds. Porous bioactive glass scaffolds are generally prepared by various techniques which all incorporate heating (sintering) the glass particles to bond the particles into a strong glass phase containing an interpenetrating network of pores (Rahaman *et al.*, 2011).

While devitrification does not inhibit the ability of 45S5 glass to form an HA-like surface layer, it has the effect of reducing the rate of conversion to HA, (Filho *et al.*, 1996). Another limitation of 45S5 glass is its slow degradation rate and conversion to an HA-like material (Huang *et al.*, 2006a); (Huang *et al.*, 2006b) as this makes it difficult to match the degradation rate of the scaffold with the rate of new tissue formation (Rahaman *et al.*, 2011). This is a vital characteristic of any bioactive scaffold to prevent any undesirable conditions during in vivo.

For this reason, various compositions have been developed to control the crystallization tendencies of bioactive glasses. Network formers and modifiers such as B_2O_3, K_2O, MgO, SrO etc. have been introduced into the SiO_2-Na_2O-CaO-P_2O_5 over the years to control crystallization during thermal treatment as well as to enhance the bioactivity and mechanical properties of the glasses (Brink, 1997).

One such bioactive silicate glass is 13-93, which is based on the 45S5 composition, but with higher SiO_2 content and additional network modifiers such as K_2O and MgO when compared to 45S5. Table 2.7 shows the compositions of some of the most widely studied bioactive glasses. Another distinguishing feature of the composition is the low phosphorus content (Sriranganathan *et al.*, 2016). Studies by (O'Donnell *et al.*, 2009) have shown that with increasing phosphorus content there is a faster apatite formation and a smaller pH rise. This is advantageous as it maintains the stability of

the internal environment and there is an increased bioactivity. However, 13-93 degrades at a much slower rate than 45S5.

Table 2-8: Compositions of various bioactive glasses (Rahaman *et al.*, 2011)

Composition (wt. %)	45S5	13-93	6P53B	58S	70S30C	13-93B1	13-93B3	$P_{50}C_{35}N_{15}$
Na_2O	24.5	6.0	10.3	0	0	5.8	5.5	9.3
K_2O	0	12.0	2.8	0	0	11.7	11.1	0
MgO	0	5.0	10.2	0	0	4.9	4.6	0
CaO	24.5	20.0	18.0	32.6	28.6	19.5	18.5	19.7
SiO_2	45.0	53.0	52.7	58.2	71.4	34.4	0	0
P_2O_5	6.0	4.0	6.0	9.2	0	3.8	3.7	71.0
B_2O_3	0	0	0	0	0	19.9	56.6	0

When comparing the processing window of the two silicate glasses, 13-93 has a larger gap between the glass transition and the onset of crystallization than 45S5, hence, porous scaffolds can be created and sintered without enduring any crystallization during heating (sintering) (Fagerlund *et al.*, 2012b). Therefore, this makes it easier to turn 13-93 into scaffolds for implantation in vivo (Brown *et al.*, 2008). However, the huge processing window for 13-93 comes with a reduced bioactivity. (Watts *et al.*, 2010) showed the magnesium oxide extends the sintering window by inhibiting crystallization but the side effect is that it limits the bioactivity by reducing apatite formation.

Another silicate bioactive glass that has been widely studied in the past years is glass S53P4 developed by (Anderson *et al.*, 1990). It is commercially available as Bonalive® with a composition of $53SiO_2$-$23Na_2O$-$20CaO$-$4P_2O_5$ in wt. % and is mostly used in the form of granules (0.8-3.15mm) but it can also be used in the form of nonporous plates or discs in various shapes , (Gestel *et al.*, 2015) . The bioactivity of the silicate glasses in both 45S5 and S53P4 is related to their low silica content, which gives them a special reaction in biological solution, (Massera *et al.*, 2013) and are able to convert slowly to HA. For this reason, S53P4 has been used in various clinical applications such as bone cavity filling in orthopaedic and cranio-maxillofacial surgery (Kinnunen *et al.*, 2000), (Peltola *et al.*, 2006) . Additionally, S53P4 has shown the abilities to facilitate and stimulate bone formation and bone

defect healing and has an antibacterial effect in various applications (Jones, 2013). However, the conversion of S53P4 to HA is often incomplete when compared to 45S5.

To determine the crystallization mechanisms of glasses 45S5 and S53P4, a study was conducted by (Massera *et al.*, 2012). According to their findings, S53P4 has shown to have a preference for surface crystallization whereas 45S5 had a more complicated mechanism which could not be described by the Johnson-Mehl-Avrami model. This could explain why S53P4 cannot be hot-worked without enduring crystallization. In another study by (McAndrew *et al.*, 2013), S53P4 was used in the treatment of chronic osteomyelitis. According to (McAndrew *et al.*, 2013), this is a destructive bone lesion caused by infecting pathogenic organisms. To achieve these, three patients who had previously undergone multiple debridements and antimicrobial regimes with no success were chosen. All tests required the patients to go through debridement and sequestrectomy procedures which involved the insertion of S53P4 followed by antimicrobial regimes with the aim of isolating pathogens sensitivities. After a mean follow up of 17.3 months, they found that all haematological and biochemical parameters have returned to normal, pain has ceased and function has returned in affected limbs. Apart from these excellent results, there were no radiological evidence of osteomyelitis and S53P4 has integrated with the surrounding bone.

2.3.2.1.3 Borate bioactive glasses

Another class of bioactive glasses which have received much attention in recent years are the borate glasses, based on the composition of 13-93 but with SiO_2 completely or partially substituted by B_2O_3. Examples include 13-93B1 and 13-93B3 as shown in Table 2.7. Due to their lower chemical durability, some borate bioactive glasses are able to degrade faster and convert more completely to an HA-like material, when compared to silicate 45S5 or 13-93 (Huang *et al.*, 2006a); (Huang *et al.*, 2006b), (Yao *et al.*, 2007); (Fu *et al.*, 2010a). The conversion of borate bioactive glass to HA appear to follow a process similar to that described for 45S5 glass, but without the formation of SiO_2-rich layer (Huang *et al.*, 2006a); (Huang *et al.*, 2006b). Unfortunately, there is a concern associated with borate bioactive glasses which is the toxicity of boron released into the solution as borate ions, $(BO_3)^{3-}$ (Rahaman *et al.*, 2011) .

Scaffolds of a borate bioactive glass, designated 13-93B3, with a composition obtained by replacing all the SiO_2 in 13-93 glass (Table 2.7) were found to be toxic to murine MLO-A5 osteogenic cells in vitro (Fu *et al.*, 2010b). However, when the same scaffold were treated in vivo, they did not show any toxicity to cells and supported new tissue infiltration implanted subcutaneously in rats (Fu *et al.*, 2010b).

Recent work has shown the ability to control the degradation rate of bioactive glass by manipulating its composition (Rahaman *et al.*, 2011). For example, by partially replacing the SiO_2 in silicate 45S5 or 13-93 glass with B_2O_3 (yielding a borosilicate bioactive glass), or fully replacing the SiO_2 with B_2O_3 (producing a borate glass), the degradation rate can be varied over a wide range (Huang *et al.*, 2006a); (Huang *et al.*, 2006b), (Yao *et al.*, 2007). However, it should be noted that the bioactivity of any glass depends on its composition; therefore, it is essential to avoid drastic changes to the glass composition to ensure that the glass degradation and bone regeneration rate still matches.

2.3.2.1.4 Phosphate bioactive glasses

Apart from silicate glasses which are well recognised for their applications in bone regeneration, phosphate glasses in the P_2O_5-CaO-Na_2O system have been found to be potential replacement of silicate glasses as they are not only good alternative in bone repair and reconstruction (Massera *et al.*, 2015a) and their compositions can be tailored to possess low melting temperature, high concentrations of rare and other metal ions (Gapontsev *et al.*, 1982);(Ahmed *et al.*, 2011). Phosphate glasses are recognised for their high solubility in aqueous media giving them the potential of being used as resorbable materials. In addition, phosphate glasses have also proved to be simple, easy to produce, biodegradable and biocompatible with many human connective tissues (Elwan *et al.*, 2014). Phosphates are common in nature because phosphorus also has an affinity to oxygen. Their tetrahedral unit, PO_4, is shown in Figure 2.9.

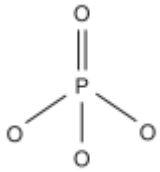

Figure 2-9: Tetrahedral unit of a phosphate

The PO_4 unit is distinguished from the SiO_4 unit by the double bond which results from the oxygen atoms that are not shared between the phosphates tetrahedral but are shared by the two unpaired electrons with the P^{5+} ions (Neel *et al.*, 2009). Additionally, when comparing vitreous phosphorus to silica, vitreous phosphorus tends to be chemically unstable however, the addition of modifying oxides does not disrupt the glass network as it does with the silica but, interestingly improves its stability (Neel *et al.*, 2009). This is due to the P-O-M^+ (when M = metal cation) bonds which are generally more stable towards atmospheric hydrolysis in contrast to the hydrolysis of P-O-P alone (Bae *et al.*, 1991). This led to the incorporation of modifying oxides such as SrO to the P_2O_5-CaO-Na_2O system to substitute CaO. Not only is Sr a naturally occurring trace element in the body (Isaac *et al.*, 2011), but it often acts similarly to Ca in the human body; both have strong bone-seeking properties, and Sr can be substituted with Ca in the apatitic phase of bone mineral (Vaughan, 1981). This is also attributed by the fact that, they are both network modifier and have similar coordination number; hence, they are expected to have the same effect in the glass structure (Massera *et al.*, 2013).

Studies have been carried out to demonstrate the behaviour of bioactive glasses in the SiO_2-Na_2O-CaO-P_2O_5 and P_2O_5-CaO-Na_2O systems by substituting SiO_2 and CaO contents with B_2O_3 and SrO, respectively.

The substitution of CaO with SrO was due to its beneficial effects on bone healing. For example, strontium renelate has proved to be an effective treatment against osteoporosis in postmenopausal women, acting via a mechanism combining the inhibition of bone resorption within the simulation of new bone tissue formation. Evidence has also shown that strontium is able to inhibit osteoclast differentiation (Santocildes-romero *et al.*, 2015) and can have a positive impact on preventing caries (Curzon, 1985). Additionally strontium is the only known element which can correlate to an increase in bone compression strength. A few studies have reported the effects of strontium-substituted bioactive glasses. Goel *et al.*, (2011) reported that up to 10 mol. % of SrO substituted for CaO decreased significantly the apatite forming ability. However, (Fredholm *et al.*, 2012) demonstrated that full substitution of SrO for CaO allows for enhanced apatite formation.

In a recent study by (Massera *et al.*, 2015b) to investigate the influence of SrO and CaO in silicate and phosphate bioactive glasses on human gingival fibroblasts; SrO was added to both silicate and phosphate glasses with nominal compositions of $53.85SiO_2$-$22.66Na_2O$-$1.72P_2O_5$-(21.77-x) CaO-xSrO with x ranging from 0 to 10 and; $50P_2O_5$-$10Na_2O$-(40-x) CaO-xSrO where x varied from 0 to 40; respectively. These glasses were immersed in the culture medium with and without cells and their behaviour in the cell culture was correlated to their SrO content. From their finding; SrO gave a faster initial dissolution in the cell culture medium for the silicate glasses. This is attributed by the expansion of the network as a result of SrO. Additionally, the formation of hydroxyapatite layer started earlier for the SrO-containing glasses in comparison to the SrO-free glasses. Consequently, the SrO-containing silicate glass led to a slight enhancement in the activity of the gingival fibroblasts cells when compared to the SrO-free reference glass, S53P4.

In contrast to the silicate glasses, SrO was found to decrease the dissolution process in the phosphate glasses as a result of a more cross linked network. The mass loss for the SrO-free glass was much greater than for the SrO-containing glasses. Although the SrO-free phosphate glass had a fast dissolution, it did not provide a good substrate for the CaP surface to attach. As a result, the human gingival cells to, did not attach to and proliferate at the SrO-free glass. This results shows that strontium does indeed have bone healing abilities.

Meanwhile, the B_2O_3-containing bioactive glasses have also attracted much interest in the past years for potential biomedical applications in tissue engineering as scaffold materials due to their low chemical durability, faster and ease to completely convert to hydroxyapatite when they are immersed in simulated body fluid (Day *et al.*, 2003). In addition, it has also been shown that the ratio between tetrahedral and trigonal boron species can influence the mechanical strength of a glass system owing to the fact that boron speciation plays a dominant role in controlling the fragility of the samples (Ciceo *et al.*, 2014); (Zheng *et al.*, 2012).

In addition, several studies were conducted on the replacement of SiO_2 with B_2O_3. The first investigation on the replacement of SiO_2 with B_2O_3 was conducted by (Richard, 2000) on the 45S5B1 borate glass and found that the apatite (HA) layer formed more rapidly on the borate glass than on the 45S5 glass when the glasses were

immersed in dilute K_2HPO_4 solution at 37°C. Similar observations were made by (Huang *et al.*, 2006a), they found that when the B_2O_3 content of the glass was increased, the conversion rate to HA was faster.

2.3.2.2 Synthetic and Natural polymers

A great deal of research effort has gone into developing synthetic polymers as tissue engineering scaffolds; such polymers include poly-l-lactic acid (PLLA), polyglycolic acid (PGA) and poly-dl-lactic-co-glycolic acid (PLGA). These materials have shown much success as they can be easily processed into desired configuration and their physical, chemical, mechanical, and degradative properties can be engineered to fit a particular need (Lu *et al.*, 2000). However, one main concern for the use of these polymers in bone tissue engineering is that their intermediate degradation products (specifically, lactic acid and/or glycolic acid) by non-enzymatic hydrolysis of ester bonds in their backbone reduces the local pH, which in turn induces an inflammatory reaction and damages the bone cell at the implant site. Moreover, the rapid drop of pH in vivo may accelerate the polymer's degradation rate, thus, resulting in premature loss of mechanical properties before new bone formation occurs (Liu and Webster, 2006).

Natural polymers have also been used as scaffold biomaterials. Natural polymers such as collagen, alginate and chitosan have all been used in the production of scaffold for tissue engineering. In comparison to synthetic polymer-based scaffolds, natural polymers are biologically active and typically promote excellent cell adhesion and growth. In addition, they are also biodegradable and allow host cells, over time, to produce their own extracellular matrix and replace the degraded scaffold. Despite that, fabricating scaffolds from biological materials with homogenous and reproducible structure presents a challenge. Also, the scaffolds generally have poor mechanical properties, which limit their use in, for example, load bearing orthopaedic applications (O'Brien, 2011).

2.5 Mechanical properties of scaffolds for tissue engineering

The clinical use of bioactive glasses particularly in load-bearing applications has been limited by their low fracture toughness and mechanical strength, especially in porous form (Rezwan *et al.*, 2006). Currently, there is no clear design criteria for the

mechanical properties of scaffolds intended for bone repair, particularly those to be used in load-bearing defects (Fu *et al.*, 2011). However, it is often stated that the scaffold should mimic the morphology, structure and function of bone in order to optimize integration with surrounding tissues (Hutmacher, 2000). The variability in the architecture and mechanical properties of bone, coupled with differences in age, nutritional state, activity (mechanical loading) and disease status of individuals, provide a major challenge in the design and fabrication of scaffolds for specific defect sites (Fu *et al.*, 2011), although it is required that the scaffold should also be able to withstand stress induced during implantation. Bone is structurally classified into two parts: cortical bone also referred to as compact bone and trabecular bone, also referred to as cancellous or spongy bone. The mechanical properties of bone vary between subjects, from one bone to another and within different regions of the same bone (Rahaman *et al.*, 2011). Table 2.9 summarises mechanical properties of both trabecular and cortical bones.

Table 2-9: Mechanical properties of human bone

	Compression strength (MPa)	**Flexural strength (MPa)**	**Tensile strength (MPa)**	**Modulus (GPa)**	**Fracture toughness ($MPa.m^{1/2}$)**	**Porosity (%)**
Cortical bone	100-150	135-193	50-151	10-20	2-12	5-10
Cancellous bone	2-12	10-20	1-5	0.1-5	0.1-0.8	50-90

The mechanical properties of porous scaffolds depend on the composition of the biomaterial, microstructure and the fabrication technique. Table 8 presents the compressive strength of some of the most widely studied glass compositions along with the fabrication methods. From the results, bioactive glass scaffolds prepared by methods such as polymer foam replication, gel-casting and sintering of particles or short fiber typically have strengths comparable to that of human trabecular bone. Meanwhile scaffolds prepared from methods such as rapid prototyping and unidirectional freezing of suspensions have resulted in the creation of porous bioactive glass scaffolds with compressive strength and elastic modulus which are

comparable to, or approach the values for, human cortical bone. These scaffolds have potential in the regeneration of load-bearing bones (Rahaman *et al.*, 2011).

With this said, researches have conducted numerous work to improve the mechanical properties of glass based scaffolds. However, it is still known that the mechanical strength of these scaffolds decrease with porosity. (Liu *et al.*, 2009) conducted a study on the improvement on the strength of bioactive borosilicate glass scaffolds for tissue engineering which were fabricated using the foam replication method and with pore sizes ranging between 200-500 µm. The compressive strength of the scaffolds had been found to increase with a decrease in porosity. The parameters of the scaffolds are summarized in Table 2.10

Table 2-10: Parameters of scaffolds

Sample	**Solid content (wt. %)**	**Compressive strength of scaffolds (MPa)**	**Porosity of scaffolds (%)**
1	56.8	0.8±0.2	86.7±2.2
2	62.2	1.5±0.4	80.4±3.1
3	66.4	4.6±0.8	73.3±2.8
4	71.1	9.7±1.3	67.7±2.6

A similar trend was observed by (Locs *et al.*, 2013), they prepared porous ceramics by viscous slurry foaming using hydroxyapatite powder and ammonium hydrogen carbonate as the foaming agent for the generation of pores in the glycerol-based viscous ceramic slurry. The compressive strength of the porous ceramics was also found to decrease as a function of porosity. The results are shown in Figure 2.10.

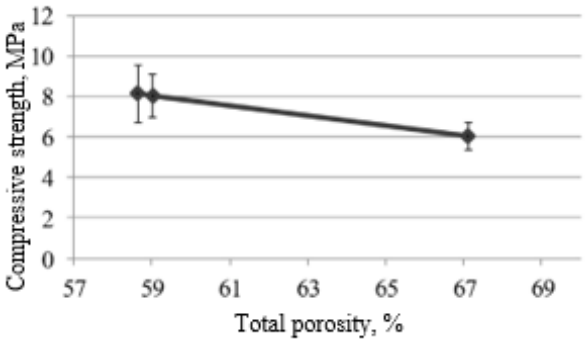

Figure 2-5: Compressive strength as a function of porosity (*Locs et al., 2013*)

Scaffolds for tissue engineering are commonly constructed from biodegradable polymers natural or synthetic (Hayashi, 1994), (Griffith, 2000) yet, the mechanical response of bone is not matched by these polymers. However, for the regeneration of load-bearing bones, the use of biodegradable polymer scaffold is challenging because of their low mechanical strength. Therefore, attempts have been made to reinforce the polymers with a biocompatible inorganic phase, commonly (HA), (Thomson *et al.*, 1998);(Rezwan *et al.*, 2006). Although brittle, scaffolds fabricated from inorganic materials such as calcium phosphate-based bioceramics and bioactive glass can provide higher mechanical strength than polymeric scaffolds.

2.6 Clinical Applications of Bioceramics

Due to their brittleness, difficulty of shaping for implantation and the inability of new bone to sustain the mechanical loading needed for remodelling (Wang, 2003), bioceramics have limitations in certain clinical applications such as load-bearing situations. However, bioceramics still found use in applications such as dental surgery to fill bone defects and orthopaedic surgery to coat metallic implant surfaces to improve implant integration with the host bone.

One of the most commonly used biomaterial in orthopaedic coating is synthetic hydroxyapatite (sHA) which is deposited on the surface through the plasma-spray method. This process uses a source material of sHA, the plasma-sprayed coatings are not pure but a mixture of crystalline calcium phosphates, of which approximately 95% is sHA, and an amorphous calcium phosphate (Tisdel *et al.*, 1994). The presence of the amorphous phase increases the degradation rate of the material (Gross *et al.*, 1998). Although sHA has excellent biocompatibility and osetconductivity, it does not

resorb in the body and therefore it will not fulfil the criteria of an ideal tissue scaffold (Jones, 2007a). However, a successful porous sHA product is Apapore® (Apatech Ltd, Elstree, UK), which is a porous HA that has an interconnected macroporosity and some microporosity. Jones, (2007a) reported that it has been successfully used in impaction grafting for the cemented revision of failed total joint athroplasties, spinal fusions and bone defect treatment.

Another commercial biomaterial that has been accepted in clinical applications is HA (Legeros, 2002). A porous bovine bone-derived HA graft is marketed under the name Bio-Oss® (Osteohealth Shirley, New York), which is an unsintered material and therefore has some resorbability in vivo (Valentini *et al.*, 2000) and osteograft-N™ (CeraMed Co, Denver, CO) and Endobon™ (Merch CO, Darmstadt, Germany), which are sintered material.

Bioactive glasses were the first biomaterials used in clinical applications. The first bioglass device was used in a middle ear surgery to treat conductive hearing loss by replacing the bones of the middle ear (Hench, 2006). The device was named the Bioglass® Ossicular Reconstruction Prothesis' and trade named' MEP®. This device offered an advantage over other devices that were in use at the time due to its ability to bond to soft tissue (tympanic membrane) as well as bone tissue.

The second bioglass device which was accepted in clinical applications was Endosseus Ridge Maintanence Implant (ERMI®) which was designed to support labial and lingual plates in both natural tooth roots and to provide a more stable ridge for denture construction following tooth extraction (Hench, 2006). These devices were simple ones of 45S5 bioglass® that were placed into fresh tooth extraction sites. They bonded to the bone tissue and proved to be extremely stable, with much lower failure rates than other materials that had been used for that same purpose. Some of the current applications of Bioceramics are summarized in Table 2.11. However, up to date, there have been no reports on the clinical application of porous bioglass devices.

Table 2-11: Current uses of Bioceramics in various clinical applications (Hench, 1998)

Applications	**Bioceramics**
Orthopedic load-bearing applications	Al_2O_3
	Stabilized zirconia
	PE-HA composite
Coatings for chemical bonding (orthopedic; dental; and maxillofacial prosthetics)	HA
	Bioactive glasses
	Bioactive glass-ceramics
Dental implants	Al_2O_3
	HA
	Bioactive glasses
Alveolar ridge augmentations	Al_2O_3
	HA
	HA-autogenous bone composite
	HA-PLA composite
	Bioactive glasses
Otolaryngological	Al_2O_3
	HA
	Bioactive glasses
	Bioactive glass-ceramics
Artificial tendon and ligament	PLA-carbon-fiber composite
Artificial heart valves	Pyrolytic carbon coatings
Coatings for tissue growth (cardiovascular;	

orthopedic; dental; and maxillofacial prosthetics	Al_2O_3
Temporary bone space fillers	TCP
	Calcium and phosphate salts
Periodontal pocket obliteration	HA
	HA-PLA composite
	TCP
	Calcium and phosphate salts
	Bioactive glasses
Maxillofacial reconstruction	Al_2O_3
	HA
	HA-PLA composite
	Bioactive glasses
Percutaneous access devices	Bioactive glass-ceramics
	Bioactive glasses
	HA
Orthopedic fixation devices	PLA-carbon fibers
	PLA-calcium phosphate-based glass fibers
Spinal surgery	Bioactive glass-ceramic
	HA

CHAPTER 3: METHODOLOGY

This chapter of the dissertation discusses the experimental procedures used to achieve the objectives of the project. Various experiments were performed to determine the optimum conditions at which the glasses could be sintered without or with minor crystallization as well as achieve the required porosity for scaffold use. These optimum conditions were dependent on the following factors; sintering temperature, holding time, heating rate, volume content of NH_4 (HCO_3) used in this dissertation as foaming agent. The work in this project was done in four stages which involved sintering with and without NH_4 (HCO_3), followed by biocompatibility tests and mechanical tests.

3.1 Materials and chemicals

The materials that were required for the successful completion of this project are listed in Table 3.1 and Table 3.2 below. The Tables also include the suppliers from which the materials were obtained.

Table 3-1: Supplier of all glass materials used in this project

Glass name	Chemical composition	Supplier
S53B50	$26.93SiO_2$-$26.93B_2O_3$-$22.66Na_2O$-$1.72P_2O_5$-21.77CaO	Tampere University of Technology, Finland
P40B10	$40P_2O_5$-$10B_2O_3$-20CaO-20SrO-$10Na_2O$	
Sr	50 P_2O_5-20SrO-$10Na_2O$	

Table 3-2: Supplier of all chemicals used in this project

Material	Supplier
Ammonium bicarbonate $NH_4(CO_3)$	Sigma Aldrich (Pty) Ltd.
PEG	Sigma Aldrich (Pty) Ltd.
Dolapix CE 64	Zchimmer and Schwarz, GmbH & Co KG, chemischefabriken. Lahnstein, Germany

3.2 Glass and powder preparation

3.2.1 Synthesis

The starting materials for the borosilicate glass designated S53B50 were analytical reagent grades of Na_2CO_3, H_3BO_3, CaCO3, $CaHPO_4.2H_2O$ and 99.4% pure SiO_2, while the borophosphate and phosphate glasses designated P40B10 and Sr respectively were prepared using $NaPO_3$, H_3BO_3, $SrCO_3$, $CaCO_3$ and $(NH_4)_2HPO_4$ as raw materials. $Ca(PO_3)_2$ and $Sr(PO_3)_2$ were used as precursors for the phosphate glasses and were prepared independently using a slow heating rate up to 900°C.

The three nominal glass compositions studied are given in Table 3.3. Glass S53B50 had a nominal oxide composition of $26.93SiO_2$-$26.93B_2O_3$-$22.66Na_2O$-$1.72P_2O_5$-21.77CaO, while glass P40B10 and Sr had a nominal composition of (50-x) P_2O_5-xB_2O_3-20CaO-20SrO-$10Na_2O$; where x = 0 (Sr) or 10 (P40B10). Proportions of relevant oxides of the starting materials were mixed together in a platinum crucible and melted at 1250°C for glass S53B50 and 1100°C for glass P40B10 and Sr for 1 hour. The melt was poured onto a graphite mould and annealed at 40°C below their respective T_g to release internal stresses; and allowed to slowly cool down to room temperature in the annealing furnace. The obtained glass ingots were then crushed using a metallic mortar and pestle for 1 hour and sieved.

Table 3-3: Composition of S53B50, P40B10 and Sr glasses presented in (mol. %)

Composition (mol. %)	**S53B50**	**P40B10**	**Sr**
SiO_2	26.93	0	0
Na_2O	22.66	10	10
CaO	21.77	20	0
B_2O_3	26.93	10	0
P_2O_5	1.72	40	50
SrO	0	20	40

3.2.2 Milling

The crushed powders were charged in a tungsten carbide grinding bowl (76 mm) and milled in a planetary ball mill (Fritsch Pulverisette 6) using alumina balls (2 mm diameter) for 1 hour at 150 rpm, with distilled water as a grinding media. The charge to ball ratio was kept at 1:1. Dolapix C64 and PEG (polyethylene glycol) were added at 3 wt. % to the mixture as a dispersant and binder respectively. In this mill operation, the grinding balls and material in the grinding bowl were acted upon by the centrifugal forces due to the rotation of the grinding bowl about its own axis and the rotating supporting disc. The grinding bowl and the supporting disc rotate in opposite directions (shown in Figure 3.1) and this results in (1) a frictional effect, were the grinding balls run along the inner wall of the grinding bowl and (2) an impact effect, were the balls impact against the opposite wall of the grinding bowl (Operating Instructions Planetary Mono Mill pulverisette 6, n.d.)

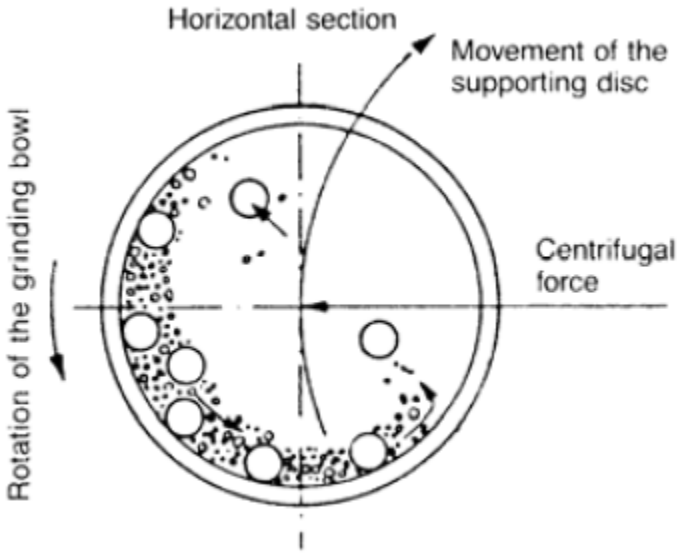

Figure 3-1: Milling mechanism if the planetary ball mill (Operating Instructions Planetary Mono Mill pulverisette 6, n.d.)

3.2.3 Drying and sieving powder

After milling, the powders were dried in the Ecotherm economy labotec oven at 70°C for 24 hours. Once the powders were completely dry, the cake formed during drying was granulated using a porcelain mortar and pestle prior to sieving. The powders were then passed through a 106 µm Retsch® stainless steel sieve using a Retsch® AS-200 control "G" sieve shaker. This stage was essential as it allows for better green

compacts and enables the powder to flow appropriately during the sintering process as the large agglomerates have been removed.

3.2.4 Mixing and Compaction of powders

To ensure that the $NH_4(HCO_3)$ foaming agent was evenly distributed into the glass powders, a dry mixing route was implemented. The equipment used for this was the Turbula T2F mixer Willy A, Bachofen, AG. The $NH_4(HCO_3)$ foaming agent and glass powder mixtures were prepared by mixing 2 grams which were rotated in the Turbula unit at a speed of 96 rpm for 30 minutes where 12 alumina milling balls (2 mm) were used to aid in the homogenization . The $NH_4(HCO_3)$ foaming agent was added at a content of 60 vol. % and 70 vol. %.

A hydraulic press is a device used to crush or press/compact samples in a piston-cylinder arrangement by applying a load. In this study the powders were pressed using a hydraulic press (Tinius Olsen, DBBSTOL-50kN, AP32092) at a pressure of 19.63MPa to produce pellets of 18.01mm diameter and 4 mm thick using a displacement range of 5 mm.

3.3 Sintering

3.3.1 Sintering with and without $NH_4(HCO_3)$

In order to determine the sintering behaviour and produce porous bioactive glass scaffolds, the samples were sintered with and without $NH_4(HCO_3)$ foaming agent, respectively. The samples prepared without $NH_4(HCO_3)$ were sintered using a heating rate of 10ºC/min and sintering temperatures ranging between 480ºC and 600ºC and at a holding time of 2 hours. The samples with $NH_4(HCO_3)$ were sintered for 1 hour at 540ºC for S53B50 and 500ºC for P40B10 and Sr after burning off the $NH_4(HCO_3)$ foaming agent at 67ºC for 2 hours. All the samples were sintered in a Muffle furnace in air (Elite Thermal system BRF 18/5E-2416+2116). Cooling was achieved by switching off the furnace immediately after the sintering time.

3.4 In vitro bioactivity

To assess the *in vitro* bioactivity of the scaffolds, they were immersed in simulated body fluid (SBF) solution at 37°C as proposed by Kokubo *et al.*, (1990). The SBF solution mimics the ionic composition of the blood plasma and the ion concentrations

of the solutions are summarized in Table 3.4. The simulated body fluid was prepared using 7.996g NaCl, 350 mg $NaHCO_3$, 224 mg KCl, 228 mg $K_2HPO_4 \cdot 3H_2O$, 305 $MgCl_2 \cdot 6H_2O$, 40 ml 1M HCl acid, 368 mg $CaCl_2 \cdot 2H_2O$, 71 mg Na_2SO_4 and 6.057 g tris (hydroxymethyl) amino methane, $(CH_2OH)_3CNH_2$, (Tris) per litre SBF using deionized water. The pH was adjusted to 7.40 using 1 N hydrochloric acid with the aid of a pH meter.

Table 3-4: Comparison of the ion concentration of SBF K9 with those of blood plasma (Kokubo *et al.*, 1990)

	Concentration mM	
	SBF K9	**Blood Plasma**
Na^+	142.0	142.0
K^+	5.0	5.0
Mg^{2+}	1.5	1.5
Ca^{2+}	2.5	2.5
Cl^-	147.8	103.0
$(HCO_3)^-$	4.2	27.0
$(HPO_4)^{2-}$	1.0	1.0
SO_4^{2-}	0.5	0.5

The mass of sample to volume of SBF ratio (1 m1/40mg) was kept constant for all the experiments. About 19-25 ml SBF was measured into 50 ml PP conical tubes and 900-1070 mg of scaffolds were dispersed in the solution for 24, 48, 72 and 168 hours at 37°C in an incubating shaker (HT Infors Multitron) at an agitation speed of 100 rpm. The experiments were conducted in duplicate. At the end of each time period, the change in the solution pH was measured and 5 ml were removed from the solution which were then diluted with deionised water. About15 ml was measured into a 15 ml PP conical tube and stored at 4°C for inductively coupled Plasma-Optical emission spectroscopy analysis. After testing, the scaffolds were removed from the solution, rinsed with ethanol to stop any further reaction, dried at 37°C and the weight loss was measured.

3.5 Characterization techniques

3.5.1 Particle size measurements

Particle size analysis was carried out on the powders after milling. This was done to establish the particles sizes of the powders that were required for sintering. A Mastersizer 2000 (Malvern Instruments, Germany) was used to measure the particle size distribution of the powders. This equipment makes use of light scattering patterns, which are produced by passing particles through a focused laser beam. Small particles scatter light at large angles whereas the large particles scatter light at small angles. The patterns that are produced are then analysed using the Fraunhofer model in order to calculate the size of the particles producing the relative scattering patterns (Malvern: Mastersizer 2000- Integrated systems for particle sizing, 2005).

3.5.2 Thermal Properties

The thermal properties of the glasses were determined using differential thermal analyses (SDTA, Netzch F1 JUPITER^{e}) at a heating rate of 10°C/min for particle size of 125-250 µm. The measurements were performed on 30 mg samples in platinum pans in N_2 atmosphere. The glass transition temperature T_g was taken at the inflection point of the first endotherm, obtained by taking the first derivative of the DTA curve. The onset of crystallization T_c and the crystallization temperature T_p were found at the onset and maximum of the exothermic peak; respectively.

3.5.3 Density measurements

Due to the different structures of the samples prepared with and without $NH_4(HCO_3)$ two separate methods were used to determine the density of the samples, respectively. The density of the samples sintered with $NH_4(HCO_3)$ was determined using the geometric density and not Archimedes Principle due to the fact the some gas bubbles; voids and pores cannot be accessed by water. Whereas the density of the samples prepared with $NH_4(HCO_3)$ was determined using Archimedes Principle.

3.5.3.1 Density of samples sintered with $NH_4(HCO_3)$

The density of the samples was determined using Archimedes principle. Firstly, the samples were immersed in distilled water (in a beaker) and then boiled for 3 hours, using a hot plate, in order to displace air from the pores in the sample. The thickness of the sintered samples was about 4 mm, therefore it was decided that 3 hours of

boiling is enough. After boiling the samples were cooled down to ambient temperature.

The density of the material was calculated by first determining the mass of the water impregnated sample, i.e. suspended in water mass (m_s). The sample is then removed from the water and dried lightly on the surface using a paper towel to remove excess water from the surface, and the water saturated mass (m_w) is then determined. Finally, the dry mass (m_d) of the sample was measured after the sample had been dried in an oven for 24hours, and then cooled to ambient temperature. For accuracy each mass was determined five times in order to calculate a mean value which was then used to determine the density (ρ_s) and the porosity (P_o) of the samples. The equation used to determine the density of the sample is given in equation 3.3 and the porosity in equation 3.4

$$\rho_s = \frac{m_d \rho_{water}}{m_{w-m_s}} \quad 3.3$$

$$P_o = \left(\frac{m_{w-} m_d}{m_{w-} m_s}\right) x\ 100 \quad 3.4$$

3.5.3.2 Density of samples sintered without $NH_4(HCO_3)$

To calculate the density of the porous scaffolds, a micrometre screw gauge was used. In principle, the samples were placed between the end of the screw and the stud. The measurements were taken by adding the readings on the pitch scale and the circular scale. The additional 0.5 mm from the subdivision was only added when there was an extra line below the datum line.

Density ρ of any substance is defined as the mass *m* of a unit volume of that substance given below:

$$\rho = \frac{m}{V} \quad 3.1$$

The volume of the samples was calculated using the equation below:

$$V = \pi r^2 h \quad 3.2$$

Where;

r = radius obtained from the measured diameter $\left(\frac{D}{2}\right)$ of the samples

h = measured thickness of the samples

The mass of the samples was weighed using a balance scale

3.5.4 Cutting the sintered samples

After the densities of the samples had been determined, they were cut in half in order to examine their cross sections. This was done using a Struers Secotom-10 precision cut-off machine and a Struers diamond cut off wheel with a 12 cm diameter. The speed used for the cutting wheel was 3500 rpm and the sample was fed at a rate of 0,025 mm/s.

3.5.5 XRD analysis of powder and sintered samples

A Bruker D2 Phaser XRD analysis instrument was used to examine the presence of any crystalline phases formed during the powder preparation stage as well as after sintering and immersion in simulated body fluid (SBF). The D2 Phaser uses Co kα radiation produced at 30kV and 10mA. Measurements were taken under the following conditions: 2θ value ranging from 10° - 90° 2θ with a step sizes of 0.02° (2θ). After the completion of the XRD scans, the phases present were then identified by using the DIFFRAC.EVA 4.0 software.

3.5.6 SEM analysis of powder and sintered samples

The morphology of the starting powders was investigated using a FEI Quanta 400 FEG SEM. A small amount of the powder was carefully placed onto a graphite tape which was attached to a stub. To improve the conductivity of the powders and that of the sintered samples, they were further coated with gold and palladium. Images were taken at various magnifications in order to confirm the chemical composition of the powder.

The sintered samples were not mounted nor polished to prevent the polyfast from clogging the pores on the cut surface. The samples made with 60 and 70 vol. % $NH_4(HCO_3)$ foaming agent addition were both analysed using SEM to examine the homogeneity of the pore distribution in the samples as well as to confirm if a good

interconnection between pores was achieved. The samples sintered without any additive were also analysed to observe the influence of the sintering temperature on the crystallization.

3.6.7 ICP analysis

Inductively Coupled Plasma analysis was performed on immersion liquid diluted 10X except for the Sr scaffolds which were diluted 100X, due to the large amount of P present in them. Na was not quantified due to the high Na content in SBF leading to high inaccuracy. The emission lines used were 253.56 nm for P; 393,366 nm for Ca; 421.552 nm for Sr; 249.772 nm for B; and 251.611nm for Si.

3.5.8 Analysis of the porous scaffolds

The structural properties of the porous scaffolds were conducted using both Mercury Porosimetry and X-ray micro computed tomography. These techniques are used to determine the porosity, pore size and pore size distribution of porous materials

3.5.8.1 Mercury Porosimetry Intrusion

Mercury Porosimetry intrusion is a technique used to measure pore size, total porosity as well as pore size distribution. The scaffolds are loaded into a penetrometer, which consist of a sample cup connected to a metal-clad, precision-bore, and glass capillary stem. The penetrometer's cup and capillary stem are then infused with mercury. As pressure on the filled penetrometer increases mercury intrudes into the scaffold pores, beginning with pores of large diameter. The relation between the pressure (*P*) and the radius of the pores (*r*) that can be filled is given by Washburn's equation (Maspero *et al.*, 2001)

$$P = \frac{2\sigma \cos\theta}{r} \qquad 3.5$$

Where;

σ = surface tension mercury

θ = contact angle

The open porosity of (π) is given by

$$\pi = \frac{V_{intrusion}}{V_{scaffold}} \quad 3.6$$

Where;

π = open porosity

$V_{intrusion}$ = total intrusion volume of mercury

$V_{scaffold}$ = volume of the scaffold

In this study, the pore size distribution measurement was conducted using a (AutoPore IV 9500 V1.09, serial 833). The applied mercury pressure was 0.52 psi at an equilibration time of 10 seconds using an evacuation pressure and time of 50 µmHg and 30 minutes, respectively.

3.5.8.2 X-ray micro computed tomography

Micro computed tomography or microCT is a non-destructive technique used to examine internal structure of objects by creating a three-dimensional (3D) image using x-ray radiation. MicroCT equipment is composed of the following principle components: x-ray tube, radiation filters and collimator (which focuses the beam geometry to either a fan or cone-beam projection), specimen stand and a phosphor-detector/charge coupled device camera (Figure 3.2).

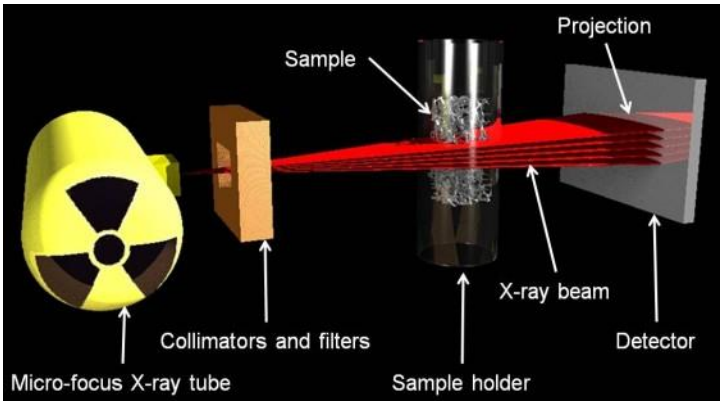

Figure 3-2: Principle components of a MicroCT scanner (Micro-Computed Tomography, 2016).

In principle, a micro-focus x-ray tube produces radiation which is collimated and illuminates the object being imaged. The radiation is attenuated by the object which is

then detected by a charge-coupled device (CCD) camera with a phosphor layer to convert x-ray to visible light. A three-dimensional (3D) image of the object is then created by scanning at different angles as the object rotates and by reconstructing the two-dimensional (2D) projections into a three-dimensional image (Micro-Computed Tomography, 2016).

In this study, the porosity analysis was conducted using micro-computational tomography (µCT). MicroXCT-400 (Carl Zeiss X-ray Microscopy, Inc., Pleasanton, USA) was used with tube voltage 140kV and current 71µA. Pixel size was 5.6 µm. Porosity analysis was done with Fiji using BoneJ plugin. µCT visualizations were done with Avizo 9.1 (FEI Visualization Sciences Group).

3.6 Mechanical properties

The compressive strength of the scaffolds (17 mm in diameter x 4 mm) as prepared and after immersion in the SBF for the selected durations, was measured using an Instron testing machine (Model 1175-K5942; Instron , Advanced laboratory solutions, SA) at a crosshead speed of 0.5 mm/min. For the scaffolds immersed in SBF, the compressive strength was measured after drying the scaffolds. Two samples were measured for each duration, and the mean strength and standard deviation were determined. Ten samples were used for the as prepared scaffolds.

CHAPTER 4: EXPERIMENTAL RESULTS

This chapter presents the results obtained from the synthesis of the borosilicate; borophosphate and phosphate bioactive glass; milling of the powders; mixing of the powders with NH4(HCO3); sintering of the powder; in vitro properties of the scaffolds in SBF; characterization of the as-sintered samples using XRD; ICP and SEM/EDS as well as the density and compressive strength.

4.1 Preparation of glass powders

The glass powder of the glasses under investigation was milled in a planetary ball mill as described in section 3.2.2. This produced the following particle size distributions with d_{10}, d_{50} and d_{90} values as presented in Table 4.1 and 4.2 for the glasses prepared with and without NH_4 (HCO_3), respectively. From the analyses it was observed that all glasses had a d_{50} less than 53 µm.

Table 4-1: Results obtained from the particle size analysis after milling for samples sintered without NH_4 (HCO_3)

Powder	d_{10} (µm)	d_{50} (µm)	d_{90} (µm)
S53B50	4.770	20.539	61.499
P40B10	4.928	18.369	47.636
Sr	6.460	26.365	78.221

Table 4-2: Results obtained from the particle size analysis after milling for samples sintered with NH_4 (HCO_3)

Powder	d_{10} (µm)	d_{50} (µm)	d_{90} (µm)
S53B50	7.788	39.899	102.310
P40B10	9.131	32.769	83.304
Sr	11.982	46.258	102.413

Figure 4-1 and 4-2 shows the XRD analysis of the glass powders after milling. The diffraction pattern showed the commonly observed hollow broad band; which is a

typical characteristic of any amorphous material and free of any significant crystalline phases.

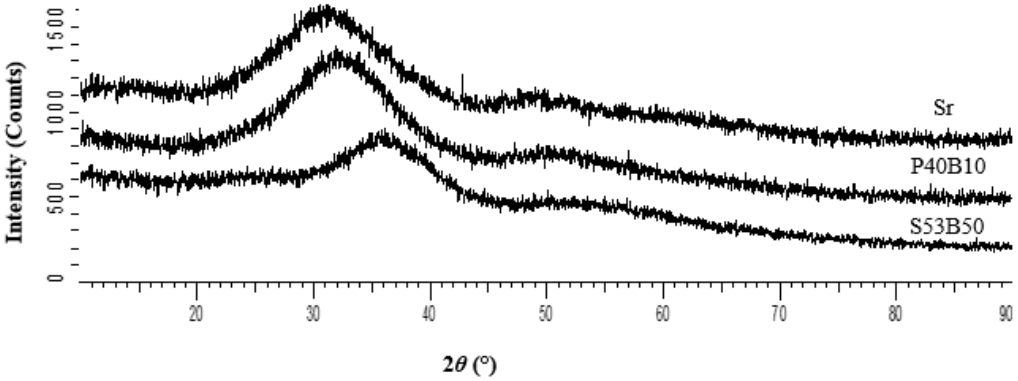

Figure 4-1: X-ray diffraction patterns of S53B50, P40B10 and Sr bioactive glasses after milling presented in Table 4-1

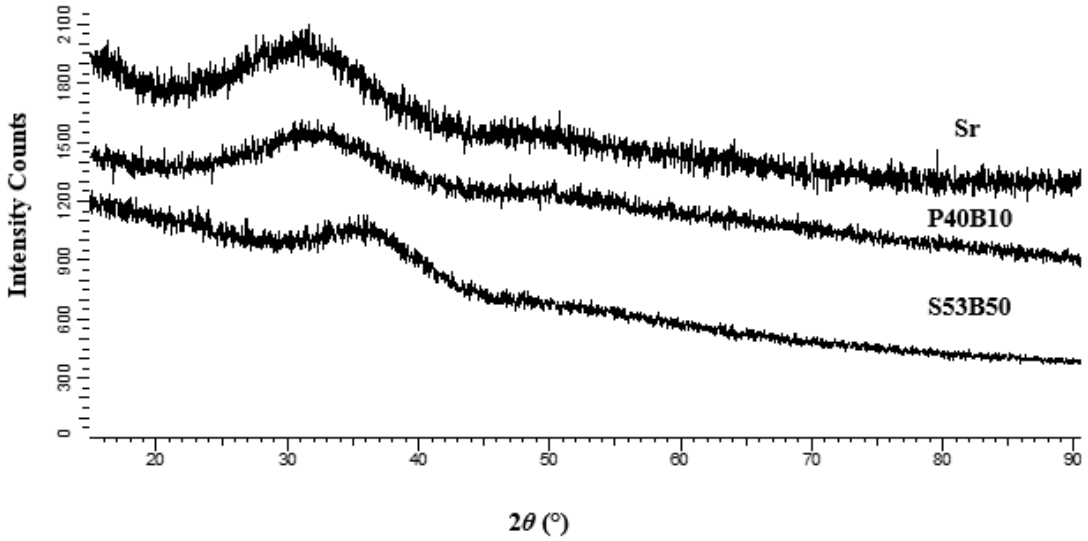

Figure 4-2: X-ray diffraction patterns of S53B50, P40B10 and Sr bioactive glasses after milling presented in Table 4-2

It was also observed that the amorphous peak shifted to lower 2θ values with increasing Strontium content as shown by the patterns of P40B10 and Sr. This shift may be attributed to the fact that Strontium has a higher atomic number than Calcium and thus scatters X-rays more effectively.

SEM analysis was performed on each of the powders in order to show the morphology of the particles. Figure 4-3 reveals that the bioactive glass powders were

composed of particles exhibiting irregular shapes and a wide size distribution, with small particles tending to attach themselves to the surfaces of the larger ones.

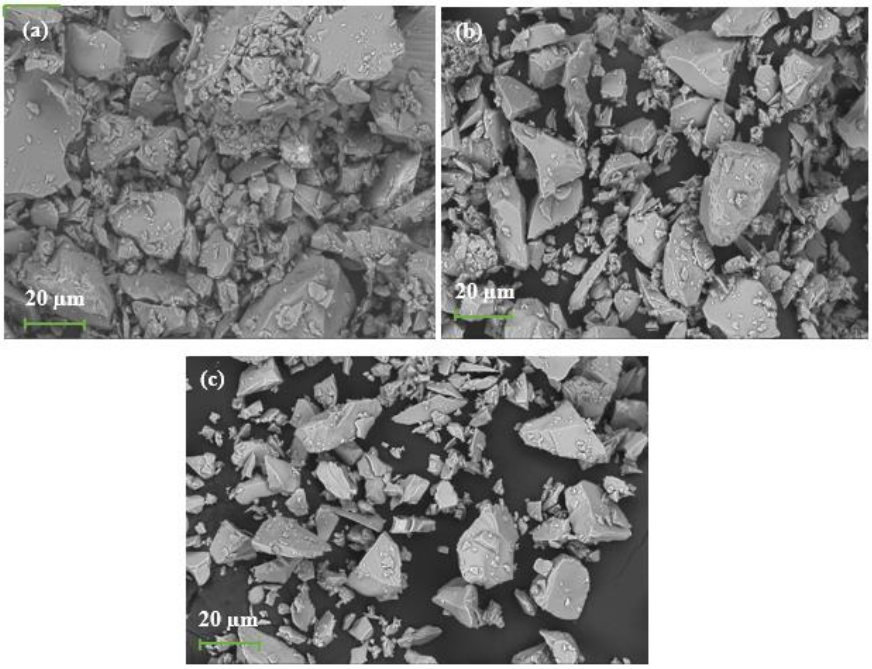

Figure 4-3: SEM images of (a) S53B50 (b) P40B10 and (c) Sr bioactive glass powder showing the particle size and shape prepared without $NH_4(HCO_3)$.

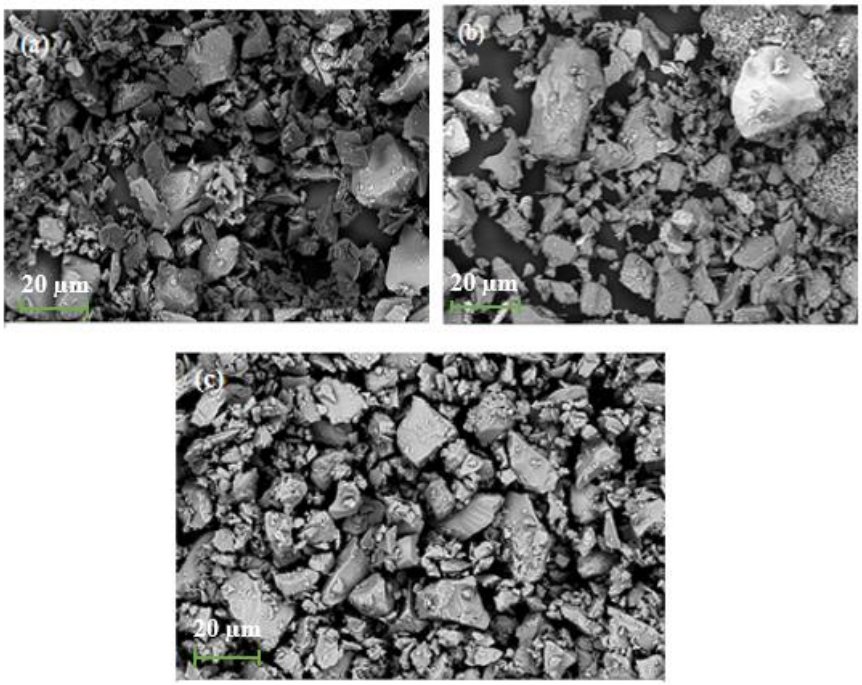

Figure 4-4: SEM images of (a) S53B50 (b) P40B10 and (c) Sr bioactive glass powder showing the particle size and shape prepared with $NH_4(HCO_3)$.

A similar trend was observed for the bioactive glass powders prepared with $NH_4(HCO_3)$; the glasses were amorphous and had no significant crystalline phases after milling and the glass particles also exhibited irregular shapes with a wide size distribution (see Figure 4.4). It is noteworthy to mention that the large particle size obtained for these glasses was due to the small force that was used during crushing compared to the force applied during crushing of the glasses that were prepared without $NH_4(HCO_3)$. This increase in particle size was crucial in that, fine particles were reported to enhance crystallization of bioactive glass powders (Massera *et al.*, 2012).

4.2 Thermal properties of the glasses

The thermal properties of the glasses, such as the glass transition temperature T_g and the onset of crystallization T_x were measured using a differential thermal analysis DTA. Figure 4-5 shows the DTA traces of the glasses S53B50, P40B10 and Sr respectively, recorded at a heating rate of 10ºC/min on powder samples of 125-250 µm particle size.

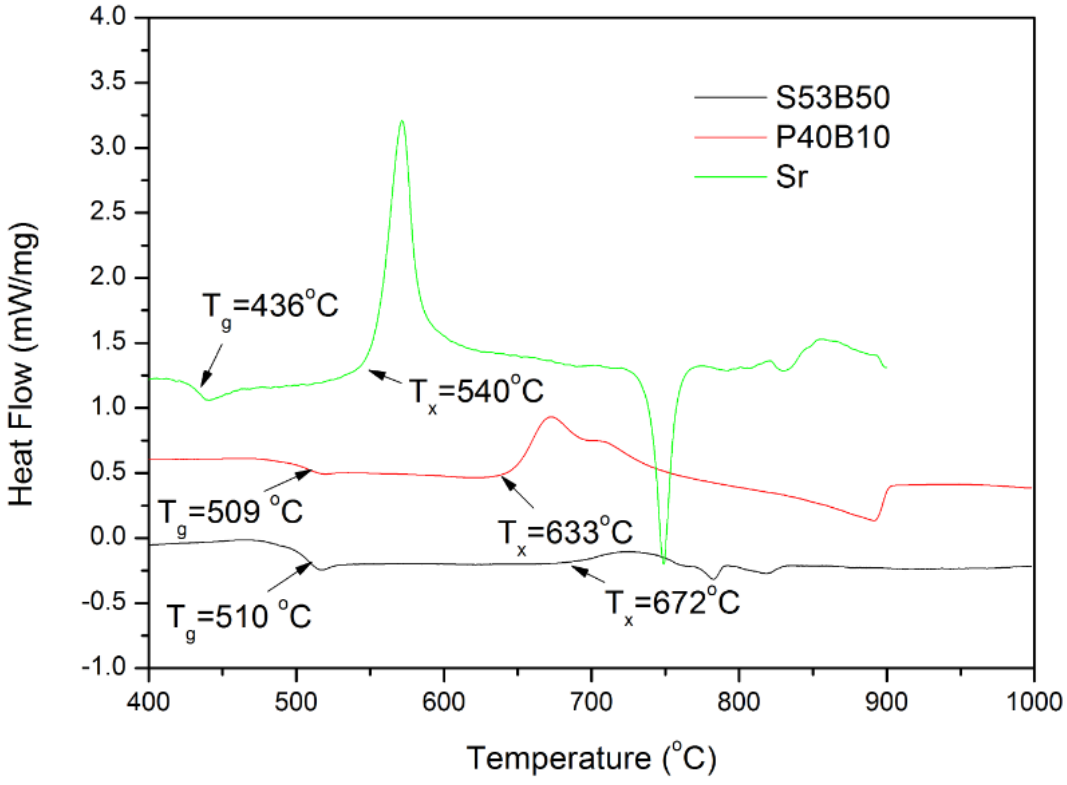

Figure 4-5: DTA thermographs of the glasses of investigation

The DTA traces of the powders of S53B50; P40B10 and Sr exhibit an endothermic effect at the glass transition temperature T_g (around 510°C; 509°C and 436°C; respectively); corresponding to the inflection point of the endotherm; followed by the onset temperature of crystallization T_x (672°C; 633°C and 540°C; respectively) corresponding to the inflection point of the endothermic and exothermic peak. In this study, the crystallization temperature (T_p) which is at the maximum of the exothermic peak was not measured. Table 4.3 summarizes the thermal properties of the glasses.

Table 4-3: Glass transition temperature (T_g), onset of crystallization temperature (T_x) and working range (ΔT) of S53B50, P40B10 and Sr bioactive glasses; as determined by differential thermal analysis (DTA)

Characteristic temperature (°C)	**S53B50**	**P40B10**	**Sr**
Glass transition temperature ($T_g \pm 2$°C)	510	509	436
Onset of crystallization temperature ($T_x \pm 2$°C)	672	633	540
Crystallization temperature ($T_p \pm 2$°C)	725	672/704	527
Working range ($\Delta T = T_x - T_g \pm 4$°C)	162	124	104

4.3 Sintering of glass powder

4.3.1 Samples sintered without $NH_4(HCO_3)$

The glass samples were sintered without the foaming agent in order to determine the sintering behavior of the glasses at the same time determine the optimum sintering conditions that would be used to fabricate the porous glass scaffolds. The obtained densities of the sintered bioactive glasses are shown in Table 4.4. The density was found to increase up to certain temperature followed by a decrease upon further increase in temperature to 600°C. This indicates that densification is inhibited at high sintering temperatures.

Table 4-4: Composition, Temperature, Time, Density, Open porosity and Relative density

Composition	Temperature (°C), Time (Hr)	Density (g/cm^3)	Open porosity (%)	Relative Den (%)
S53B50_1	520, 2	2.22±0.01	15±0.62	85
S53B50_2	540, 2	2.31±0.01	11±0.44	89
S53B50_3	560, 2	2.44±0.01	7±0.20	93
S53B50 _4	580, 2	2.30±0.01	12±0.43	88
S53B50_5	600, 2	2.30±0.01	12±0.15	88
P40B10_1	520,2	2.12±0.01	28±0.45	72
P40B10_2	540,2	2.27±0.01	23±0.27	77
P40B10_3	560,2	2.03±0.01	31±0.52	69
P40B10_4	580,2	2.08±0.01	29±0.34	71
B40B10_6	600,2	2.06±0.01	30±0.00	70
Sr_1	480.2	2.37±0.01	16±0.35	84
Sr_2	520.2	2.49±0.01	12±0.24	88
Sr_3	540,2	2.54±0.01	10±0.12	90
Sr_4	560,2	2.60±0.01	8±0.33	92
Sr_5	580,2	2.46±0.01	13±0.68	87
Sr_6	600,2	2.39±0.01	15±0.19	85

XRD analysis was performed on all sintered samples. Figure 4-6-4-8 shows the XRD patterns of the bioactive glasses for each sintering temperature for S53B50, P40B10 and Sr, respectively. From the XRD data, it was observed that glass S53B50 and P40B10 had a similar behavior in maintaining an amorphous structure at the sintering temperature of 520 °C. On the other hand, glass Sr displayed crystallization at the same temperature. However as the sintering temperature was increased in all the

glasses, the samples began to crystallize as evidenced by the presence of sharp diffraction peaks with pronounced crystallization at 600°C.

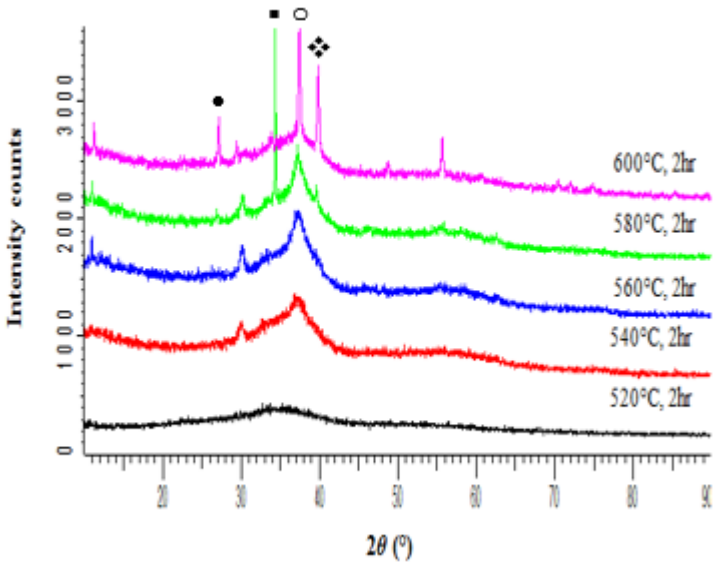

• $Ca_2(SiO_4)$ ○ $CaSiO_3$ ▪ $Na_{2.2}Ca_{1.9}Si_3O_9$ ❖ Si

Figure 4-6: XRD pattern for glass S53B50 as a function of temperature

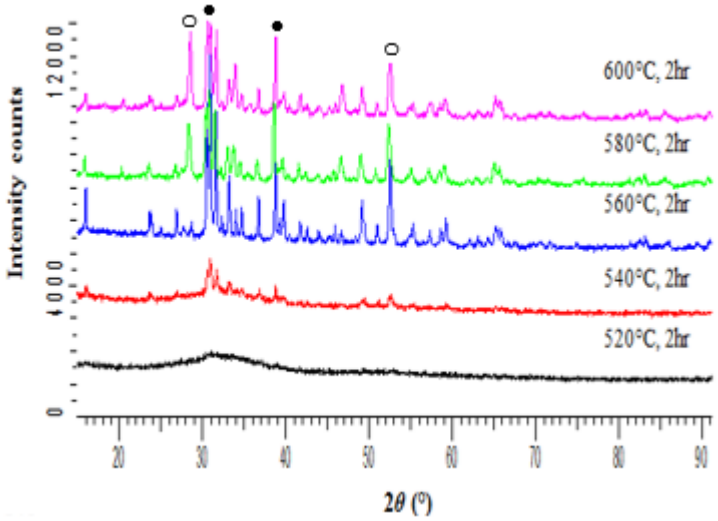

○ $Sr(PO_3)_2$ • $B(PO_4)$

Figure 4-7: XRD patterns for glass P40B10 as a function of temperature

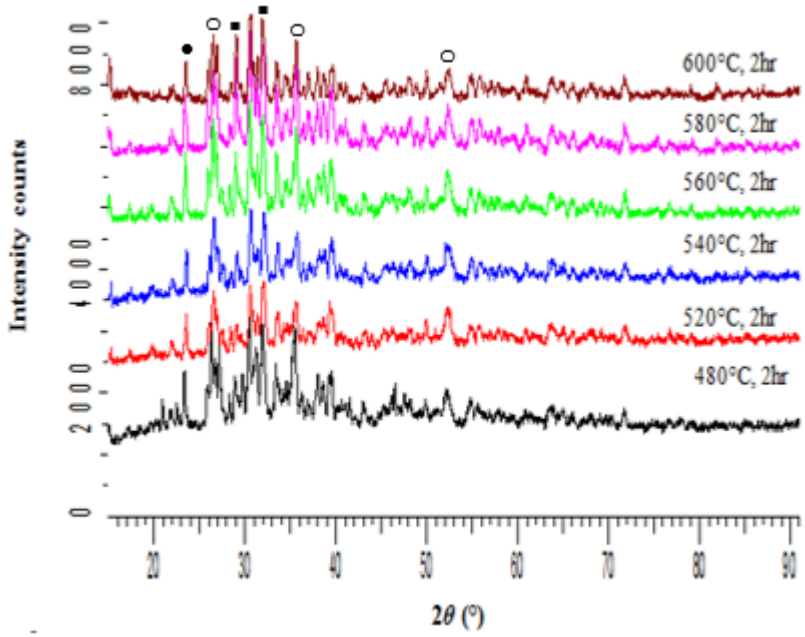

- $Na_4(P_2O_7)$ ○ $Sr(PO_3)_2$ ▪ $Sr_2(PO_2)_7$

Figure 4-8: XRD patterns for glass Sr as a function of temperature

The samples were further characterized using SEM in order to examine the microstructure of the samples after sintering. SEM investigations of the sintered bodies' cross sections in Figure 4-9-4-11 reveal dense microstructures which correlate with the densification results in Table 4.4. The presence of micropores is also evident which could have contributed to the reduction in the density of the samples. These micropores might be residual porosity as a result of the incomplete sintering process. Furthermore; cracks were also observed on the microstructure of glass P40B10 as evident in Figure.4-10. This may be due to the stress exerted on the samples during cutting. In addition the presence of craters were also observed on the surface of glass Sr presented in Figure 4-11. It is possible that these craters might have been caused by the chirped section of the cutting blade resulting in the pull out of some materials as evidenced. In order to further examine the crystals formed during sintering, SEM micrographs were taken at high magnification as shown in Figure 4.12

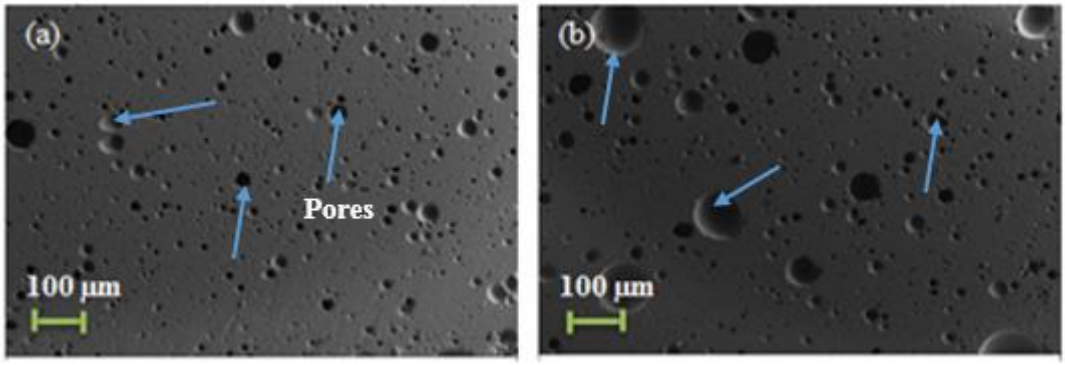

Figure 4-9: SEM micrographs of the cross section of glass S53B50 samples sintered at (a) 580°C and (b) 600°C

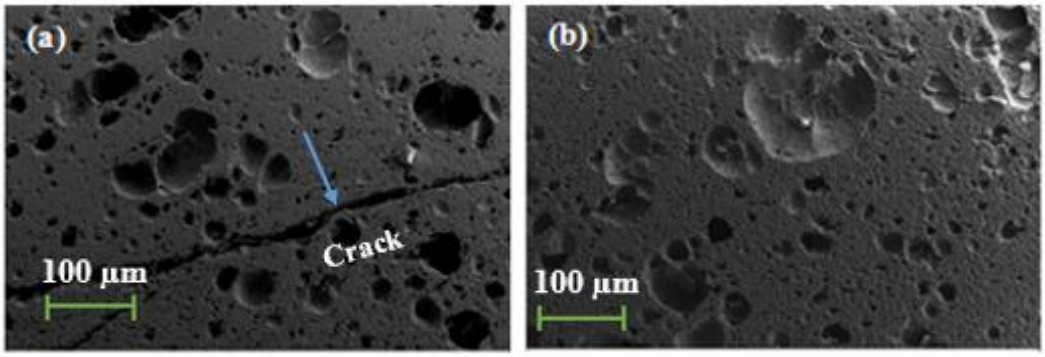

Figure 4-10: SEM micrographs of the cross section of glass P40B10 sintered at (a) 580°C and (b) 600°C

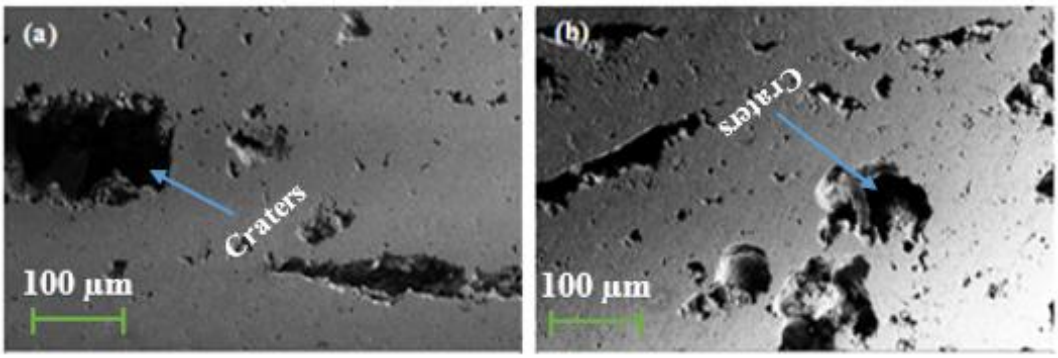

Figure 4-11: SEM micrographs of the cross section of glass Sr samples sintered at (a) 580°C and (b) 600°C

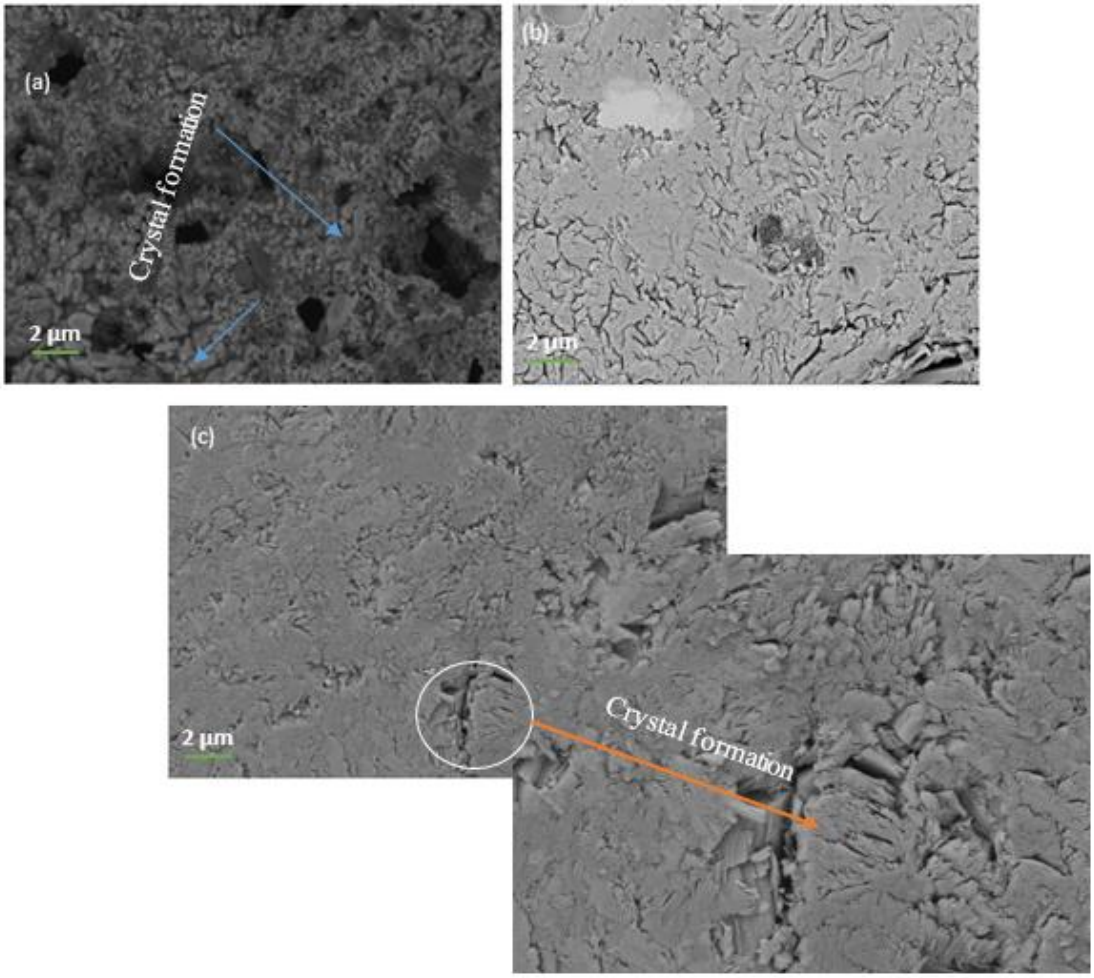

Figure 4-12: SEM micrographs of the cross section of glass samples sintered at 600°C for glass (a) P40B10 (b) S53B50 and (c) Sr

4.3.2 Samples sintered with $NH_4(HCO_3)$

One of the objectives of this project is the fabrication of porous scaffolds which will be achieved by sintering the glass powders with $NH_4(HCO_3)$ foaming agent with the sole aim of increasing the porosity of the scaffolds using the optimum conditions obtained from sintering the samples without $NH_4(HCO_3)$.

The compacted pellets were sintered in the muffle furnace using a heating rate of 10°C/min at temperatures of 500°C for glass Sr and 540°C for glass S53B50 and P40B10 with a holding time of 1 hour at the sintering temperature. The use of $NH_4(HCO_3)$ is motivated by the high density of the samples sintered without porogens. The $NH_4(HCO_3)$ was burned of at 67°C for 2 hours , prior to the sintering temperature. The obtained scaffolds were characterized in terms of density and the

results are shown in Table 4.5. The density was found to decrease with increasing $NH_4(HCO_3)$ content, hence, the high porosity in the samples.

Table 4-5: Composition, Density and Open porosity of sintered scaffolds

Composition	Temperature (°C), Time (Hr)	Density (g/cm^3)	Open porosity (%)	Relative Den (%)
S53B50 – 60 vol.% $NH_4(HCO_3)$	540, 1	1,07±0.01	59±0.47	41
S53B50 – 70 vol.% $NH_4(HCO_3)$	540, 1	0,86±0.01	67±0.60	33
P40B10 – 60 vol.% $NH_4(HCO_3)$	540, 1	1,19±0.01	59±0.45	41
P40B10 – 70 vol.% $NH_4(HCO_3)$	540, 1	0,95±0.01	68±0.48	32
Sr – 60 vol.% $NH_4(HCO_3)$	500, 1	1,02±0.01	64±0.34	36
Sr – 70 vol.% $NH_4(HCO_3)$	500, 1	0,79±0.01	72±0.00	28

The XRD patterns for glass S53B50; P40B10 and Sr are shown in Figure 4.13. The results confirm that the two glasses had a broad shallow peak which indicates the glasses retained the amorphous state during sintering, while glass Sr still showed a glass-crystalline transition at 500°C. However, it is worth mentioning that the intensity of the diffraction pattern was more pronounced when the glass was sintered without $NH_4(HCO_3)$ foaming agent.

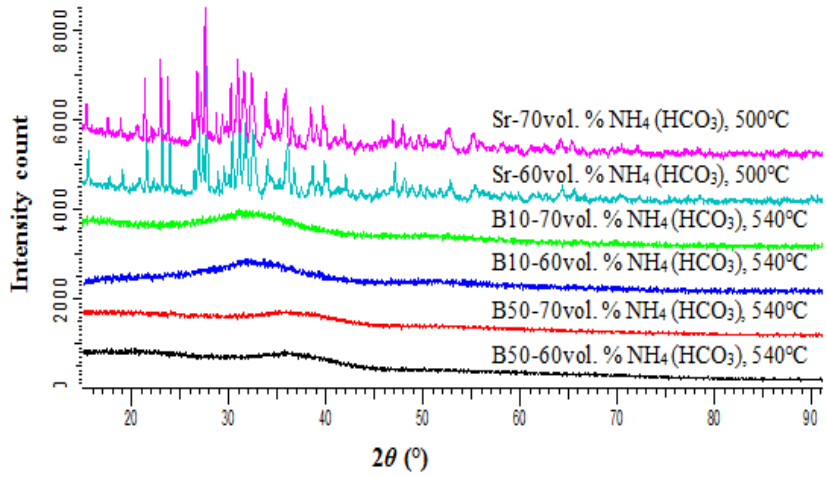

Figure 4-13: XRD patterns of the as prepared porous glass scaffolds for S53B50, P40B10 and Sr

SEM analysis of the cross sections was performed to show the morphology of the porous structures. The images of the porous scaffolds of S53B50, P40B10 and Sr are shown in Figure 4-14. The results reveal porous microstructures with well-connected open porosity and irregularly shaped pores; hence, the low density. The interconnection between the pores is clearly presented in the SEM micrographs. Homogeneity of pore distribution is also evident on the cross section of the scaffolds. All the glasses had a similar microstructure.

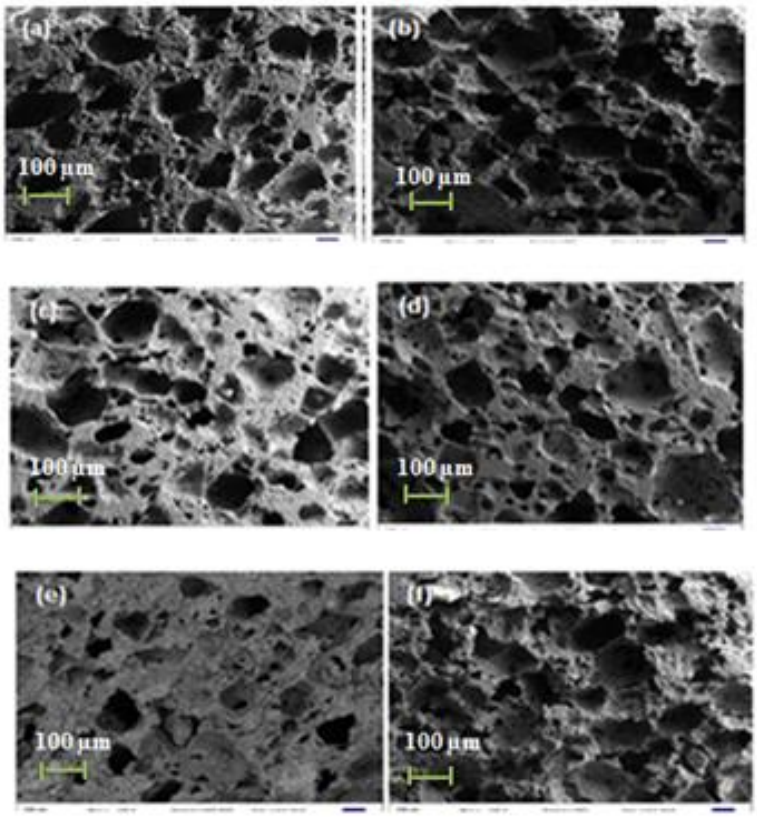

Figure 4-14: SEM micrographs of porous S53B50; P40B10 and Sr bioactive scaffolds mixed with (a),(c) and (e) 60 vol. % $NH_4(HCO_3)$ and (b), (d) and (f) 70 vol. % $NH_4(HCO_3)$, sintered at 540°C and 500°C for 1 hour, respectively

In addition, the pore walls were composed of dual microstructures (see Figure 4.15) with micro pores observed on the pore struts as well as all over the surface. This was probably due to the gas released during the sintering process. However, the micro pore were only clearly visible on glass P40B10 and Sr. The presence of micro pores is also another important feature of these scaffolds, as it is known that small pores favour and aid cell adhesion and allow the physiological fluids to enter the inner part of the scaffold (Brovarone *et al.*, 2006). Whereas large pores >100 µm are required by the vascular tissues to circulate body fluids.

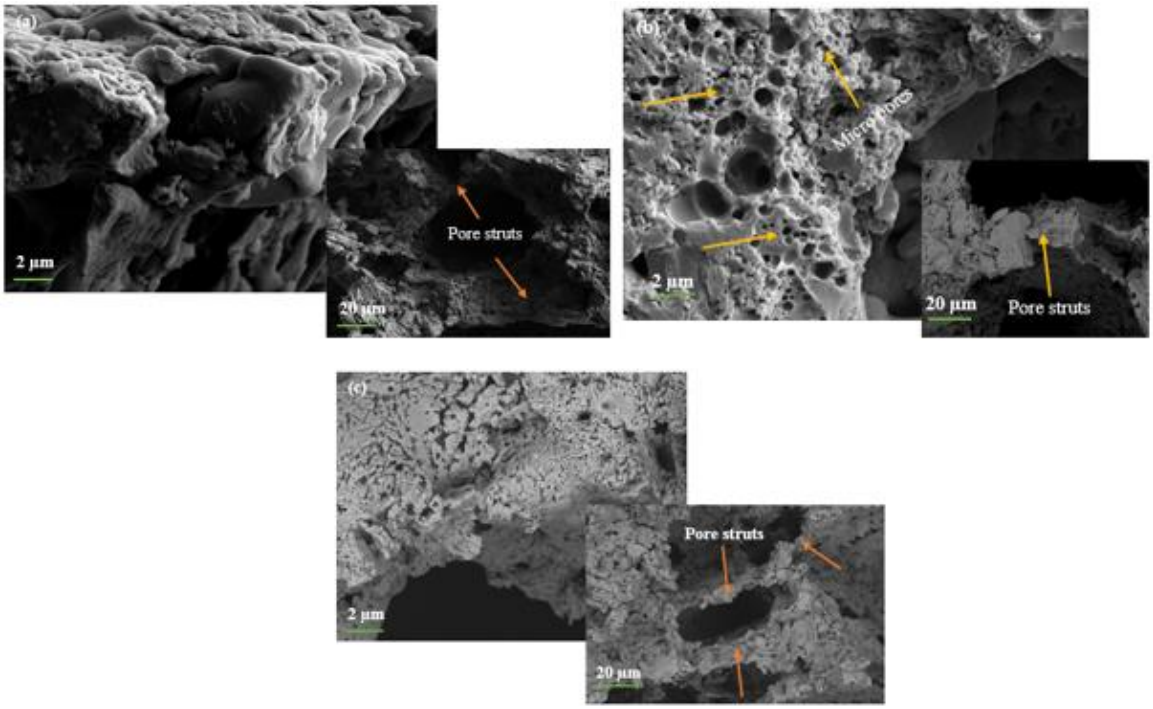

Figure 4-15: High magnification SEM micrographs of porous S53B50, P40B10 and Sr bioactive glasses mixed with (a); (b) and (c) 70 vol. % $NH_4(HCO_3)$, respectively

4.4 Analysis of the porous scaffolds

For a scaffold to be ideal for any tissue engineering application, the most important architectural feature of the scaffold is the interconnection of the pores. To determine the porosity and the pore size distribution, Mercury Porosimetry Intrusion and µCT were performed on the scaffolds. Figure 4-16 - 4-18 shows the pore size distribution of S53B50, P40B10 and Sr glass scaffolds, respectively, obtained from mercury intrusion porosimetry. The vertical axis is a derivative of the volume of mercury intruded into the scaffold relative to the pore diameter (Lowell, 1984). The Figures show that the scaffolds have a wide pore distribution with interconnected pores in the range of 0.003 µm – 90. 84 µm. However, the pore network obtained from mercury intrusion porosimetry did not correlate with the SEM analysis which showed that the scaffolds had large and a wide distribution of interconnected pores; therefore, the scaffolds were further analysed using micro computed tomography to determine the pore size distribution.

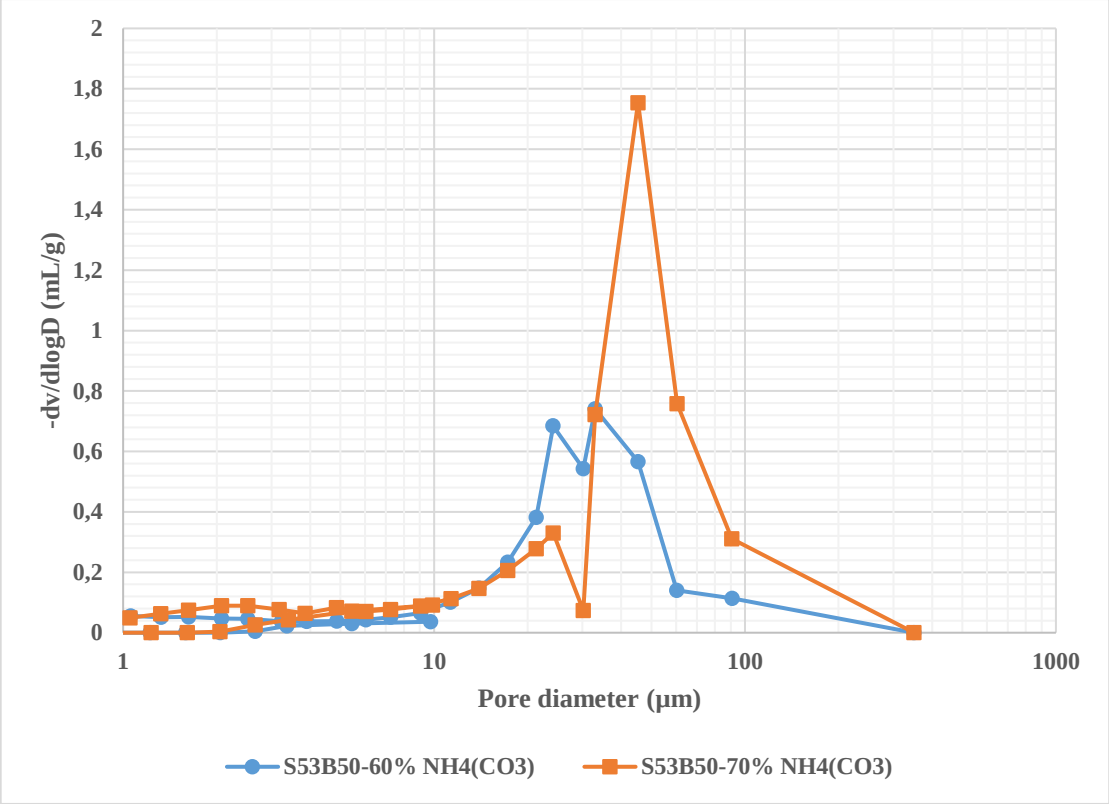

Figure 4-16: Pore size distribution of S53B50 glass scaffolds at different $NH_4(HCO_3)$ content; obtained from mercury intrusion porosimetry

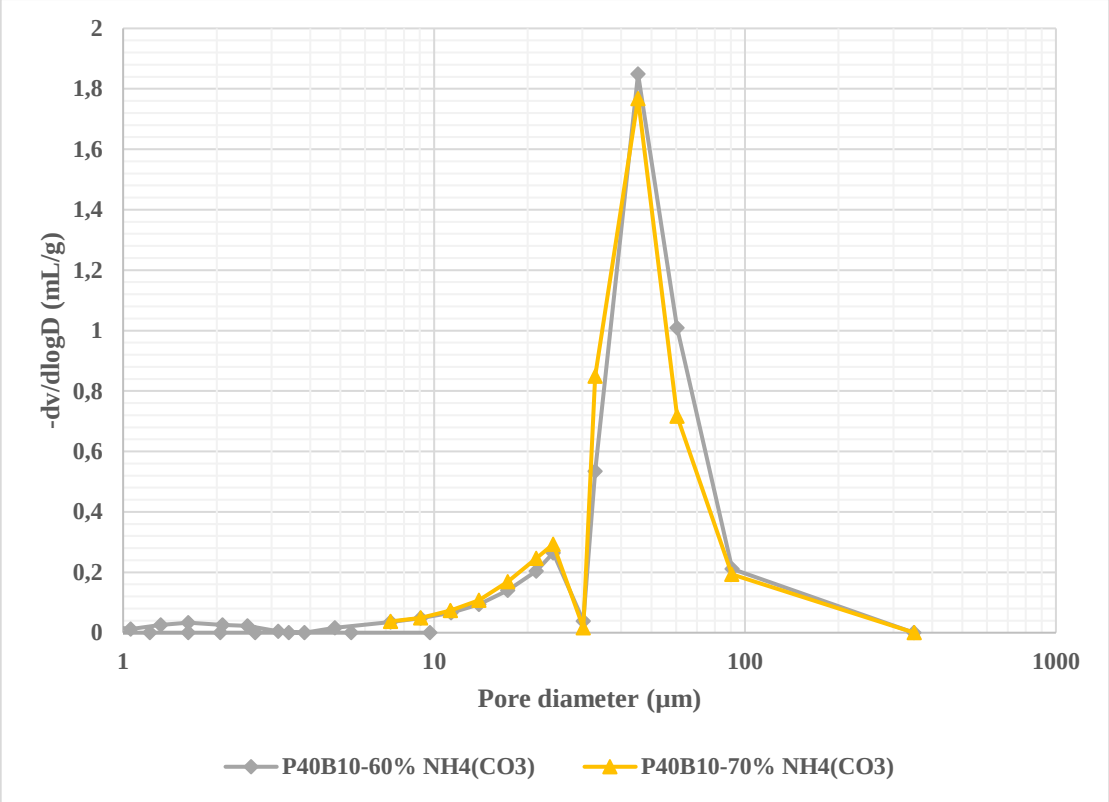

Figure 4-17: Pore size distribution of P40B10 scaffolds at different $NH_4(HCO_3)$ content; obtained from mercury intrusion porosimetry

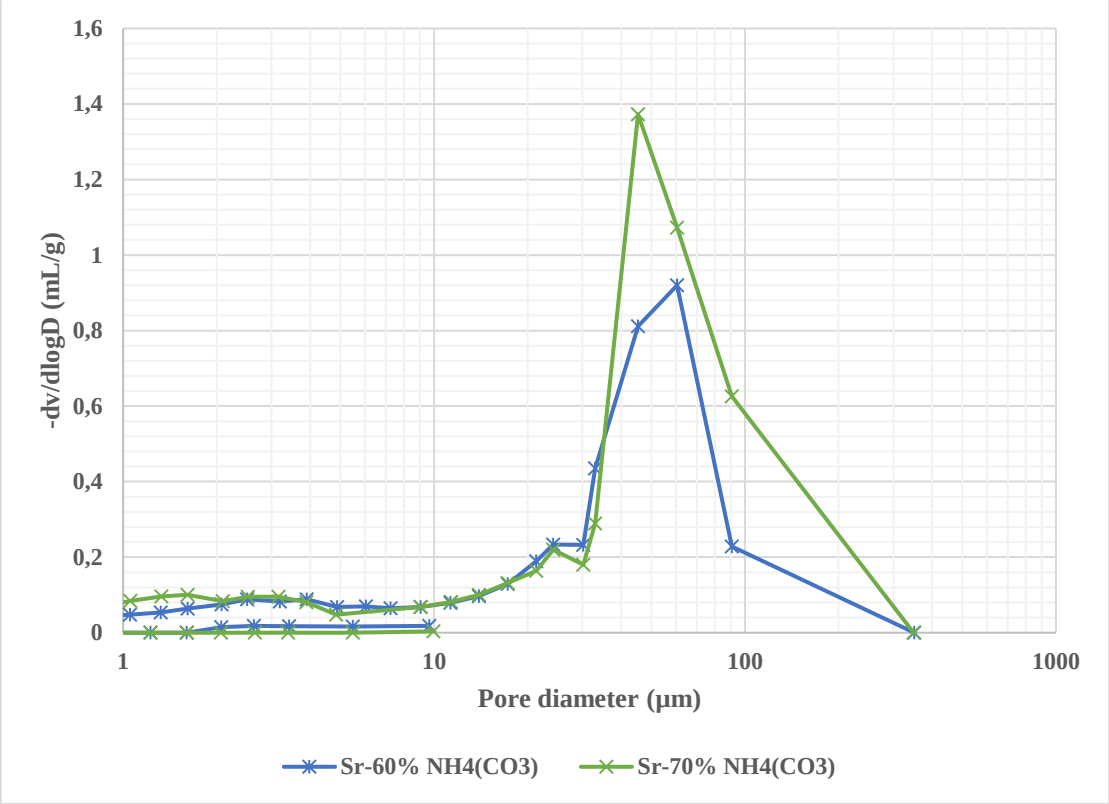

Figure 4-18: Pore size distribution of Sr glass scaffolds at different $NH_4(HCO_3)$ content; obtained from mercury intrusion porosimetry

The 3-D µCT images of the structure of the optimized scaffolds at different $NH_4(HCO_3)$ content are shown in Figure 4-19 – 4-21 for glass S53B50, P40B10 and Sr, respectively. From the images, it is evident that the pores generated and porosity increased with the $NH_4(HCO_3)$ as observed with the SEM analysis. There is also clear visual evidence of the high interconnectivity and porosity of the scaffolds. In addition, there appears to be a homogenous distribution of pores which are distributed uniformly all over the scaffolds. This trend was observed for all scaffolds.

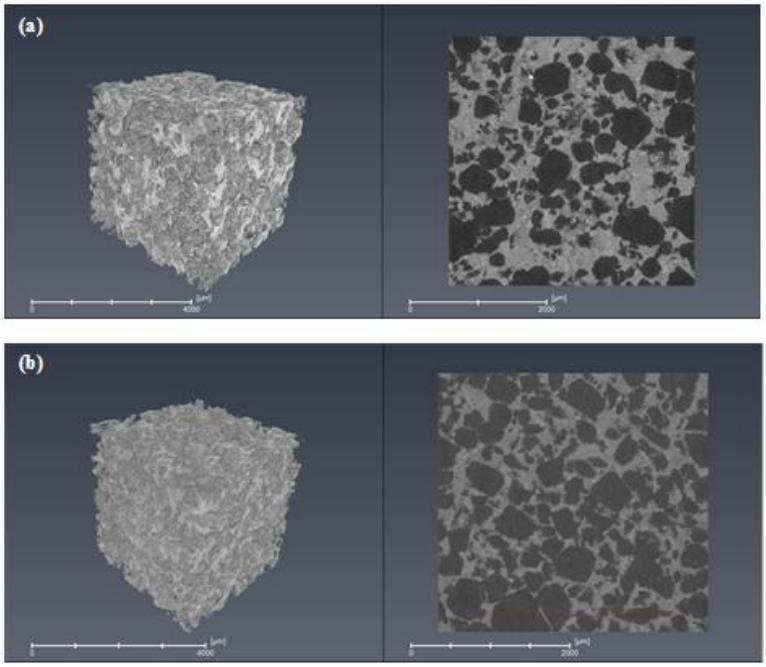

Figure 4-19: An X-ray micro tomography (µCT) image of S53B50 glass scaffold mixed with (a) 60 vol. % $NH_4(HCO_3)$ (b) 70 vol. % $NH_4(HCO_3)$

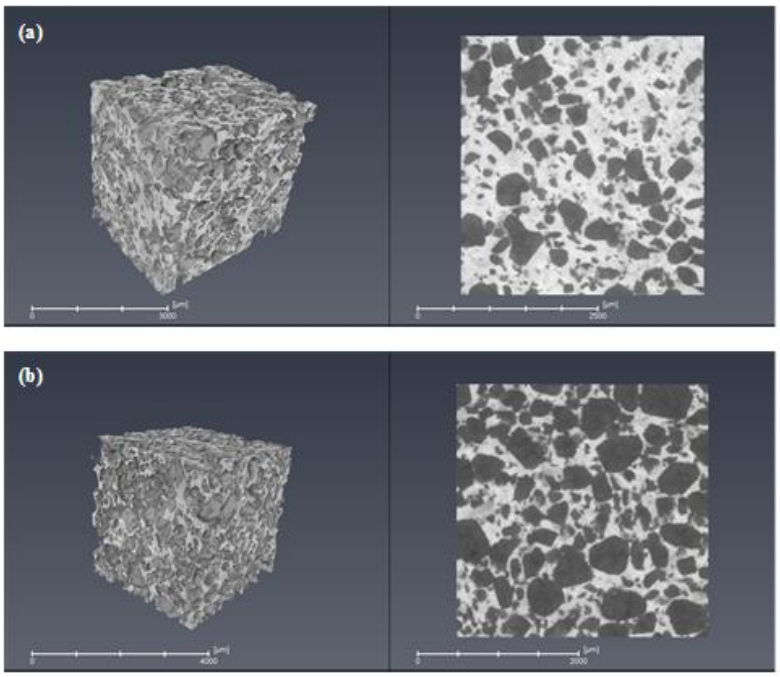

Figure 4-20: An X-ray micro tomography (µCT) image of P40B10 glass scaffold mixed with (a) 60 vol. % $NH_4(HCO_3)$ and (b) 70 vol. % $NH_4(HCO_3)$

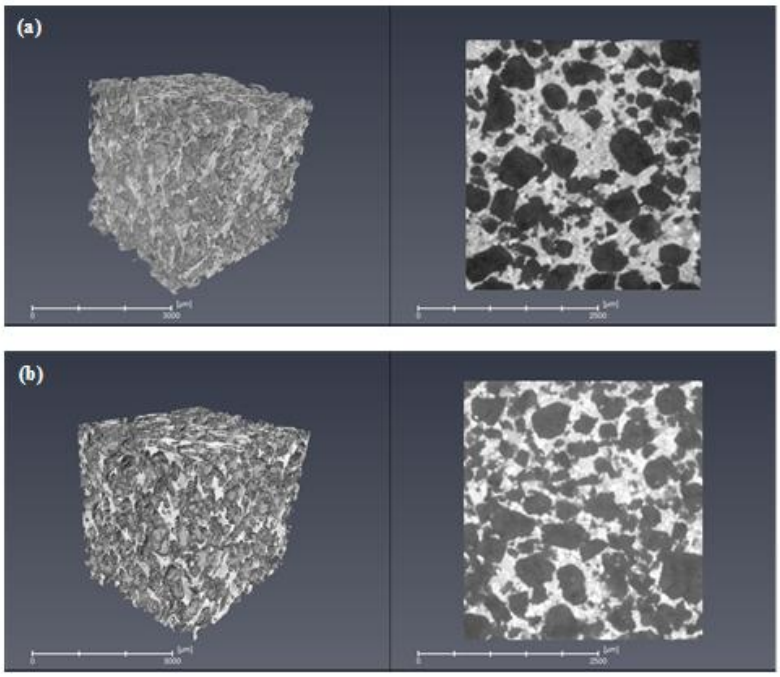

Figure 4-21: An X-ray micro tomography (µCT) image of Sr glass scaffold mixed with (a) 60 vol. % $NH_4(HCO_3)$ and (b) 70 vol. % $NH_4(HCO_3)$

Table 4.6 summarises the characterization data of the scaffolds obtained from the analysis. From the results, as expected, the average pore size and porosity increased as a function of $NH_4(HCO_3)$ content. µCT also confirmed the expected pore size range of the scaffolds in contrast to those obtained from the mercury intrusion method. The high discrepancy between the results collected by Mercury Intrusion Porosimetry (MIP) and micro-computated tomography (µCT) might be attributed to the different resolutions used during the operation. The MIP can measure pore diameters in the range of 3 nm to 200 µm (Westermarek, 2000). The pores measured are often the ones that reach the surface of the samples. On the other hand; µCT measure pore diameters in the range of 1 µm to 200 µm or more as observed in Table 4.6. This is due to the fact that the X-ray can penetrate through the material and measure pores on the surface and the internal structure of the materials. Furthermore, one should keep in mind that the porosimetry does not provide measure of the pores but rather, the interconnected size (Qin et al, 2007), (Gao, 2013) whereas µCT the general pore size as it cannot properly measure the interconnects.

Table 4-6: Composition; Average pore diameter and % Porosity of scaffolds

Composition	From Porosimetry			From µCT		
	Average pore diameter (µm)	Median pore diameter (Volume) µm	Porosity (%)	Average pore diameter (µm)	Maximum pore diameter µm	Porosity (%)
S53B50 – 60 vol.% $NH_4(HCO_3)$	0.32	32.63	54.62	257.2±0.00	513.4±112.3	54.1
S53B50 – 70 vol.% $NH_4(HCO_3)$	3.34	52.83	67.63	257.5±146.2	518.5±102.6	61.8
P40B10 – 60 vol.% $NH_4(HCO_3)$	0.19	55.06	66.34	259.8±150.3	570.0±103.2	46.9
P40B10 – 70 vol.% $NH_4(HCO_3)$	47.55	53.07	62.52	262.3±149.1	509.3±106.3	60.2
Sr – 60 vol.% $NH_4(HCO_3)$	2.75	56.42	67.13	243.8±165.2	482.0±109.1	58.0
Sr – 70 vol.% $NH_4(HCO_3)$	3.09	68.60	75.64	285.5±138.0	519.0±89.3	64.7

4.5 In vitro properties

4.5.1 Variation of pH

The glass scaffolds were immersed in the simulated body fluid (SBF) for 24, 48, 72 and 168 hours. Figure 4-22 - 4-24 presents the average pH values of the SBF solutions containing glass scaffolds of S53B50, P40B10 and Sr, respectively, as a function of immersion time and for varying contents of $NH_4(HCO_3)$ at 37°C. The pH value of the SBF before immersion is 7.4. The pH was found to increase with increasing immersion time for S53B50. Additionally, the pH values of the scaffolds with 70 vol. % $NH_4(HCO_3)$ was found to be slightly higher than that of the scaffolds with 60 vol. % content. The increase in pH was due to the leaching of Na^+ and Ca^{2+} into the solution with simultaneous SiO_2 rich layer formation leading to more basic pH.

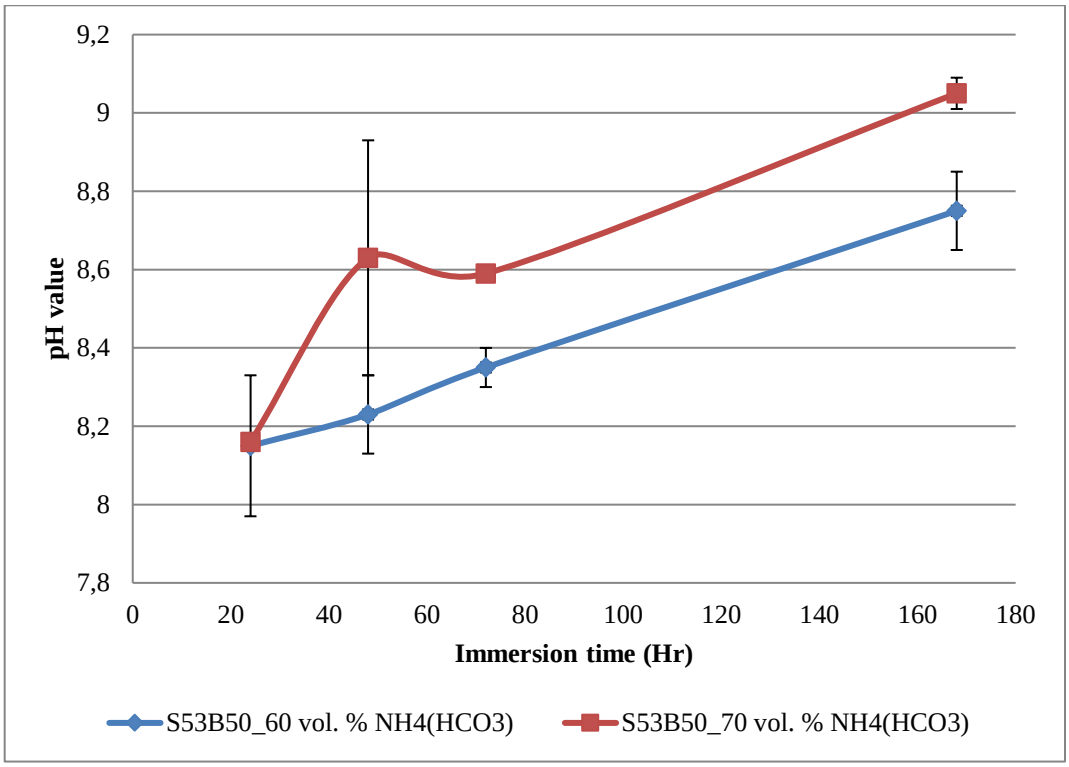

Figure 4-22: pH of SBF as a function of immersion time for glass S53B50 scaffolds

The pH results for glass P40B10 and Sr scaffolds are shown in Figure 4-23 and 4-24, respectively. The pH of the SBF solutions was found to decrease with respect to immersion time. As observed with the glass scaffolds of S53B50 the pH value of the scaffolds with 70 vol. % NH_4 (HCO_3) was found to be slightly higher than those with 60 vol. %. Meanwhile the pH values of the glass scaffolds of P40B10 and Sr with 70 vol. % NH_4 (HCO_3) were also found to be slightly lower than those with 60 vol. %. This shows that high porosity is crucial for better permeability of fluids and release of ions.

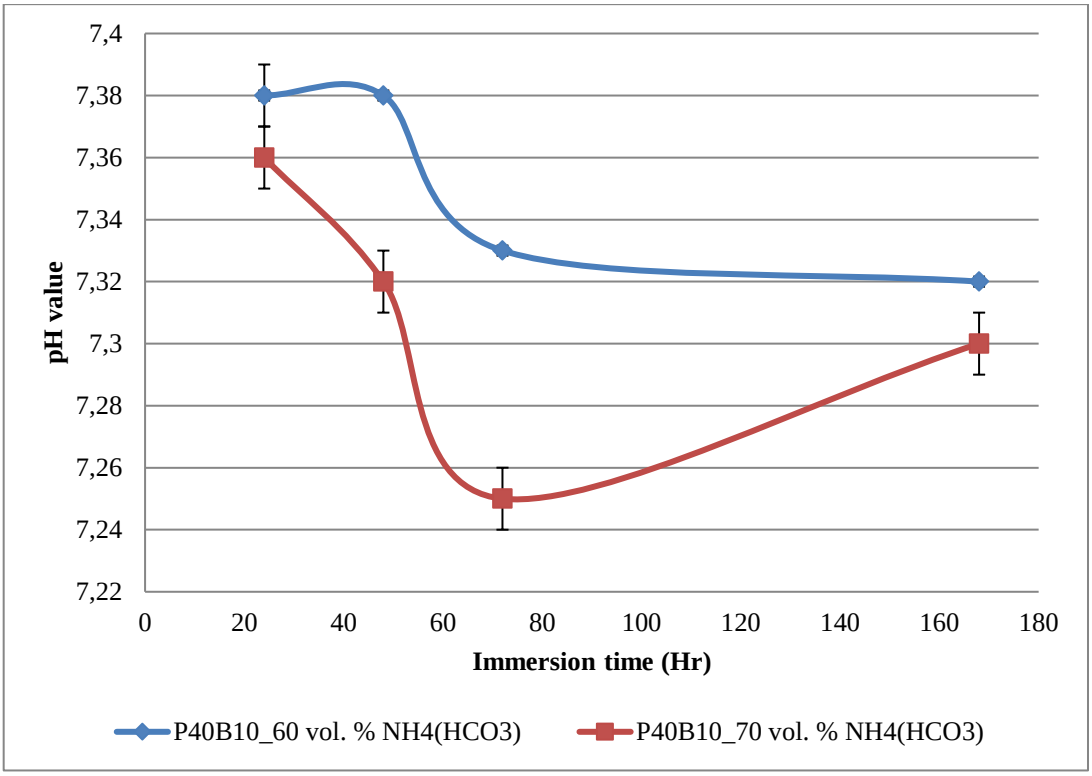

Figure 4-23: pH of SBF as a function of immersion time for glass P40B10 scaffolds

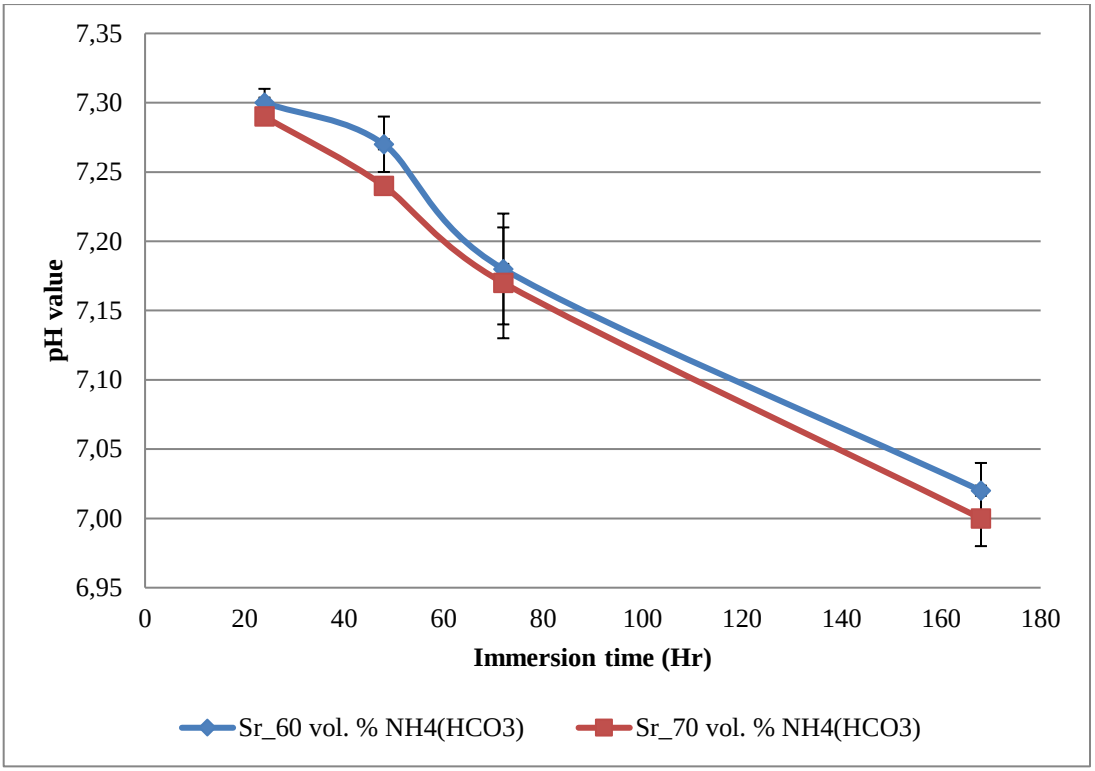

Figure 4-24: pH of SBF as a function of immersion time for glass Sr scaffolds

4.5.2 Variation of mass

The change in mass of the scaffolds was also calculated in order to determine how much was lost during immersion. Upon immersion of the scaffolds into the SBF solution, the dissolution and conversion reactions that led to weight loss of the glasses were also the same reactions that controlled the pH of the solution, therefore, it is expected that the weight loss and pH data will show approximately the same trend.

The change in mass of glass S53B50, P40B10 and Sr scaffolds as a function of immersion time are displayed in Figure 4-25 - 4.27, respectively. It is worth noting that while S53B50 continued to show a gradual increase in weight loss after the initial rapid increase; Sr showed a constant weight after the initial increase period and P40B10 showed almost no weight loss. Furthermore; the weight loss was found to be slightly higher at 70 vol. NH_4 (HCO_3) than at 60 vol. % for all three glasses. Accordingly the amount of weight loss is depended on the pH endured during immersion. It was observed that at higher pH the weight loss encountered was also high as seen with S53B50 at 70 vol. % than 60 vol. % $NH_4(HCO_3)$. Whereas at lower pH values as seen with P40B10 and Sr; a lower pH was associated with a high

percentage of weight loss. However; this observation was more evident to Sr than P40B10 with the scaffolds of prepared with 70 vol. %.

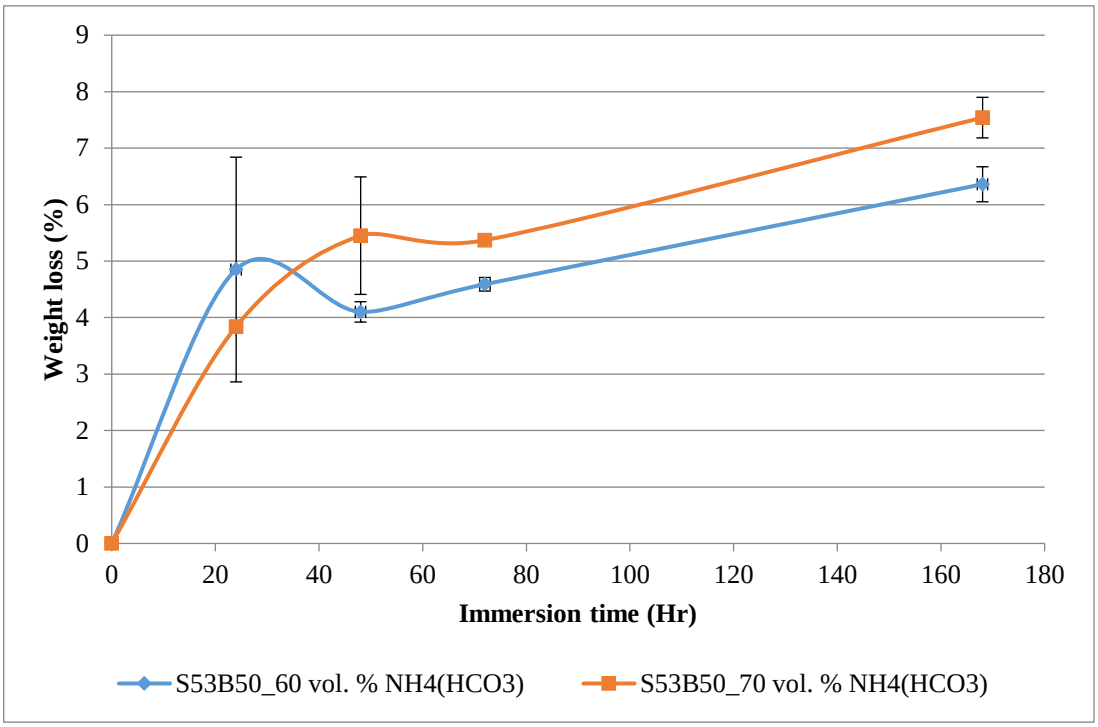

Figure 4-25: Weight loss (%) as a function of immersion time for glass S53B50 scaffolds

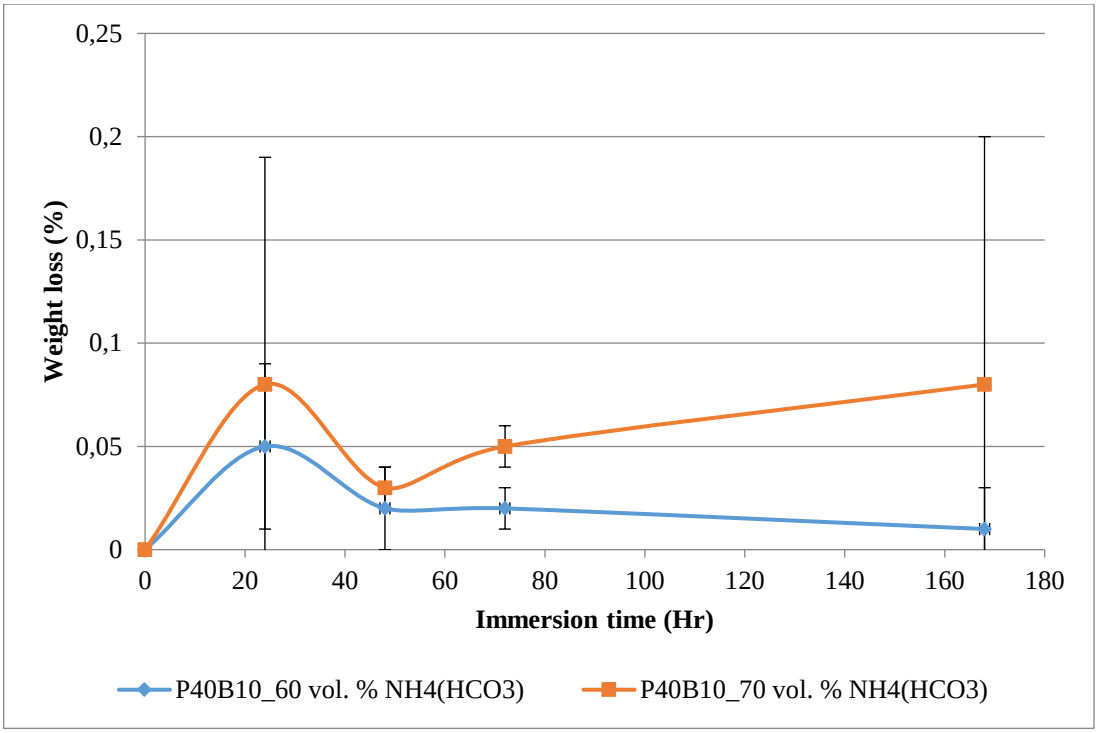

Figure 4-26: Weight loss (%) as a function of immersion time for glass P40B10 scaffolds

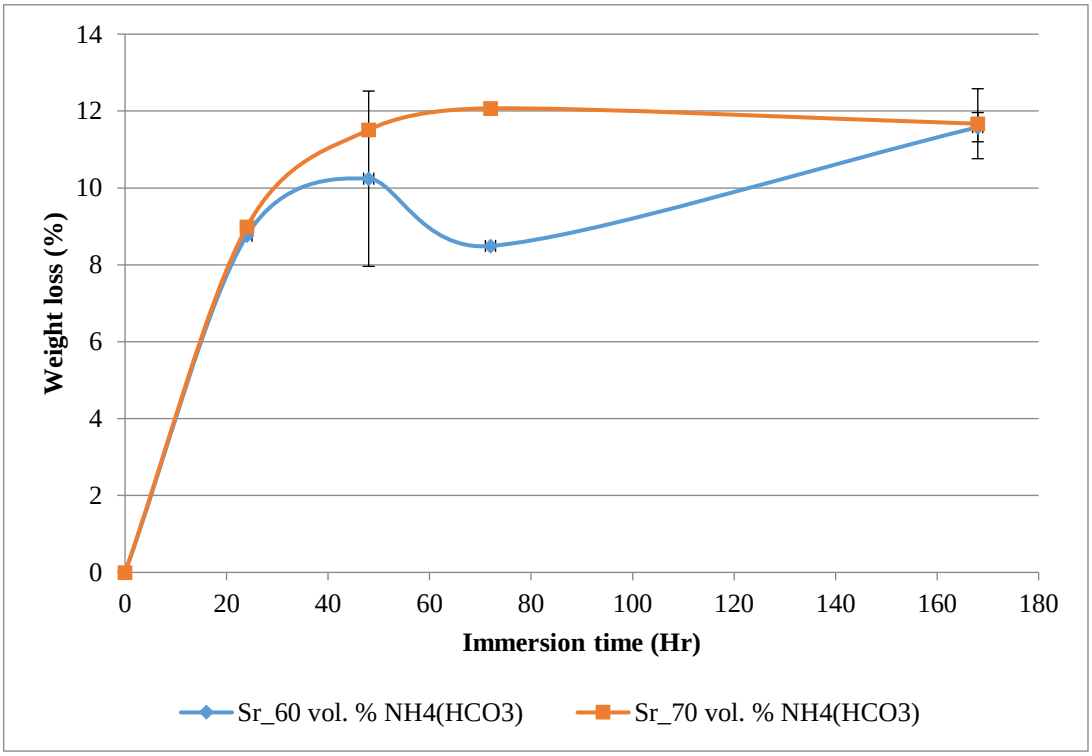

Figure 4-27: Weight loss (%) as a function of immersion time for glass Sr scaffolds

4.5.3 ICP analysis

After immersion, the ion concentration in the immersion solution was quantified using inductive coupled plasma. Figure 4-28 presents the (a) [B], (b) [Ca], (c) P and (d) [Si] ion concentration upon immersion of the borosilicate glass. Upon immersion; the [B]; [Ca] and [Si] increases. The [P]; however was found to decrease with increasing immersion time. While; up to 24h of immersion; no significant differences in concentration could be measured; between the immersion solution containing the scaffolds with 60 or 70 vol. %; the later showed drastically increased ion concentration at longer immersion time.

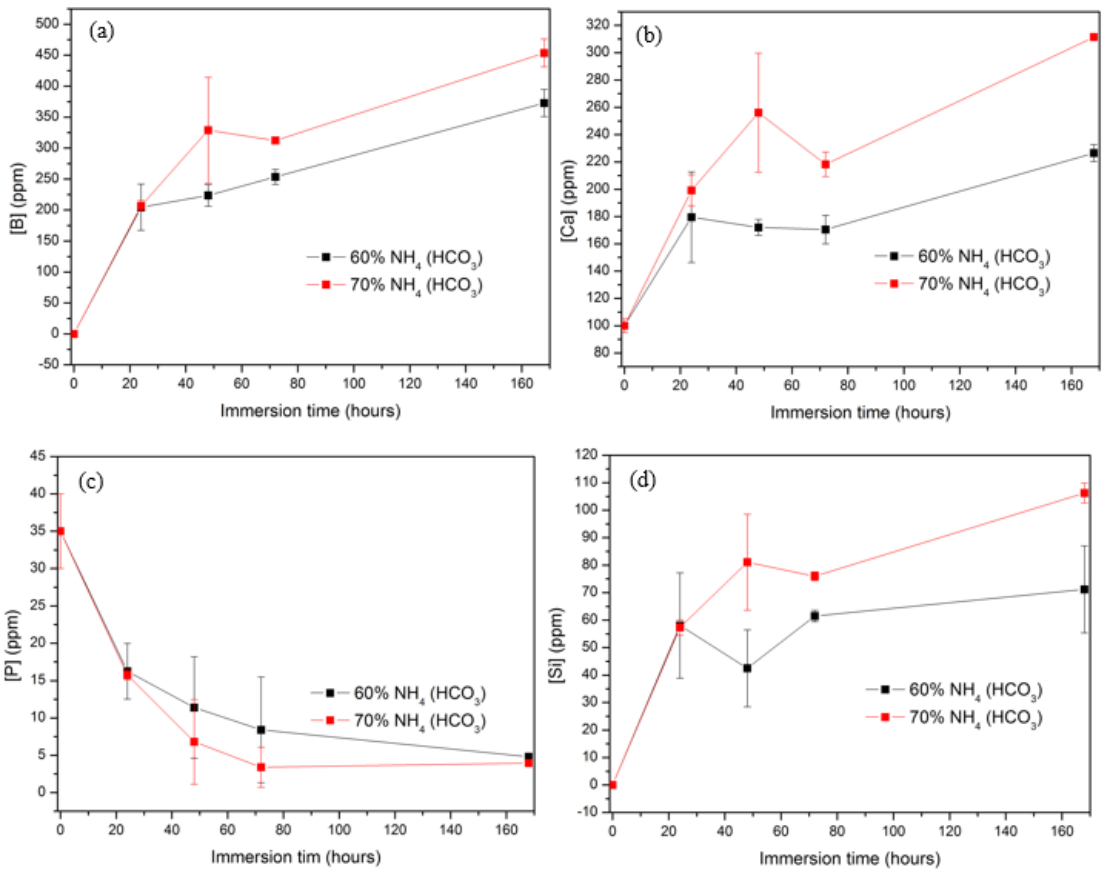

Figure 4-28: Ion concentration in the immersion solution of S53B50 for (a) [B] , (b) [Ca], (c) [P] and (d) [Si] as a function of time

Figure 4-29 presents the (a) [B]; (b) [Ca]; (c) [P] and (d) [Sr] ion concentration upon immersion of the borophosphate glass. While a general increase in [B]; [P] and [Sr] can be seen; the [Ca] was found to decrease. As explained in Fig 3; all variation are more pronounced in when scaffolds containing 70 vol. % are immersed in SBF. It is also interesting to point out the change in ion release of the borosilicate glass (Figure 4-28) compared to the borophosphate glass (Figure 4-29). Indeed the scale for the ion being released (especially [B]) are lower upon immersion of the borophosphate compared to the borosilicate.

Figure 4-30 presents the (a) [Ca]; (b) [P] and (c) [Sr] ion concentration upon immersion of the phosphate glass. Upon immersion for 24h; the [P] and [Sr] increases and then remain almost constant for longer immersion time. The [Ca]; however; decreases during all imersion test. As opposed to the other tested materials; here no significant differences could be seen between the scaffolds produced with 60 or 70 vol. % of $NH_4(HCO_3)$.

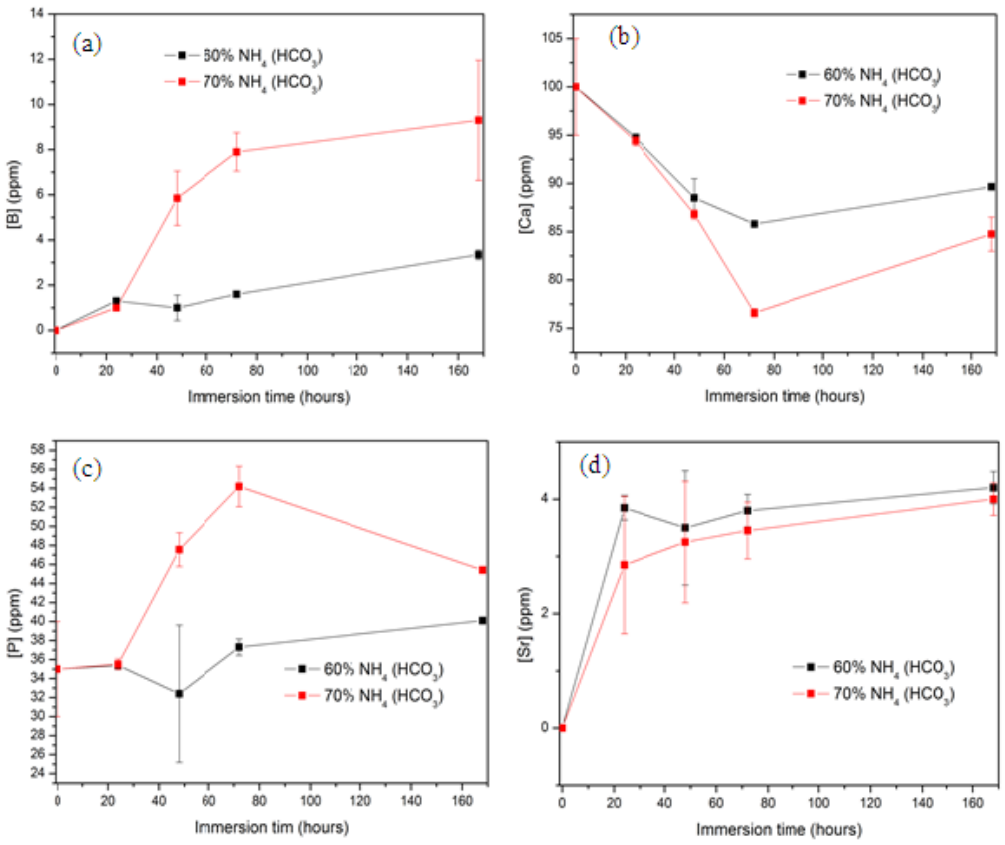

Figure 4-29: Ion concentration in the immersion solution of P40B10 for (a) [B], (b) [Ca], (c) [P] and (d) [Sr] as a function of time

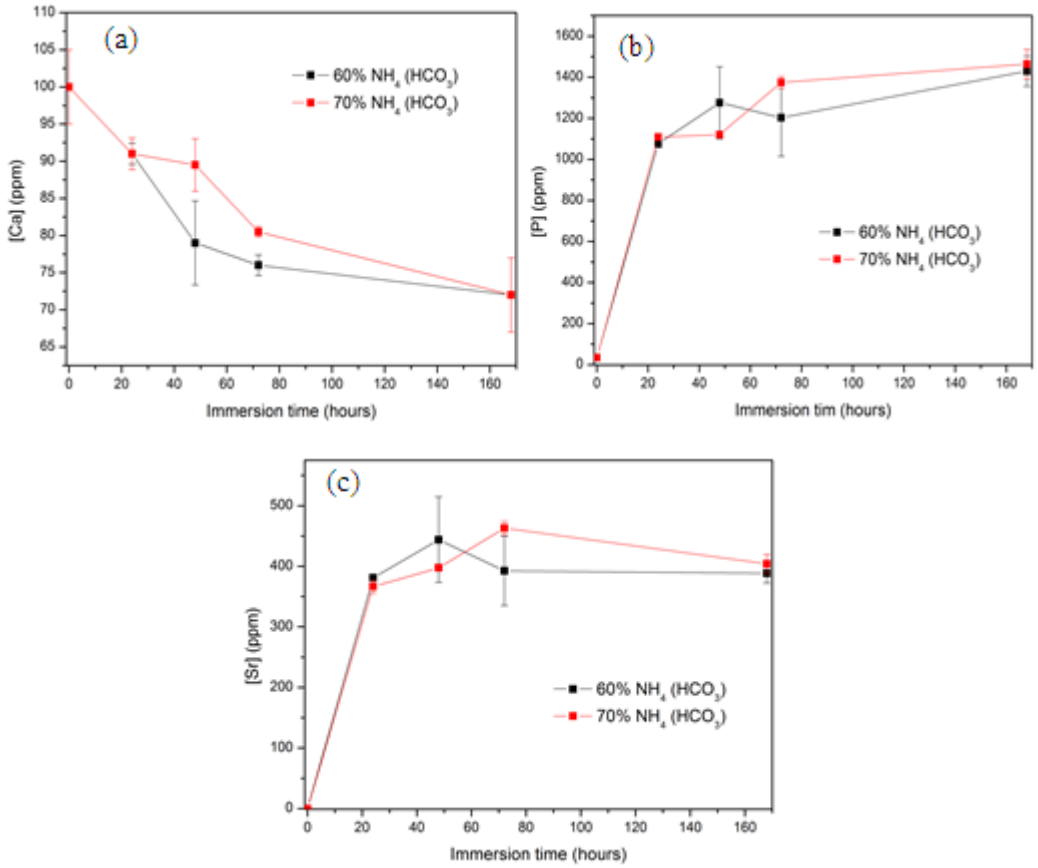

Figure 4-30: Ion concentration in the immersion solution of Sr for (a) [Ca], (b) [P] and (c) [Sr] as a function of time

4.5.4 Phase and Microstructural analysis

4.5.4.1 XRD analysis

To confirm that the spherical particles formed on the glasses surfaces was indeed HA particles; a phase analysis was carried out using XRD on the scaffolds immersed for 24, 48, 72 and 168 hours in SBF. Figure 4-31 - 4-32 presents the XRD patterns for glass S53B50 scaffolds. The as prepared glass scaffold (seen in Figure 4.12) showed the commonly observed shallow broad peak, which is a typical characteristic of any amorphous glass material. On the other hand, the XRD patterns of the immersed samples showed a major peak at 36° corresponding to that of HA as reported (Erasmus *et al*, 2017).This results shows that SBF dissolves the scaffolds with the formation of a weak crystalline phase of $Ca_4O(PO_4)_2$.Normally this peak is found at about 32° when using Cu K_α; however in this case the use of Co K_α may have caused a shift in the peak position. These peaks increased in intensity as the immersion time

and porosity increased. However, as observed by Fu *et al.*, (2007), the peak intensities were still well below those for a standard crystalline HA; this clearly indicates that the as-formed HA was incompletely crystallized or only weakly crystalline.

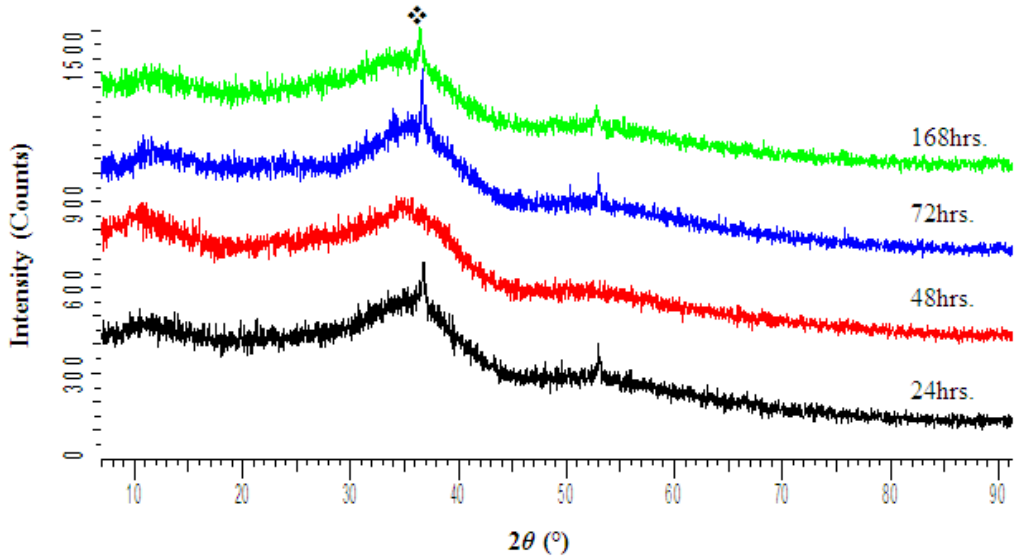

❖ $Ca_4O(PO_4)_2$

Figure 4-31: XRD traces of S53B50-60 vol. % $NH_4(HCO_3)$ immersed in SBF for 24; 48;72 and 168 hours

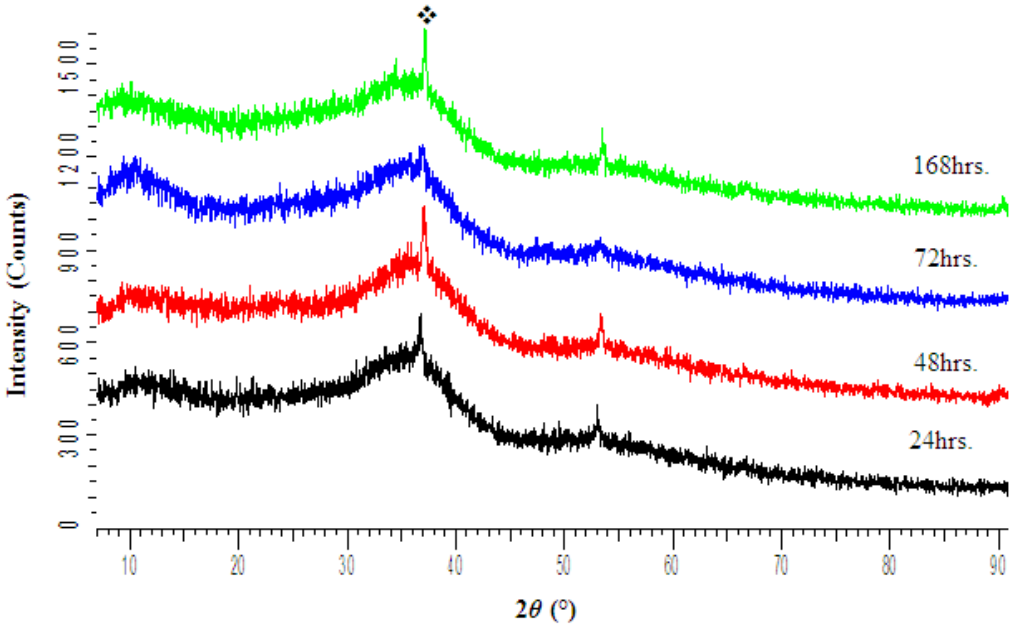

❖ $Ca_4O(PO_4)_2$

Figure 4-32: XRD traces of S53B50-70 vol. % $NH_4(HCO_3)$ immersed in SBF for 24, 48, 72 and 168 hours

The phase analysis for glass P40B10 and Sr was only carried out on scaffolds immersed for 168 hours in SBF as presented in Figure 4-33 and 4-34 respectively. The XRD results for both compositions (60 and 70 vol. %) were chosen at 168hrs to assess the formation of the HA layer only. The XRD pattern of P40B10 immersed for 168hrs remained identical to the untreated one. This shows that SBF dissolves the scaffolds without the formation of crystalline phase. On the other hand, a phase difference was observed for the Sr scaffolds before and after immersion in SBF. This is evident by the reduction in peak intensity, formation of new peaks as well as the disappearance of some peaks.

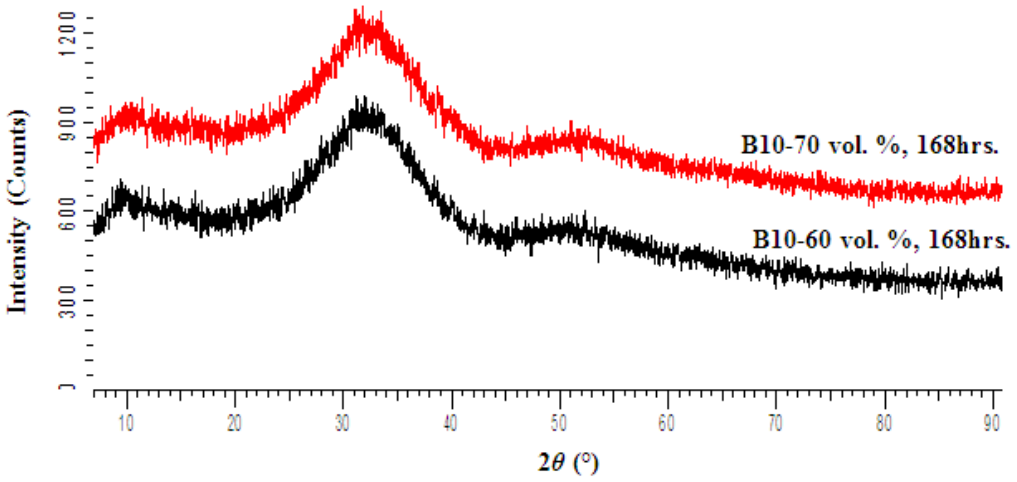

Figure 4-33: XRD traces of P40B10 mixed with 60 and 70 vol. % NH_4 (HCO_3) immersed in SBF for 168 hours

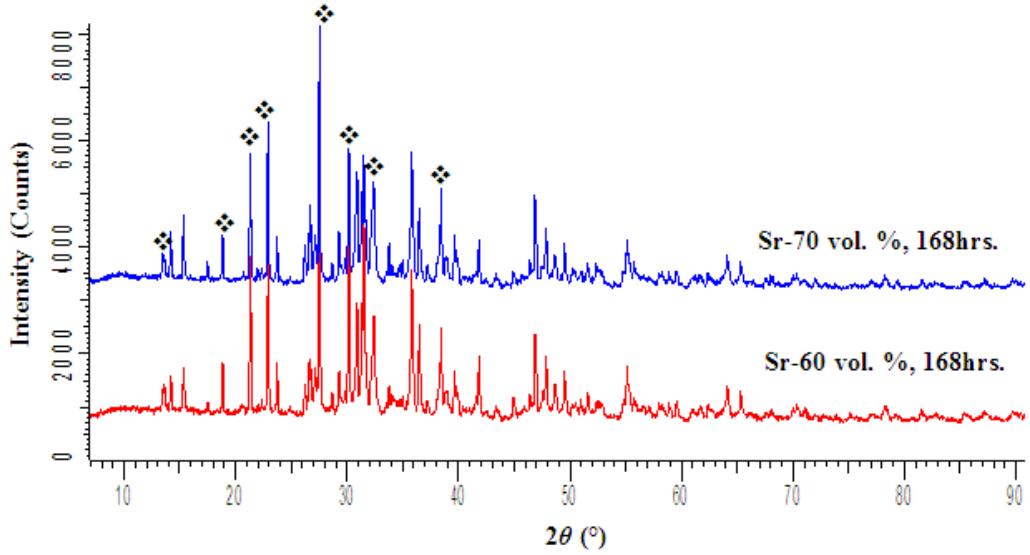

❖ Sr P_2O_6

Figure 4-34: XRD traces of Sr mixed with 60 and 70 vol. % NH_4 (HCO_3) immersed in SBF for 168 hours

4.5.4.2 SEM images

Figure 4-35 – 4-36 presents SEM micrographs of the scaffold surfaces of glass S53B50 after immersion in SBF for 24, 48, 72 and 168 hours. The images show that upon immersion precipitation of spherical particles occurs. These particles were also

found inside the pores of the scaffolds; which indicates good interconnectivity; hence; good permeability of the fluid. Interestingly; apart from the particles that were formed at the glass surface; a reactive layer also formed around the mouth of the pores.

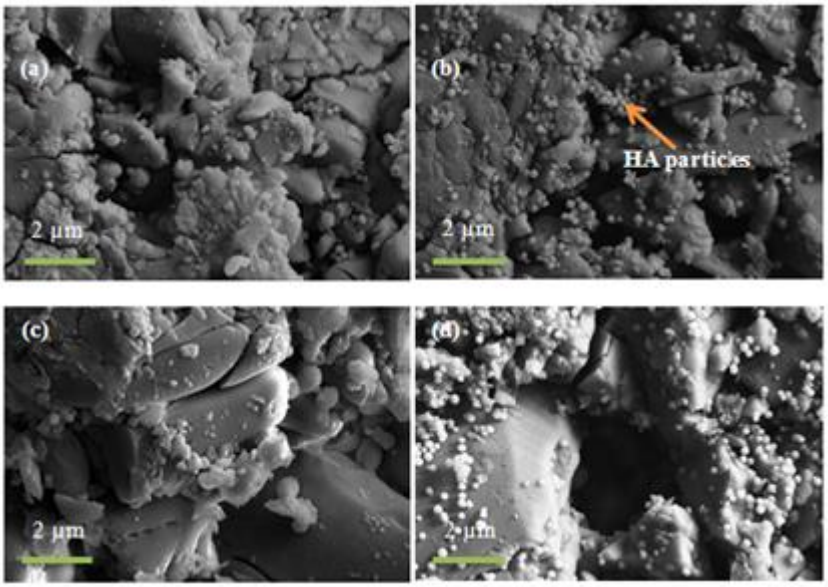

Figure 4-35: SEM images of the surface of S53B50-60 vol. % NH_4 (HCO_3) bioactive glass scaffolds after immersion in SBF for (a) 24, (b) 48 , (c) 72 and (d) 168 hours

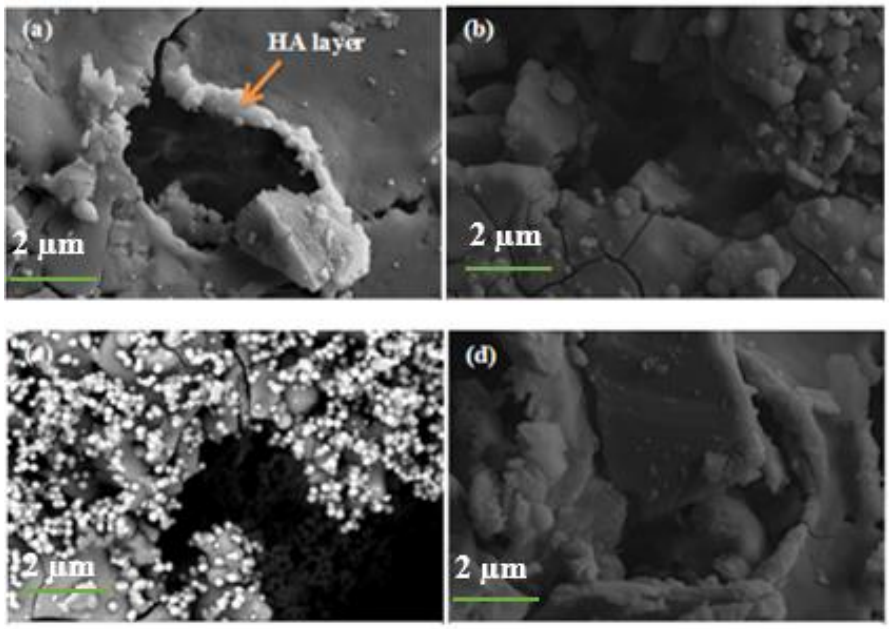

Figure 4-36: SEM images of the surface of S53B50-70 vol. % NH_4 (HCO_3) bioactive glass scaffolds after immersion in SBF for (a) 24, (b) 48, (c) 72 and (d) 168 hours

Figure 4-37 presents the SEM image and corresponding EDX analysis of one of the particle. From EDX analysis the Ca/P ratio is found to be 1.65. The presence of Si and Na come most likely from the glass underneath the particles. This is expected given the high penetration of X-ray.

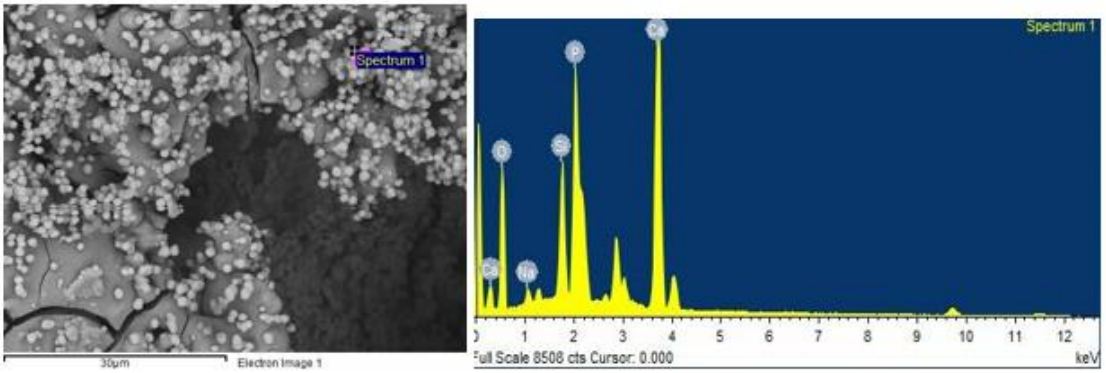

Element	Weight %	Atomic %
O	54.72	72.15
Na	1.58	1.45
Si	7.09	5.33
P	11.63	7.94
Ca	24.95	13.13

Figure 4-37: EDS spot analysis of as-formed HA particles on glass S53B50-70 vol. % $NH_4(HCO_3)$ after immersion in SBF for 24 hours

SEM images of the glass scaffold surface of P40B10 and Sr shown in Figure 4-38 and 4-39, respectively. In the case of the borophosphate scaffolds (Figure 4-38); signs of a reactive layer formation could be seen. However the surface coverage and the amount of globular particles was low. The phosphate scaffolds SEM images exhibit the evolution of a surface texture which cannot be related with the deposition of a reactive layer.

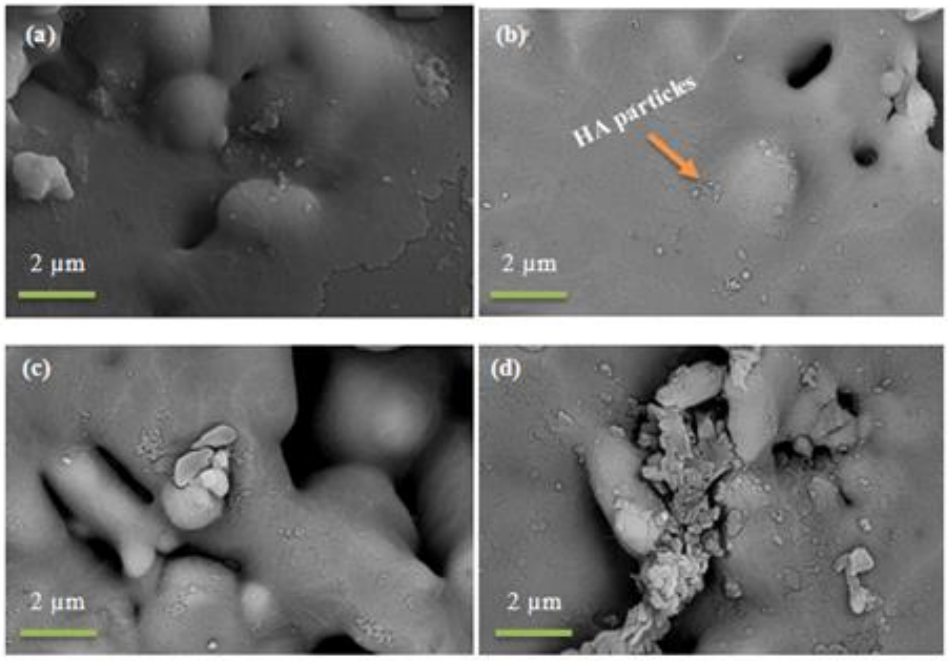

Figure 4-38: SEM images of the surface of P40B10-60 vol. % NH_4 (HCO_3) bioactive glass scaffolds after immersion in SBF for (a) 24, (b) 48, (c) 72 and (d) 168 hours

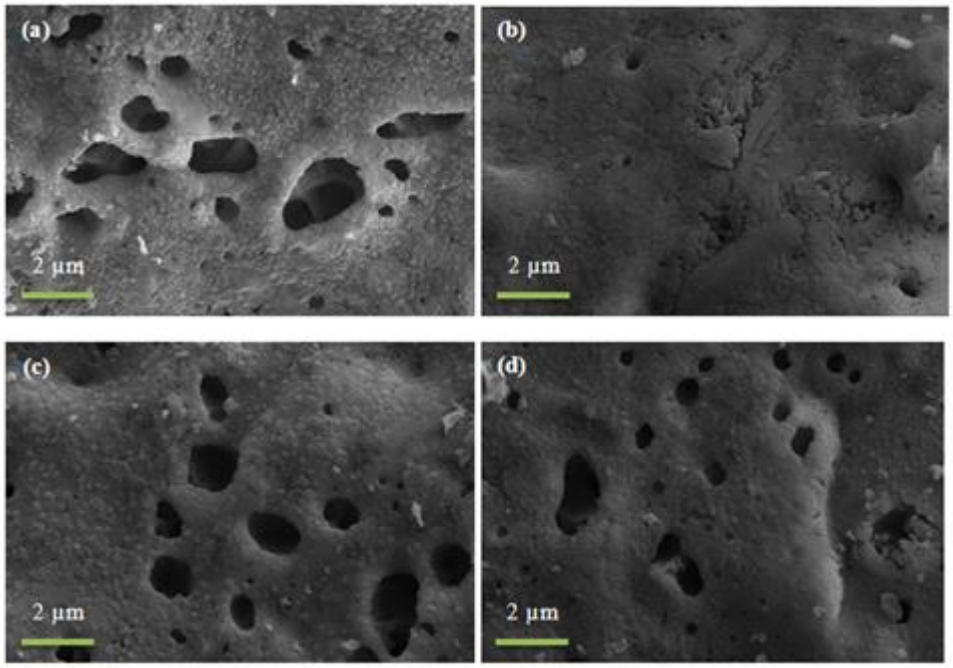

Figure 4-39: SEM images of the surface of Sr-60 vol. % NH_4 (HCO_3) bioactive glass scaffolds after immersion in SBF for (a) 24, (b) 48, (c) 72 and (d) 168 hours

Figure 4-40 presents the EDS analysis of the P40B10 surface after 168hrs immersion. From the calculation of the Ca + Sr/P ratio; the ratio was found to be 04.5 which correponds to the ratio of the original glass composition (~0.5).

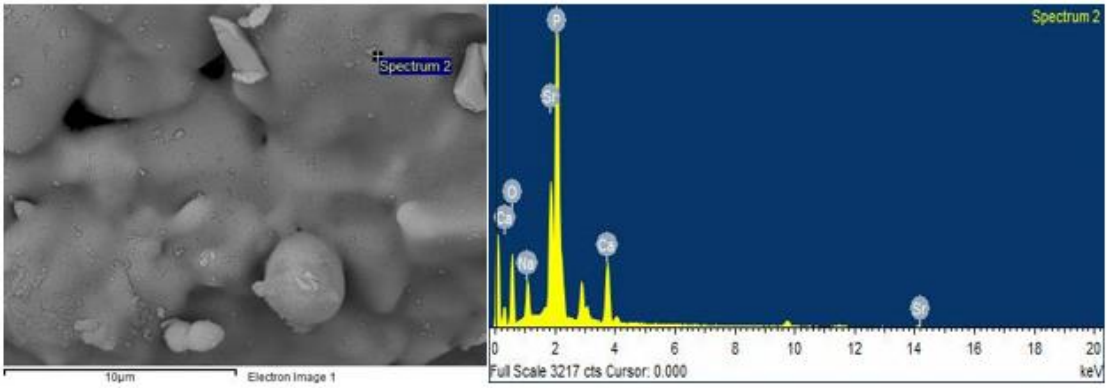

Element	Weight %	Atomic %
O	36.66	58.90
Na	4.25	4.75
P	30.10	24.99
Ca	8.18	5.25
Sr	20.81	6.11

Figure 4-40: EDS spot analysis of the as-formed HA particles on glass P40B10-70 vol. % $NH_4(HCO_3)$ after immersion in SBF for 168 hours

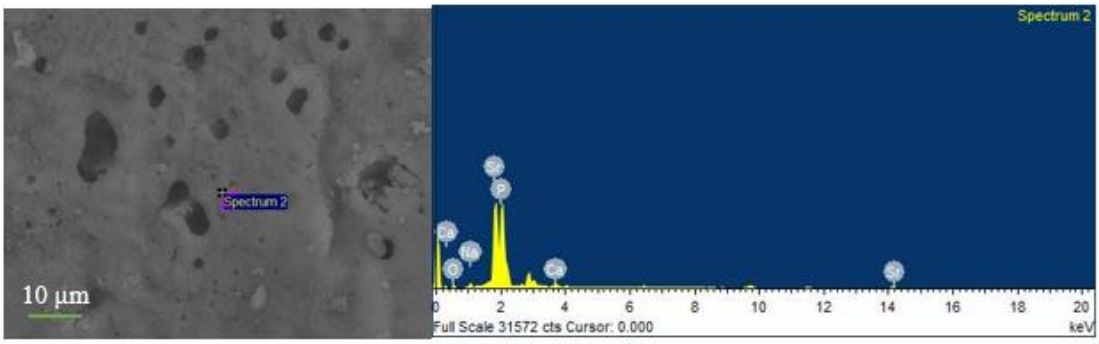

Element	Weight %	Atomic %
O	10.34	25.51
Na	1.49	2.56
P	38.28	48.78
Ca	1.27	1.25
Sr	48.63	21.91

Figure 4-41: EDS spot analysis of the as-formed HA particles on glass Sr-60 vol. % $NH_4(HCO_3)$ after immersion in SBF for 24 hours

Figure 4-41 presents the EDS analysis of the HA particles formed on the glass surface of Sr after immersion for 168 hours.

4.6 Mechanical properties

The compressive strength of the scaffolds before and after immersion in SBF as a function of immersion time and $NH_4(HCO_3)$ content are presented in Figures 4-42 and 4-43. The data in Figure 4-42 show that the compressive strength decreased significantly after 24 hours of immersion. This instant decrease in strength is a result of the porous structure of the scaffold as well as the dissolution of ions from the samples. The compressive strength of the immersed scaffolds was found to be slightly lower than the as prepared scaffolds. However, slightly higher compressive strength after immersion was also observed. Additionally lower compressive strengths were obtained at high $NH_4(HCO_3)$ content.

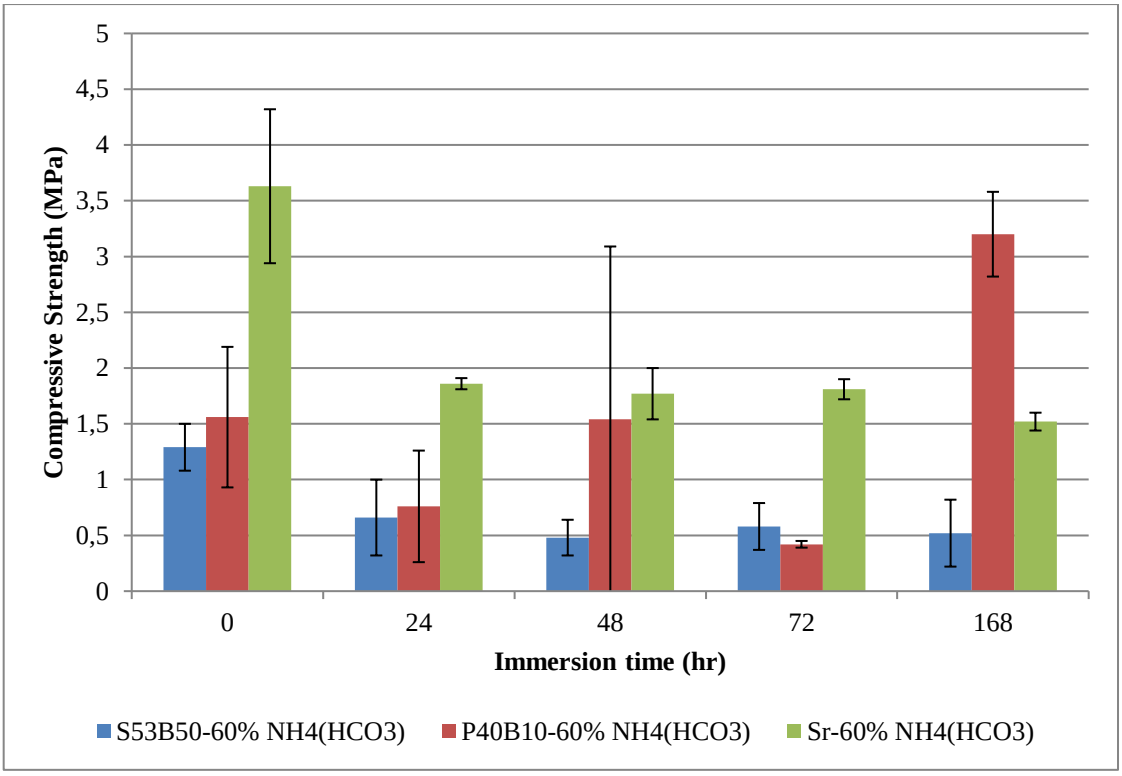

Figure 4-42: Compressive strength of scaffolds as a function of immersion time in SBF at 60 vol. % content

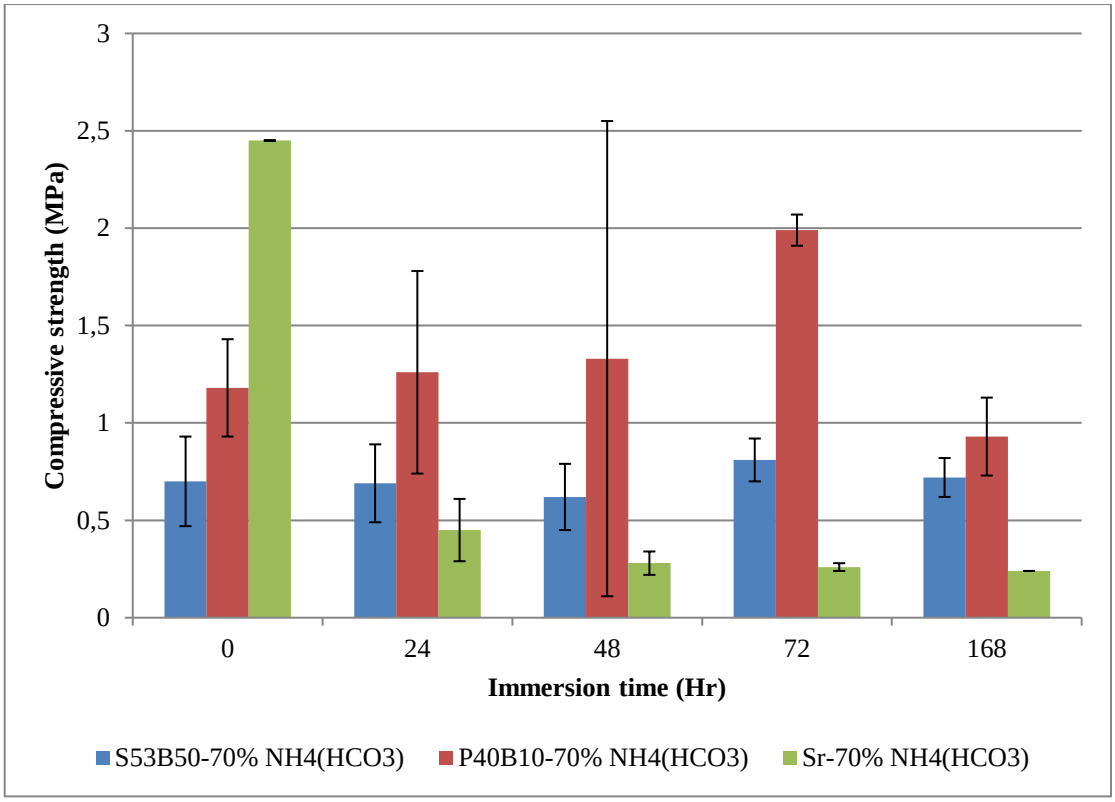

Figure 4-43: Compressive strength of scaffolds as a function of immersion time in SBF at 70 vol. % content

CHAPTER 5: DISCUSSION

This chapter gives a detailed explanation of the results obtained in Chapter 4. This includes the thermal properties of the glasses, densification and microstructural analysis of the sintered samples and their *in vitro* properties in simulated body fluid, mechanical properties

5.1 Densification and Microstructure of sintered glasses

5.1.1 Effects of particle size on crystallization

The particle size of the sintered glass powders with or without $NH_4(CO_3)$ has shown to have a critical effect on the crystallization of the glasses. The particle size for samples without $NH_4(HCO_3)$ were in average 20.5 µm, 18.4 µm and 26.4 µm for glasses S53B50, P40B10 and Sr respectively, while the average particle size for the glass powders sintered with $NH_4(HCO_3)$ was 39.9 µm, 32.8 µm and 46.3 µm for S53B50, P40B10 and Sr respectively. When the glass particles sintered without $NH_4(HCO_3)$ were used, the samples were fully dense as small particles have a greater driving force for sintering and allow better viscous flow of particles. However, small particles also have a large surface area. This not only increases the number of nucleation site, but also enhances the crystallization tendencies of the glasses by increasing the intensity of the exothermic peaks at low temperatures (Massera *et al.*, 2012). Aside from the particles size which might affect the crystallization kinetics, the presence of carbon, from the binder, at the particles surface may inhibit crystallization. This effect is mostly dominant with glass Sr, where crystallization is observed at temperatures as low as 480°C (Figure 4.7). Meanwhile, when the glass particles sintered with $NH_4(HCO_3)$ were used, the scaffold struts were fully dense and the particles were properly fused together despite the slightly larger particles. An advantage offered by the larger particles is the ability to sinter the glasses at the same temperature (as in the case of glass S53B50 and Sr sintered at 540°C (Figure 4.12) and still be able to control their crystallization. This is because large particles begin crystallising at higher temperatures for the reasons given above, thereby creating a wide sintering range. When the particle size of glass Sr was increased, it still endured crystallization but it was less pronounced.

Wu *et al.*, (2011) observed a similar behaviour, they showed that fine particles with <38 µm produced structures that were intact and well sintered with good particle packing and stacking. Unfortunately they had a large surface area which created a platform for crystal nucleation as recognised in this work. Meanwhile, the particle with >38 µm did not allow efficient sintering at 700°C as the particles were not properly fused together, hence, structures were not fully dense. Figure 5.1 presents the crystallization temperature of different bioactive glass as a function of particle size. Although these glasses have different composition, the commencement of crystallization was found to occur at temperatures lower than their onset of the crystallization temperature due to the small glass particles used during sintering.

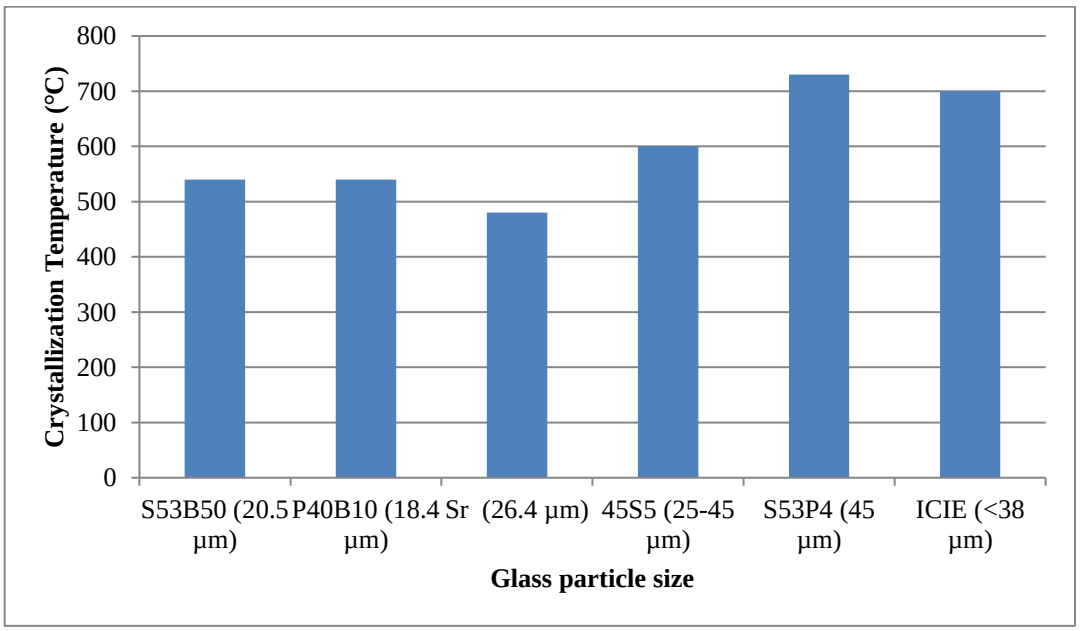

Figure 5-1: Crystallization temperature as a function of particle size (glass 45S5 (Fagerlund *et al.*, 2010)**; glass S53P4** (Massera *et al.*, 2012) **and glass ICIE** (Wu *et al.*, 2011))

5.1.2 Effect of sintering temperature on crystallization

All the DTA traces exhibited an endothermic event corresponding to the glass transition and an exothermic event corresponding to the crystallization of the glass. From the thermograph, T_g (glass transition temperature) and T_x (onset of

crystallization) were quantified and are indicated in the figures as well as in Table 4.3. ΔT ($\Delta T=T_x-T_g$), also presented in Table 4.3, is a gauge to the glass resistance to crystallization Fagerlund *et al.*, (2012a) and is often referred to as the hot working domain. According to Brauer, (2015), crystallization of bioactive glasses can be controlled by increasing the working range which is the temperature difference between crystallization and the glass transition. This stability range, ΔT, is the temperature range in which glass viscosity allows for sintering, fiber drawing, or other processing. A large temperature gap between glass transition and onset of crystallization suggests that viscous flow is more likely to occur prior to the crystallization. A small temperature gap between glass transition and onset of crystallization suggests a nucleation close to the glass transition temperature and therefore more risk of nucleation and growth of crystals, prior or during sintering. This phenomenon is depicted in Figure 5.2.

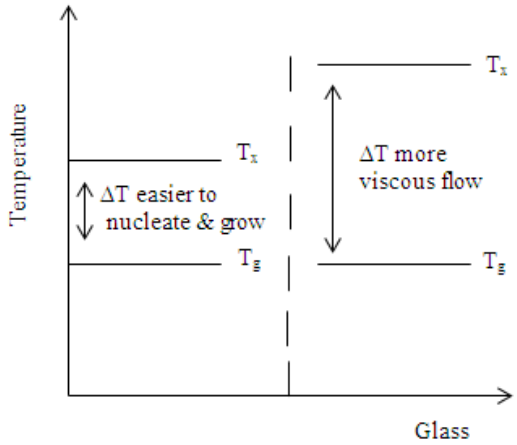

Figure 5-2: Effect of glass stability range (ΔT) on viscous flow sintering

As the primary objective is to sinter the glass particles by viscous flow sintering without any measurable crystallization, all sintering temperature should be chosen within the hot forming domain, i.e. between 510°C and 672°C, 509°C and 633°C, 430°C and 540°C for glasses S53B50, P40B10 and Sr, respectively. It is noteworthy that all glasses are expected to have a surface initiated crystallization as demonstrated for the Sr glass Massera *et al.*, (2015c) and for typical silicate bioactive glasses (Massera *et al.*, 2012) , (Massera and Hupa, 2014). It is therefore expected that with small particle size the risk of crystallization upon increasing temperature increases

due to an increase in the number of nucleation sites with increasing the surface area to volume ratio (Filho *et al.*, 1996) ,(Massera *et al.*, 2012) ,(Marrota *et al.*, 1981) ,(Ray and Day, 1997). Glass S53B50 and P40B10 have a wider processing window than glass Sr; therefore, the Sr glass is the most likely to endure crystallization during the sintering process.

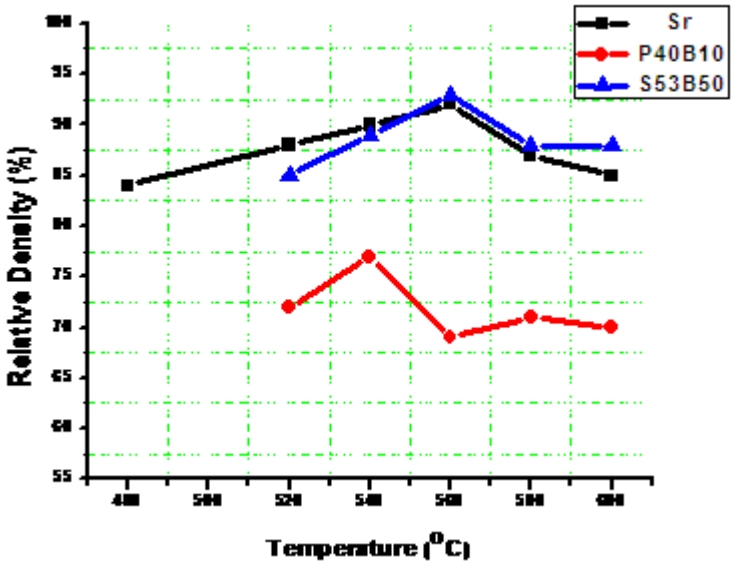

Figure 5-3: Relative density of S53B50, P40B10 and Sr bioactive glasses as a function of temperature sintered without $NH_4(HCO_3)$

The density of the sintered samples was determined by the Archimedes principle. From the density results presented in Figure 5-3, it can be seen that the relative density increased with increasing temperature. However, a decrease was observed when the temperature was increased beyond 560°C for glasses S53B50, Sr and 540°C for glass P40B10. The decrease in density may be attributed by the inhibition of the viscous flow of the particles caused by surface nucleation and/or crystallization; hence, particles may not fuse together properly during sintering resulting in poor densification of the material.

Glass P40B10 samples showed the same trend, but with slightly lower densification than S53B50 and Sr. This may be due to the fact that glass P40B10 has high activation energy for viscous flow. The maximum densification (TD %) achieved for glasses S53B50, P40B10 and Sr were 93%, 72% and 92% respectively.

From the XRD results of the samples shown in Figure 4.5 – 4.7, Figure 4.5 and 4.6 showed the onset of crystallization at temperatures between 520°C and 540°C while Figure 4.7 showed crystallization transition at 480ºC. With an increase in temperature the diffraction peaks sharpen and increase in intensity, as expected, due to an increasing crystallinity of the glass. This means that glass S53B50 and P40B10 can be sintered up to 540ºC without undergoing adverse crystallization in contrast to glass Sr, which will undergo crystallization at any sintering temperature. As expected, the crystallization occurs at lower temperature than T_c due to the small size of the glass particles sintered compared to the one analyzed by DTA. The XRD patterns also show the transitional behavior which led to the crystallization of the individual glasses. Furthermore it can also be seen that the density of the samples decreases as the intensity of the peaks increases with temperature. This evidently shows how crystallization affects the densification of amorphous materials.

SEM images of the cross section of the sintered samples revealed a dense microstructure which explains the high theoretical densities obtained between sintering temperatures of 480°C – 560°C as shown in Figure 4.8-4.10. However at 580°C - 600°C the presence of micropores is also evident, which contribute to the reduction in theoretical density as observed. These micropores might be residual porosity as a result of the incomplete sintering process. Figure 4.11 shows the SEM micrographs, recorded with backscattered electrons, of the samples sintered at 600°C for glass (a) P40B10 (b) S53B50; and (c) Sr at high magnification. There is strong evidence of crystals forming in the P40B10 glass; whereas the darker areas correspond to the crystals and the brighter areas to the remaining glass. This strongly correlates with the XRD patterns in Figure 4.6. SEM investigation of glass S53B50 showed almost no or minor presence of crystals. This is in agreement with the XRD pattern (Figure 4.5) exhibiting low number of diffraction peaks with low intensity indicating reminiscence of a mainly amorphous matrix. The XRD patterns of glass Sr (Figure 4.7) show adverse crystallization and this is clearly aided by the SEM micrographs of the glasses which reveal high volume of crystals present on the cross section of the samples. Similar results have been reported by Massera *et al.*, (2015c) where rapid surface crystallization led to fully crystallized particles at such temperatures. In contrast to the crystallization mechanism of glass S53B50; crystals of

glass P40B10 appeared to be irregularly shaped and clustered together while crystals of glass Sr exhibit a thatch like shape covering the surface of the sintered body.

As observed by the high densification results obtained in Figure 5.3, the porosity achieved during sintering was too low to meet one of the requirements of an ideal scaffold, which is high porosity; therefore it was necessary to add porogens in order to increase the porosity. In this work, the required porosity was obtained by mixing $NH_4(HCO_3)$ with the glass powder. The low densification results obtained in Table 4.5 indicates that high porosity was obtained by incorporating $NH_4(HCO_3)$ as the pore forming agent. This was achieved by burning out the pore forming agent $NH_4(HCO_3$ before sintering, thereby creating the pores as observed in Figure 5.4. As the sintering temperature was increased, the glass particles fused together and densified around the pores. This action is illustrated in Figure 5.4. In addition the formation of such high porosity may also be attributed by the high volume expansion (more than 1000 times) ratio during decomposition of $NH_4(HCO_3)$ (Locs *et al.*, 2013).

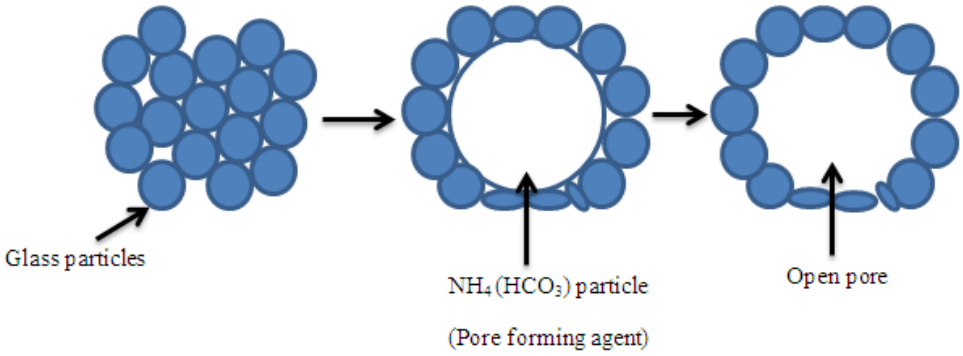

Figure 5-4: Schematic diagram on the fabrication of highly porous scaffolds during sintering

A similar trend was observed by Locs *et al.*, (2013), whereby the open and total porosity were found to increase from 25 to 69% and from 32 to 73% when $NH_4(HCO_3)$ content was varied from 0 to 2.75 wt. %. The investigated glass compositions reached an open porosity of more than 60% at the addition of 70 vol. % (0.56 wt. %) $NH_4(HCO_3)$, with glass Sr obtaining the highest open porosity of 72%. Table 5.1 presents the sample compositions as prepared by Locs *et al.*, (2013) and the glass samples investigated in this work. From the table, the low content of NH_4HCO_3 added as a function of wt. % to the HAp powder resulted in a low open porosity in contrast to the high contents of NH_4HCO_3 that was incorporated into the bioactive glass

powders; hence, the high porosity despite the glasses having a lower wt. %. The addition of the small amount of NH_4HCO_3 used by Locs *et al.*, (2013) despite having a high wt.% could be due to the fact that they used a fixed mass for HAp; whereas in this work, the overall mass (of 2 grams) was composed of both the glass powders and NH_4HCO_3 foaming agent with the mass of the foaming agent determined by the respective wt. %.

Table 5-1: List of sample compositions

HAp Sample	**HAp ,g**	**NH_4HCO_3, g**	**NH_4HCO_3, wt. %**	**Glass samples**	**Powder, g**	**NH_4HCO_3, g**	**NH_4HCO_3, wt. %**
S4	2.6	0.00	0.00	**0**	2.00	0.00	0.00
S5	2.6	0.05	0.90	**B50-60**	1.05	0.95	0.48
S6	2.6	0.06	1.10	**B50-70**	0.83	1.17	0.59
S7	2.6	0.07	1.30	**B10-60**	1.11	0.89	0.45
S8	2.6	0.08	1.40	**B10-70**	0.89	1.11	0.56
S9	2.6	0.10	1.80	**Sr-60**	1.09	0.91	0.46
S10	2.6	0.15	2.70	**Sr-70**	0.87	1.13	0.57

5.2 In vitro properties of the scaffolds

5.2.1 Variation of pH

The pH of the SBF was assessed as a function of time. As mentioned earlier; the dissolution and conversion reactions that led to weight loss of the scaffolds are expected to be the same reactions that control the pH of the SBF solution. Evidently, the increase in pH of the SBF with immersion time of the scaffolds showed similar trend with weight loss results. The increase in pH of S53B50 SBF solution (Figure 4.21) might have resulted from the dissolution of glass ions such as Si^{4-}, Na^{+}, Ca^{2+} ions which increased the pH of solution. This increase in pH is typical for silicate bioactive glasses (Zhang *et al.*, 2008) and is known to aid apatite formation (Aina *et al.*, 2009), (Brauer *et al.*, 2010), (Fredholm *et al.*, 2012). The dissolution mechanism that leads to the increase in pH is shown in Figure 5.5.

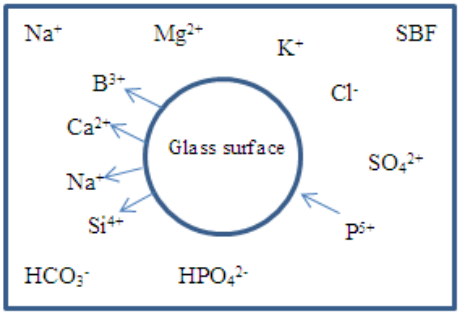

Figure 5-5: Initial ion dissolution mechanism of conversion of glass S53B50 to HA

The decrease in pH of P40B10 and Sr solutions (Figure 4.22 and 4.23, respectively) may be related to the change in P content in the solution which will reduce the alkalinity/basicity caused by the dissolution of Na^{+}, Ca^{2+} and Sr^{2+} ions as shown in Figure 5.6. In addition, glass P40B10 and Sr contain high contents of P_2O_5, and the dissolution of phosphate glasses being congruent often leads to larger amount P^{5+} ions being released into the solution. Therefore when the (P_2O_5) ions were being released into the solution, it may have reacted with water to form phosphoric acid ($H_3PO_4^{-}$) which consequentially dissociates producing H_3O^{+} and PO_4^{3-} ions causing a decrease in pH due to the increase of dissociated H_3O^{+}. Although this acidic environment is not desirable for the formation of apatite, it has been reported by Krajewshi and Ravaglioli, (2002) that a low pH is also advantageous for bioactivity as a pH of 7.2 is still optimal in physiological fluid for apatite formation.

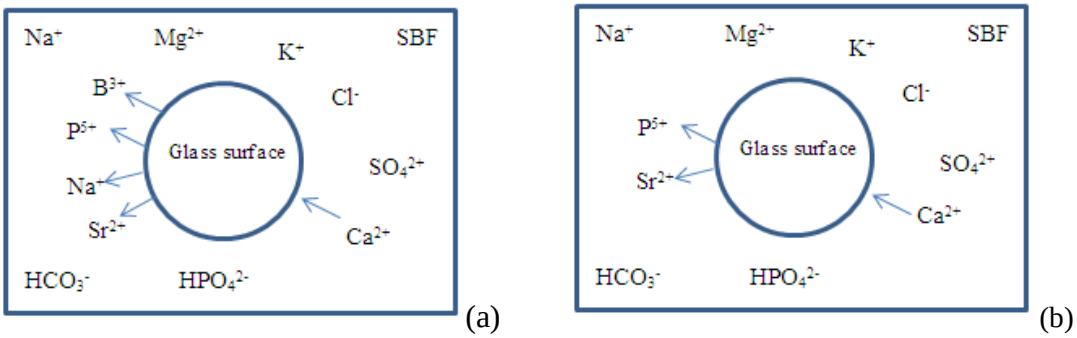

Figure 5-6: Initial ion dissolution mechanism of conversion of glass (a) P40B10 and (b) Sr to HA

5.2.2 Variation of mass

The results of the weight loss in Figure 4.24 indicate that the addition of B_2O_3 in the borosilicate glass (S53B50) composition resulted in an increase in the conversion rate of the scaffolds. It is known that the addition of B_2O_3 brings changes in the glass network which disrupts the 3D Si-O network and forms [BO_3^-] trihedral or chains of (BO_3) triangles. In contrast to Si, it is difficult for B to completely form a 3D network due to its threefold coordination number; this effect aids the apatite formation of biomaterials. On the other hand, the conversion rate of P40B10 and Sr shown in Figure 4.25 and 4.26, respectively may be associated with the substitution of CaO with SrO, since SrO and CaO are both glass modifiers and have similar coordination numbers; they are expected to have the same effect in the glass network. However, despite both compositions having similar SrO content, glass Sr had the fastest dissolution rate and weight loss. This may be due to the addition of B_2O_3 into the P40B10 composition which stabilized the system as well as the partial substitution of SrO for CaO, whereas for Sr, CaO was fully substituted by SrO as it has been reported that full substitution enhances apatite formation.

5.2.3 ICP analysis

As seen in Figure 4.21, the pH of the solution increased with immersion time. This increase in the solution's pH can be attributed to the release of B^{3-}, Ca^{2+} and Si^{4-} ions in solution as supported by the concentration in Figure 4.27a, b and c. Meanwhile the decrease in the solution's pH of P40B10 and Sr presented in Figure 4.22 and 4.23 respectively was due to the increase in P content as shown Figure 4.28 and 4.29, respectively. This increase indicates phosphorus was released into the solution from the glass surface, on the other hand, a decrease in P content as observed for glass S53B50 indicate phosphorus was taken up by the scaffold from the solution.

Normally it is expected that, with large content of P released into the solution, the amount of calcium consumed from the solution will also be high. However, in this work it has been observed that despite glass Sr having released a higher concentration of P than glass P40B10 there was no difference in the amount of Ca consumed. This also explains why glass P40B10 had a more stable or less pH variation than glass Sr. Additionally, Massera *et al.*, (2013) reported that by increasing the SrO content of phosphate glasses a large consumption of Ca is expected, however contrary to this study, it was found that an increase in SrO content in glass Sr had no effect on the Ca

consumed as both P40B10 and Sr had a similar Ca concentration profile despite the difference in SrO content. Nonetheless, the decrease in Ca content suggested that HA was progressively being formed on the glass surfaces as this indicates that the Ca^{2+} ions were consumed when the glasses were. Whilst on the other hand, an increase in Ca content for glass S53B50 shows that the Ca^{2+} ions were released from the glass surface into the solution and this action also supports the formation of HA on the glass surface. The increase in Sr concentration of glass Sr with respect to SrO was also observed by (Fredholm *et al.*, 2012), (Massera *et al.*, 2013). Si was progressively released into the solution from the glass surface and its concentration increased with immersion time as observed in Figure 4.21d. Jones *et al.*, (2006) also observed a similar behaviour from their 70S30C bioactive glass foams.

5.2.4 Phase and Microstructural analysis

5.2.4.1 XRD analysis

The XRD patterns for glass P40B10 scaffolds (see Figure 4-33) showed a broad shallow peak which indicates that even after being immersed for 168hrs, they maintained the amorphous state. This does not necessarily mean that no HA was formed, but it is possible that the precipitated HA was rather amorphous and did not fully crystallize. Meanwhile, although the as-prepared scaffolds of glass Sr showed adverse crystallization during sintering, this did not prevent the scaffolds from reacting or forming HA. When compared to the XRD patterns of the as-prepared scaffolds, the immersed scaffold (shown in Figure 4-34) showed a reduction in peak intensity, formation of new peaks as well as the disappearance of some peaks. This clearly indicates that crystallization did not inhibit the reactions that led to the formation of HA. Additionally, strontium phosphate (SrP_2O_6) was found to be the main phase formed in glass Sr; this does not necessarily mean that strontium substituted HA particles were formed on the glass surface but indicates that the glass scaffolds were enriched with Sr and P. However, it is difficult to state if the as formed HA particles were crystalline or amorphous.

5.2.4.2 SEM analysis

SEM images show the formation of HA particles on the surfaces of all glasses as indicated by the arrows in Figure 4-31 - 4-32 for S53B50. SEM/EDX analysis were

also performed on the on the scaffolds with 70 vol. % and the same HA precipitation was observed. The images show that apatite starts to grow in a spherical morphology on the glass within 24 hours and completely covers the surface within the week. These particles were also found inside the pores of the scaffolds; which indicates good interconnectivity; hence; good permeability of the fluid. Similar particles which are typical of HA deposited by precipitation from solution were observed by (Fu *et al.*, 2010), (Chen *et al.*, 2006). A typical behavior of bioactive glasses is the formation of a silica rich layer during the conversion reactions. This layer often forms on the surface of the glasses and separates the precipitated HA from the unconverted glass. This indicates that the apatite (HA) is easily nucleated on the silica gel when the starting pH of the environment increases slightly and this formation of HA clearly correlates with the pH variation in Figure 4.22. The presence of this layer/gel is often evidenced by the formation of scales on the glass surface aided with cracks endured during sample drying (see Figure 5-7). In addition alkaline solutions are known to aid apatite formation. Interestingly; apart from the HA particles that were formed on the glass surface; an HA layer was also formed around the mouth of the pores.

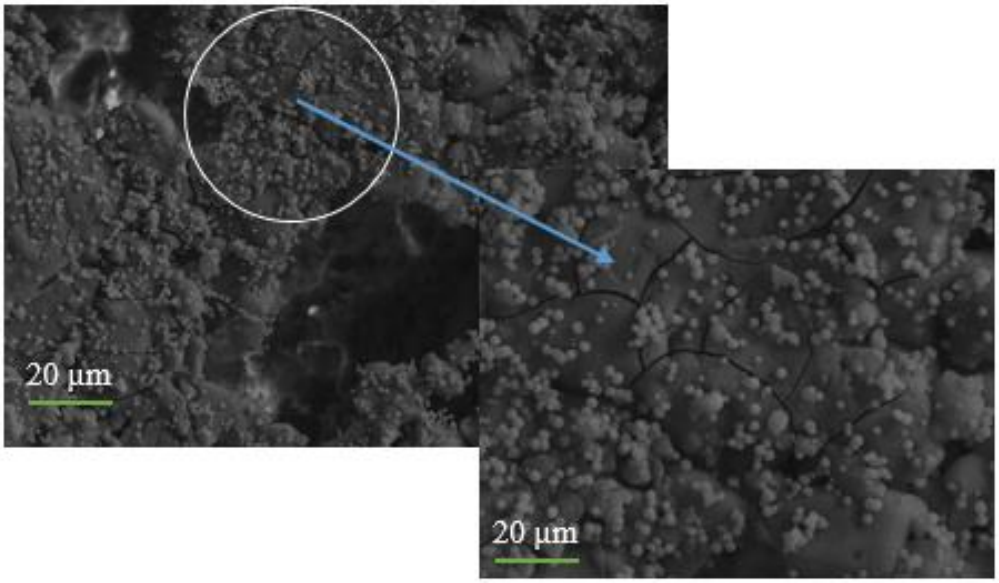

Figure 5-7: SEM images of the surface of S53B50-70 vol. % NH_4 (HCO_3) bioactive glass scaffolds after immersion in SBF for 24 hours

It is well known that the ideal stoichiomteric Ca/P ratio of HA is 1.67, therefore it was necessary to carry out EDS analysis (shown in Figure 4-37) on the as-formed HA

particles and determine its Ca/P ratio. The Ca/P atomic ratio was found to be 1.65 which is close to the value (1.67) , this indicates conversion of the S53B50 glass to HA.

The presence of these globular particles are present in all samples, however they become fewer with decreasing pH as observed for P40B10 and Sr scaffolds shown in Figure 4-38-4-39, respectively. A typical behaviour of bioactive glasses is the formation of a silica rich layer during the conversion reactions. This layer often forms on the surface of the glasses and separates the precipitated HA from the unconverted glass. Due to its porous nature there is a continuous dissolution of ions through the SiO_2-rich layer into the solution. Eventually the Ca^{2+} from the glass surface and PO_4^{3-} from the solution react resulting in the precipitation and growth of HA on the glass surface. Meanwhile the HA particles formed on glass Sr and P40B10 were a result from the reaction between Sr^{2+} and PO_4^{3-} which allowed for precipitation of strontium substituted HA particles. These mechanisms are presented in Figure 5-8 which shows the adhesion of Ca^{2+}, PO_4^{3-} and Sr^{2+} ions to the silica gel surface forming a bone-like HA.

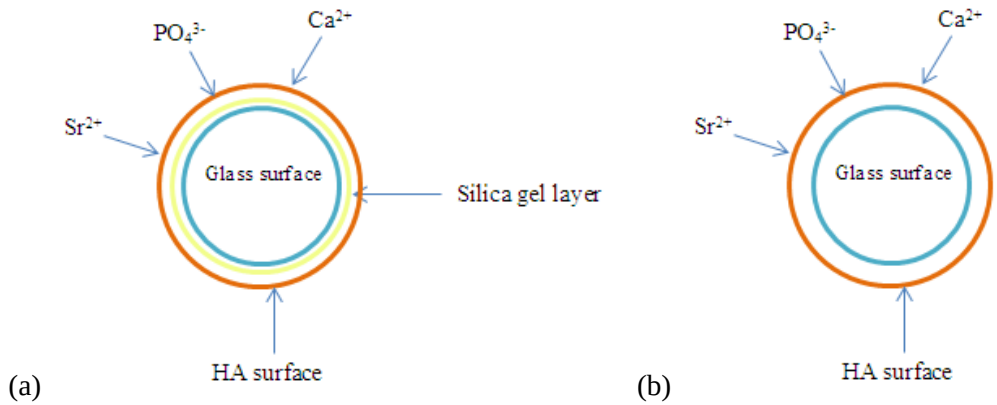

Figure 5-8: Final mechanism of conversion of glass (a) S53B50, (b) P40B10 and Sr to HA in SBF

The EDS analysis for glass P40B10 are shown in Figure 4-39 after immersion for 168 hours. From the Ca + Sr/ P ratio; the ratio was found to be 0.45 which is far from the conventional ratio of HA which has been reported to be around 1.67. This indicates that the as-formed HA particles did not fully crystallize to HA and this behaviour was also supported by the XRD results in Figure 4-32 where no HA peaks were detected.

Figure 4-40 showed the EDS analysis of the Sr scaffold after immersion for 24 hours. An observation from this analysis is the presence of Ca on the glass surface, this indicates that some Ca^{2+} has precipitated from the solution in the surface layers. It is note worthy that this was a CaO free glass.

The formation of HA is presented in the form of small spherical particles in the above Figures. When these dissolution and precipitation reactions are allowed to continue a thick reaction product layer is often formed from the surface of the particle inward. In this case; this layer is formed around the pore (see Figure 4-36a and d). It is worth noting that the cracks observed on the glass surfaces are the dried silica gel which occurred during drying of the scaffolds after immersion. In addition the presence of the HA particles on the glass surface corresponds to the HA peaks observed on the XRD traces. EDS analysis in Figure 4-37 showed that the scaffolds had a Ca/P ratio of 1.65 which is close to the stoichiometric value of HA. This essentially indicates that the reaction almost completely converted to HA.

It is noteworthy to mention that, although HA particles were formed on the glass surface of P40B10, XRD traces (in Figure 4-33) showed no HA peaks. This clearly confirms that the HA particles were incompletely crystalline hence the broad amorphous XRD pattern. Additionally, as expected, HA formed much faster on glass Sr scaffolds compared to P40B10 as a result of its fast dissolution rate and high phosphate content.

5.3 Mechanical properties

The mechanical properties of the glass scaffolds obtained from sintering of particles in different particle size with different porosities were measured. The mechanical strength was found to decrease for all particle size as the porosity of the scaffold increases. This is due to the increase in void space on the scaffold which makes the scaffold structurally prone to collapse even at lower mechanical stress. It is also well reported in literature that porous structures have relatively high porosities which consequently results in the materials having poor mechanical strength.

The compressive strength of the as-prepared scaffolds (Figure 4-42) of S53B50 was 1.29 ± 0.21 MPa. In comparison, the compressive strength of the as prepared scaffold of P40B10 was 1.56 ± 0.63 MPa while Sr had strength of 3.63 ± 0.69 MPa. This value was found to be in the range of 2 – 12 MPa which has been reported for the

cancellous bone (Rahaman *et al.*, 2011). All these values were obtained at 60 vol. % content of NH_4 (HCO_3). Figure 4-43 also shows that upon immersion in SBF, the compressive strength of the scaffolds decreased with increasing immersion time and porosity. In addition, as was expected, the compressive strength of the scaffold after immersion was found to be lower than that of the as-prepared although it was also observed that some scaffolds had high strength after immersion. Glass S53B50 had a moderate degradation rate and it is clearly evident that the foaming agent content had no significant change in the compressive strength of the scaffolds immersed from 24 to 168 hour in SBF. Meanwhile glass P40B10 which has the slowest degradation rate was found to maintain its mechanical properties for a longer time. It is worth noting that the scaffolds of glass P40B10 did not display any monotonic decrease or increase and the unusual high strength was observed for these scaffolds after immersion. Once again this might be due to some debris from degradation which filled up the pores. Lastly, glass Sr showed a trend similar to glass S53B50. However its fast degradation and reaction time lead to a drastic decrease in compressive strength as can be seen in Figure 4-42 and 4-43. In addition, the high strength of glass Sr might be due to the crystalline phases formed in the amorphous matrix, as it has been reported by Kauer *et al.*, (2014) that crystallization enhances the mechanical properties of bioactive glass. However, this strength comes at the expense of the glass bioactivity as observed with the slow conversion to HA. Furthermore it was also observed that there is no correlation between the sintering temperature and the mechanical properties of the scaffolds. Normally it is expected that at high sintering temperature a high compressive strength is to be obtained due to the well densified and strong struts of the scaffolds formed during sintering, however in this work, the compressive strength of S53B50 and P40B10 were found to be lower compared to Sr, despite Sr being sintered at a temperature 40°C lower than the sintering temperature of S53B50 and P40B10. This also indicates that Sr particles bond better during sintering compared to the particles if S53B50 and P40B10.

The stress/strain curves recorded during the compression test of the scaffolds are shown in Figure 5-9 – 5-10 for glasses S53B50, P40B10, respectively. Figure 5-9 showed a typical rupture of ceramic foam (Gibgson and Ashby, 1988): which in this case no elastic region was observed; however an initial fracture of the solid walls

between pores is clearly displayed by the curve which ends by failure of the scaffold struts normally as a result of cracking, bending or buckling. These actions provide the maximum compressive strength of the scaffolds. The curve is further characterized by the progressive failure of the pore walls until the scaffolds become powder followed by the densification region which signifies compression of the powder. This same compressive behaviour was observed by Jones *et al*., (2006) when they tested the compressive strength of their 70S30C glass foams, however their foams displayed an elastic region. The stress/extension curve for P40B10 scaffolds is shown in Figure 5-10 and exhibits a similar behaviour; however the densification region is not reached here due to the fragmentation of the scaffolds.

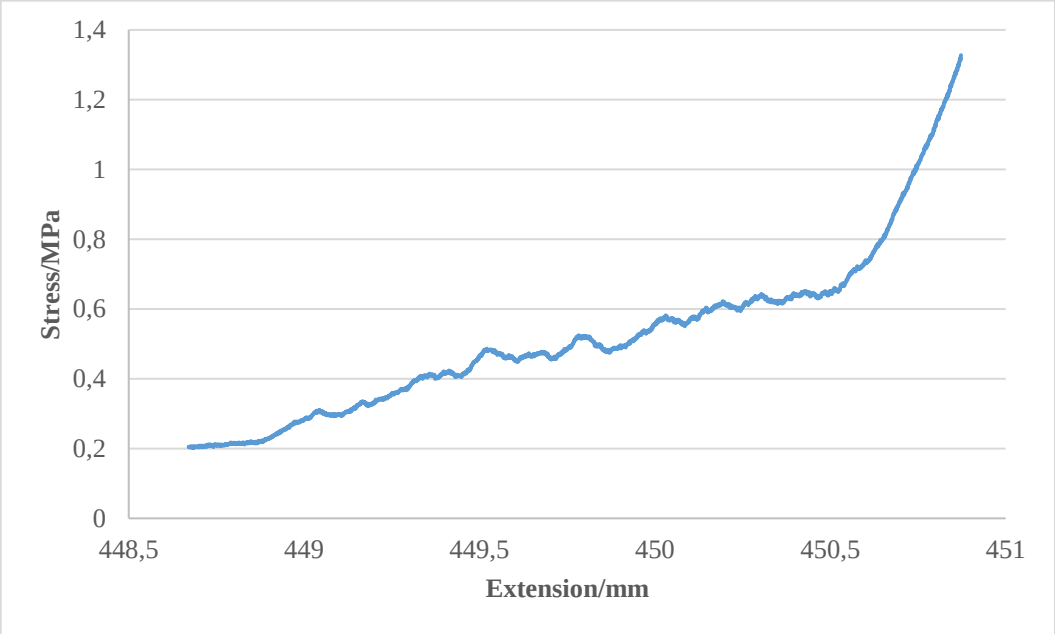

Figure 5-9: Typical stress/extension curve for S53B50 prepared with 70 vol. % $NH_4(HCO_3)$ immersed in SBF for 168 hours

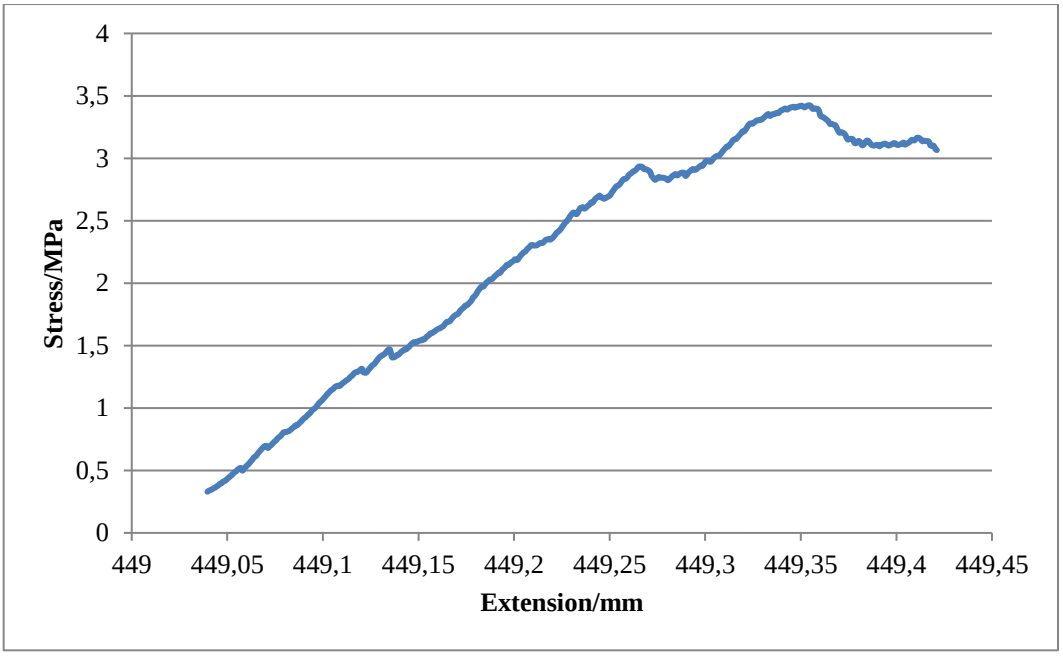

Figure 5-10: Typical stress/extension curve for P40B10 prepared with 60 vol. % $NH_4(HCO_3)$ immersed in SBF for 168 hours

CHAPTER 6: CONCLUSIONS and FUTURE WORK

In this thesis, the potential for the processing of scaffolds for tissue engineering was assessed for three glass types, i.e. borosilicate (S53B50), borophosphate (P40B10) and phosphate (Sr). These glasses were found, in the past, to have promising antimicrobial and dissolution properties towards healing of injured bones. However, in tissue engineering it is well accepted that a scaffold with large porosity and interconnected pores is required to reach optimum clinical application.

The crystallization and sintering ability of S53B50, P40B10 and Sr was investigated without the addition of $NH_4(HCO_3)$ foaming agent in the temperature range of 480°C – 600°C. Glasses S53B50 and P40B10 were found to exhibit crystalline peaks at 540°C while glass Sr does so at 480°C; this suggests that glass Sr is highly prone to crystallization due to its lower glass stability. Bioactive glass scaffolds from these compositions (S53B50, P40B10 and Sr) were produced by using a foaming agent ($NH_4(HCO_3)$) at a content of 60 and 70 vol. % followed by sintering using a heating rate of 10°C/min for 1 hour at 500°C and 540°C for glass Sr and S53B50, P40B10, respectively. It was found that, increasing the size of the glass particles inhibited to some extent the glass crystallization as observed during the sintering process where no crystallization peaks were identified at 540°C for S53B50 and P40B10 in contrast to the samples sintered without $NH_4(HCO_3)$. This indicates that the scaffolds from these two compositions maintained their amorphous nature.

Open porosity of more than 60% was achieved at 70 vol. % addition of $NH_4(HCO_3)$ and an average interconnected pore diameter in the range of 243.8 – 285.5 μm. As prepared, the S53B50 scaffold has a compressive strength of 1.29 ± 0.21 MPa, which decreased to 0.52 ± 0.3 MPa after immersion in SBF for 168 hours. In comparison, the as prepared P40B10 scaffolds had a compressive strength of 1.56 ± 0.63 MPa, which increased to 3.2 ± 0.38 after immersion for 168 hours in SBF while Sr had strength of 3.63 ± 0.69 MPa, which decreased to 1.52 ± 0.08 MPa after 168 hours immersion in SBF. These values were obtained at 60 vol. % content. After 168 hours in SBF, the weight loss of S53B50 and Sr was 6.36 ± 0.31 and 11.58 ± 0.38, respectively. This clearly indicates that Sr had a faster degradation rate. However, due to the acidic environment of the solution, the conversion rate to HA was inhibited. Similar behavior was observed for P40B10 but with slow degradation of the glass.

Despite the low weight loss of S53B50, which indicates a moderate degradation rate, S53B50 was found to have the fastest conversion rate to HA.

These glass compositions, at the exception of the glass Sr, have shown to be promising in terms of apatite formation and can be successfully processed into porous scaffolds, while maintaining their amorphous nature, which are favorable for supporting tissue ingrowth.

In addition, further work should be done to investigate the effects of $SrAl_2O_4$ luminescent on the mechanical and in vitro properties of the glasses.

REFERENCES

Ahmed, A. A., Ali, A. A., Mahmoud, D. A. R., & El-Fiqi, A.M. (2011). "Preparation and Characterization of Antibacterial P_2O_5 – CaO – Na_2O – Ag_2O Glasses", *Journal of Biomedical Materials Ressearch*, vol 98A(1).

Aina, V., Malavasi, G., Pla, A. F., Munaron, L., & Morterra, C. (2009). "Zinc-containing bioactive glasses : Surface reactivity and behaviour towards endothelial cells", *Acta Biomaterialia*, vol 5(4), pp. 1211–1222.

Ambrosio, A. M. A., Sahota, J. S., Khan, Y., & Laurencin, C. T. (2001). "A Novel Amorphous Calcium Phosphate Polymer Ceramic for Bone Repair : I . Synthesis and Characterization", *Journal of Biomedical Materials Research*, vol 58(3), pp. 295–301.

Anderson, O.H., Liu,G., Karlsson,K.H., Niemi,L., Miettinen,J., Juhanoja,J. (1990)." In vivo behaviour of glasses in the SiO_2-Na_2O-CaO-P_2O_5-Al_2O_3-B_2O_3 system", *Journal of Materials Science: Materials in Medicine*, vol 1, pp. 219-227.

Arstila, H., Hupa, L., Karlsson, K. H., & Hupa, M. (2008). Influence of heat treatment on crystallization of bioactive glasses. *Journal of Non-Crystalline Solids*, vol 354(2–9), pp. 722–728.

Bae S.B & Weinberg M.C. (1991)." Oxidation -reduction equilibrium in copper phosphate glass melted in air", *Journal of the American Ceramic Society*, vol 74(12), pp. 3039-3045.

Banno, T., Yamada, Y., & Nagae, H. (2009). "Fabrication of porous alumina ceramics by simultaneous thermal gas generating and thermal slurry solidification", J*ournal of the Ceramic Society of Japan*, vol 117(5) , pp. 713–716.

Brauer, D. S. (2015). "Bioactive Glasses — Structure and Properties", *Angewandte Chemie International Edition*, vol 54, pp. 4160–4181.

Brauer, D. S., Karpukhina, N., Donnell, M. D. O., Law, R. V, & Hill, R. G. (2010). "Fluoride-containing bioactive glasses : Effect of glass design and structure on degradation , pH and apatite formation in simulated body fluid". *Acta Biomaterialia*, vol 6(8), pp. 3275–3282.

Brink, M. (1997). "The influence of alkali and alkaline earths on the working range for bioactive glasses", *Journal of Biomedical Materials Research*, vol 36, pp. 109–117.

Brinker, C.J, Scherer, G. . (1990). "Sol-Gel Science The physics and chemistry of sol-gel processing".New York: Academic Press, Inc.

Brovarone, C., Nunzio, S. D. I., Bretcanu, O., & Verne, E. (2004). "Macroporous glass-ceramic materials with bioactive properties", *Journal of Materials Science: Materials in Medicine*, vol 15, pp. 209–217.

Brovarone, C. V., Verné, E., & Appendino, P. (2006). "Macroporous bioactive glass-ceramic scaffolds for tissue engineering", *Journal of Materials Science: Materials in Medicine*, vol 17(11), pp. 1069–1078.

Brown, R. F., Day, D. E., Day, T. E., Jung, S., Rahaman,M.M., Fu,Q. (2008). "Growth and differentiation of osteoblastic cells on 13 – 93 bioactive glass fibers and scaffolds", *Acta Biomaterialia* , vol 4, pp. 387–396.

Burg, K. J. L., Porter, S., & Kellam, J. F. (2000). "Biomaterial developments for bone tissue engineering", *Biomaterials*, vol 21, pp. 2347-2359.

Chatzistavrou,J., & Boccaccini, A.R .(2011)." Bioactive glass and glass ceramic scaffold for bone tissue engineering, Ylänen, H.O. Ed. Bioactive glasses: Materials, properties and applications, UK: Woodmead Publishing Limited

Chen, B. Q., & Boccaccini, A. R. (2006a). "Competence and Bioresorbability in Bioglass ® -Derived Tissue Engineering Scaffolds **", *Advanced Engineering Materials*,vol 8(4), pp. 285–289

Chen, Q. Z., Thompson, I. D., & Boccaccini, A. R. (2006b). "45S5 Bioglass s -derived glass – ceramic scaffolds for bone tissue engineering", *Biomaterials*, vol 27, pp. 2414–2425.

Chen, Q., Zhu, C., & Thouas, G. a. (2012). "Progress and challenges in biomaterials used for bone tissue engineering: bioactive glasses and elastomeric composites", *Progress in Biomaterials*, vol 1(1), 2.

Chen Q, Roether J.A, B. A. . (2008). "Tissue Engineering Scaffolds from Bioactive

Glass and Composite Materials", *Topics in Tissue Engineering*, vol 4.

Ciceo, R. L., Tranda, D., Radu, T., Ponta, O., & Simon, V. (2014)." Synthesis , characterisation and in vitro evaluation of sol – gel derived $SiO_2 – P_2O_5 – CaO – B_2O_3$ bioactive system", *Ceramics International*, vol 40, pp. 9517–9524.

Curzon, M. (1985)." The Relation between carries and prevalance and strontium concentrations in drinking water, plaque and surface enamel", *Journal of Dental Research*, vol 64(12), pp. 1386-1388.

Day,D.E., White, J.E., Brown,R.F & McMenamin,K.D.(2003)."Transformation of borate glasses into biological useful materials", *Glass Technology*, vol 44(2), pp. 75-81.

Elizabeth, J., Jones, J. R., & Hench, L. L. (2004). "Nodule formation and mineralisation of human primary osteoblasts cultured on a porous bioactive glass scaffold",*Biomaterials*, vol 25, pp. 2039–2046.

Elwan, RL, Al-Shathly, M. (2014). "Microstructural characterization and in vitro bioactivity of $SrO\text{-}SiO_2\text{-}Na_2O\text{-}CaO\text{-}B_2O_3\text{-}P_2O_5$ glasses", *Life Science Journal*, vol 11, pp. 36–46.

Erasmus, E.P., Johnson, O.T., Sigalas, I. & Massera, J. (2017) "Effects of Sintering Temperature on Crystallization and Fabrication of Porous Bioactive Glass Scaffolds for Bone Regeneration, *Sci.Reports*. **7**.

Fagerlund, S., Massera, J., Hupa, M., & Hupa, L. (2012b). "T – T – T behaviour of bioactive glasses 1 – 98 and 13 – 93", *Journal of the European Ceramic Society*, vol 32, pp. 2731–2738.

Fagerlund, S., Massera, J., Moritz, N., Hupa, L., & Hupa, M. (2012a). "Phase composition and in vitro bioactivity of porous implants made of bioactive glass S53P4", *Acta Biomaterialia*, vol 8(6), pp. 2331–2339.

Filho, O. P., Latorre, G. P., & Hench, L. L. (1996). "Effect of crystallization on apatite-layer formation of bioactive glass 45S5", *Journal of Biomedical Materials Research*, vol 30(4), pp. 509–514.

Fredholm, Y. C., Karpukhina, N., Brauer, D. S., Jones, J. R., Law, R. V, & Hill, R. G.

(2012)."Influence of strontium for calcium substitution in bioactive glasses on degradation , ion release and apatite formation", *Journal of the Royal Society Interface*, vol 9, pp. 880–889.

Fu, Q, Rahaman, M.N, Bal,B.S, Brown,R.F,Day, D. . (2008). "Mechanical and InVitro Performance of 13 – 93 Bioactive Glass Scaffolds Prepared By a Polymer Foam Replication Technique", *Acta Biomaterialia*, vol 4, pp. 1854–1864.

Fu, Q., Rahaman, M. N., Bal, B. S., Bonewald, L. F., Kuroki, K., & Brown, R. F. (2010b). "Silicate , borosilicate , and borate bioactive glass scaffolds with controllable degradation rate for bone tissue engineering applications . II . In vitro and in vivo biological evaluation", *Journal of Biomedical Materials Research* , vol 95A (1), pp. 172–179.

Fu, Q., Rahaman, M. N., Bal, B. S., Huang, W., & Day, D. E. (2007). "Preparation and bioactive characteristics of a porous 13 – 93 glass , and fabrication into the articulating surface of a proximal tibia", *Journal of Biomedical Materials Research.*

Fu, Q., Rahaman, M. N., Fu, H., & Liu, X. (2010a). "Silicate , borosilicate , and borate bioactive glass scaffolds with controllable degradation rate for bone tissue engineering applications . I . Preparation and in vitro degradation", *Journal of Biomedical Materials Research*, vol 95A (1), pp. 164–171.

Fu, Q., Saiz, E., Rahaman, M. N., & Tomsia, A. P. (2011). "Bioactive glass scaffolds for bone tissue engineering : state of the art and future perspectives", *Materials Science & Engineering C*, vol 31(7), pp. 1245–1256.

Gao, Z. (2013). "Estimating permeability using median pore throat radius obtained deom mercury intrusion porosimetry" , *J. Geophys. Eng*, vol. 10(2), pp.1-7.

Gapontsev, V. P., Matitsin, S. M., Isineev, A. A., & Kravchenko, V. B. (1982). "Erbium glass lasers and their applications", *Optics and Lase Technology*, pp. 189–196.

Gerhardt, L., & Boccaccini, A. R. (2010). "Bioactive Glass and Glass-Ceramic Scaffolds for Bone Tissue Engineering", *Materials*, vol 3, pp. 3867–3910.

Gestel, N. A. P. Van, Geurts, J., Hulsen, D. J. W., Rietbergen, B. Van, Hofmann, S., & Arts, J. J. (2015). "Clinical Applications of S53P4 Bioactive Glass in Bone Healing and Osteomyelitic Treatment : A Literature Review", *BioMed Research International*.

Gibgson, L.J., & Ashby,M.F.(1988)."Cellular solids and Properties", Oxford: Pergamon Press.

Goel, A., Raman, R., & Ferreira, J. M. F. (2011). "Acta Biomaterialia Influence of strontium on structure , sintering and biodegradation behaviour", *Acta Biomaterialia*, vol 7, pp. 4071–4080.

Griffith, L. G. (2000). "Polymeric biomaterials", *Acta Materialia*, vol 48, pp. 263-277.

Gross, U, Raimund, K, Schmitz, H. (1988). "The response of bone to surface-active glasses / glass-ceramics", *CrC Critical Reviews in Biocompatibility*, vol 4 (2), pp. 159-179.

Gross, K., Berndt, C. C., Herman, H., Gross, K. A., Berndt, C. C., & Herman, H. (1998). "Amorphous Phase Formation in Plasma- Sprayed Hydroxyapatite Coatings Amorphous phase formation in plasma-sprayed hydroxyapatite coatings", *Journal of Biomedical Materials Research*, vol 39 (5) , pp. 407-417.

Hayashi, T. (1994). "Biodegradable polymers for biomedical use", *Progress in Polymer Science*, vol 19, pp. 663-702.

Hench, L, L, West, J. . K. (1990). "The Sol-Gel Process", *Chemical Reviews*, vol 90(1), pp. 33-72.

Hench, LL, Paschall, H. (1973). "Direct Chemical Bond of Bioactive Glass-Ceramic Materials to Bone and Muscle", *Journal of Biomedical Materials Research Symposium*, vol 42(4), pp. 25–42.

Hench, L. L. (1991). "Bioceramics: From Concept to Clinic", *Journal of the American Ceramic Society*, vol 74(7), pp. 1487–1510.

Hench, L. L. (1998). "Bioceramics", *Journal of American Ceramics Society*, vol 81(7), pp. 1705-1728.

Hench, L. L. (2006). The story of Bioglass?? *Journal of Materials Science: Materials in Medicine*, vol 17(11), pp. 967–978.

Hench, L. L., Paschall, H. A., (1974). "Histochemical Responses at a Biomaterial ' s Interface", *Journal of Biomedical Materials Research Symposium*, vol 5(5), pp. 49–64.

Hench, L. L., Splinter, R. J., Allen, W. C., & Greenlee, T. K. (1971). "Bonding mechanisms at the interface of ceramic prosthetic materials", *Journal of Biomedical Materials Research*, vol 5(6), pp. 117–141.

Hench, L. L., & Wilson, J. (1984). "Surface-Active Biomaterials", *Science*, vol 226, pp. 630-635.

Hench LL, Polak. J.M. (2002). "Third-Generation Biomedical Materials", *Science*, vol 295(5557), pp. 1014-1017.

Hench, L.L., & Wilson, J. Eds. (1993)." An introduction to bioceramics", Singapore: World Scientific Publising.

Hill, R. G. (1996). "An Alternative View of the Degradation of Bioglass", *Journal of Materials Science Letters*, vol 15, pp. 1122-1125.

Huang, W., Day, D. E., Kittiratanapiboon, K., & Rahaman, M. N. (2006). "Kinetics and mechanisms of the conversion of silicate (45S5), borate , and borosilicate glasses to hydroxyapatite in dilute phosphate solutions", *Journal of Material Science: Materials in Medicine*, vol 17, pp. 583–596.

Huang, W., Rahaman, M. N., Day, D. E., & Li, Y. (2006). "Mechanisms for converting bioactive silicate , borate , and borosilicate glasses to hydroxyapatite in dilute phosphate solutions", *Physics and Chemistry of Glass:European Journal of Glass Science and Technology B*, vol 47(6), pp. 647-358.

Huang, J., & Best, S.M. 2007. "Ceramic biomaterials", Boccaccini,A.R.,& Gough, J.E. Ed., Tissue Engineering using ceramics and polymers, New York: CrC Press Boca Raton

Hulbert, S.F., Bokros,J.C., Hench,L.L., Wilson,J., & Heimke,G.(1987). "Ceramics in clinical applications: Past, Present and future", Vincenzini,P. Ed., High Tech

Ceramics, Amsterdam: Elsevier.

Hutmacher, D. W. (2000). "Scaffolds in tissue engineering bone and cartilage", *Biomaterials*, vol 21, pp. 2529–2543.

Isaac, J, Nohra J, Lao, J, Jallot, E, Nedelec, J. (2011). "Effects of strontium-doped bioactive glass on the differentiation of cultured osteogenic cells", *European Cells and Materials*, vol 21, pp. 130–143.

Jamieson, Christie, K., Ainsworth, R. I., & Leeuw, N. H. De. (2016). "Investigating structural features which control the dissolution of bioactive phosphate glasses : Beyond the network connectivity", *Journal of Non-Crystalline Solids*, vol 432, pp. 31–34.

Jones, J. R. (2013). "Review of bioactive glass : From Hench to hybrids", *Acta Biomaterialia*, vol 9(1), pp. 4457–4486.

Jones, J. R., Ehrenfried, L. M., & Hench, L. L. (2006). "Optimising bioactive glass scaffolds for bone tissue engineering", *Biomaterials*, vol 27, pp. 964–973.

Jones, J. R., & Hench, L. L. (2003). "Regeneration of trabecular bone using porous ceramics", *Current Opinion in Solid State and Materials Science* , vol 7, pp. 301–307.

Jones, J. R., Lin, S., Yue, S., Lee, P. D., Hanna, J. V, Smith, M. E., & Newport, R. J. (2009). "Bioactive glass scaffolds for bone regeneration and their hierarchical characterisation", *Journal of Engineering in Medicine*, vol 224, pp. 1373–1387.

Jones, J. R., Lin, S., Yue, S., Lee, P. D., Hanna, J. V, Smith, M. E., & Newport, R. J. (2010)." Bioactive glass scaffolds for bone regeneration and their hierarchical characterisation", *Proceedings of the Institution of Mechanical Engineers. Part H, Journal of Engineering in Medicine*, vol 224(12), 1373–1387.

Jones, J.R.(2007a)." Bioactive ceramics and glasses", Boccaccini,A.R.,& Gough, J.E. Ed., Tissue Engineering using ceramics and polymers, New York: CrC Press Boca Raton

Jones, J. R., Tsigkou, O., Coates, E. E., Stevens, M. M., Polak, J. M., & Hench, L. L. (2007b). "Extracellular matrix formation and mineralization on a phosphate-free

porous bioactive glass scaffold using primary human osteoblast (HOB) cells", *Biomaterials*, vol 28, pp. 1653–1663.

Karageorgiou, V., & Kaplan ,D. (2005). "Porosity of 3D biomaterial scaffolds and osteogenesis", *Biomaterials*, vol 26, pp. 5474–5491.

Kauer,G., Pandey,O.P., Singh,K., Homa,D., Scott,B., & Pickrell,G.(2014)." A review of bioactive glasses: Their structure, properties, fabrication, and apatite formation", *Journal of Biomedical Materials Research*, vol 102A, pp. 254-274.

Kazutaka, Hyodo, Shimizu, Y., Kamitani, T., & Egashira, M. (2009). "Fabrication of highly porous alumina-based ceramics with connected spaces by employing PMMA microspheres as a template", *Advances in Materials Science and Engineering*, pp. 1687-1696.

Kinnunen, I., Aitasalo, K., & Po, M. (2000). "Reconstruction of orbital floor fractures using bioactive glass", *Journal of Cranio-Maxillofacial Surgery*, vol 28, pp. 229–234.

Kokubo, T., Kushitani, H., Sakka, S., Kitsugi, T., & Yamamum, T. (1990). " Solutions able to produce *in vivo* surface-structure changes in bioactive", *Journal of Biomedical Materials Research*, vol 24, pp. 721–734.

Krajewshi,A., Ravaglioli,A. (2002)."Bioceramics and biological glasses", Barbucci, R, Ed. Integrated biomaterials science, New York: Kluwer Academic/Plenum.

Laurencin, Cato, T, Khan Yusuf, Kofron Michele, El-Amin, Saadiq, Botchwey , Edward, Yu, XiaojunCooper, J. A. (2006). "Regular and special features the abjs nicolas andry award Tissue Engineering of Bone and Ligament", *Clinical Orthopaedics and Related Research*, (447), pp. 221–236.

Legeros, R. Z. (2002). "Properties of Osteoconductive Biomaterials : Calcium Phosphates", *Clinical Orthopaedics and Related Research* ,(395), pp. 81–98.

Liu, H., & Webster, T. J. (2006). "Less harmful acidic degradation of poly (lactic- co-glycolic acid) bone tissue engineering scaffolds through titania nanoparticle addition", *International Journal of Nanomedicine*, vol 1(4), pp. 541–545.

Liu, X., Huang, W., Fu,H., Yao,A., Wang, D., Pan,H., & Lu, W. W. (2009).

"Bioactive borosilicate glass scaffolds : improvement on the strength of glass-based scaffolds for tissue engineering", *Journal of Material Science: Materials in Medicine*, vol 20, pp. 365–372.

Locs, J., Zalite, V., Berzina-Cimdina, L., & Sokolova, M. (2013). "Ammonium hydrogen carbonate provided viscous slurry foaming-A novel technology for the preparation of porous ceramics", *Journal of the European Ceramic Society*, vol 33(15–16), pp. 3437–3443.

Lowell. (1984). "Theory of Mercury Porosimetry", *Powder Technology*, vol 38, pp. 121–124.

Lu, L., Peter, S. J., D. Lyman, M., Lai, H. L., Leite, S. M., Tamada, J. A., … Mikos, A. G. (2000). "In vitro and in vivo degradation of porous poly(DL-lactic-co-glycolic acid) foams", *Biomaterials*, vol 21(18), pp. 1837–1845.

Ma, P. X. (2004). "Scaffolds for tissue fabrication", *Materials Today*, vol 7(5), pp. 30–40.

Malvern: Mastersizer 2000 - Integrated systems for particle sizing (2005). Malvern Instruments Ltd., Brochure MRK501-02.

Marrota A, Buri A, B. F. (1981). "Nucleation in glass and differential thermal analysis", *Journal of Materials Science*, vol 16(2), pp. 341–344.

Maspero, F, A, Ruffieux, K, Muller, B, Wintermantel, E. (2001). "Resorbable defect analog PLGA scaffolds using CO 2 as solvent : Structural characterization", *Journal of Biomedical Materials Research*, vol 62(1), pp. 89-98.

Massera, J., Fagerlund, S., Hupa, L., & Hupa, M. (2012). "Crystallization mechanism of the bioactive glasses, 45S5 and S53P4", *Journal of the American Ceramic Society*, vol 95(2), pp. 607–613.

Massera, J., & Hupa, L. (2014). "Influence of SrO substitution for CaO on the properties of bioactive glass S53P4", *Journal of Materials Science: Materials in Medicine*, vol 25, pp. 657–668.

Massera, J., Petit, L., Cardinal, T., Videau, J. J., Hupa, M., & Hupa, L. (2013). "Thermal properties and surface reactivity in simulated body fluid of new

strontium ion-containing phosphate glasses", *Journal of Materials Science: Materials in Medicine* , vol 24, pp. 1407–1416.

Massera, J., Shpotyuk, Y., Sabatier, F., Jouan, T., Boussard-plédel, C., Roiland, C., … Hupa, L. (2015a). "Processing and characterization of novel borophosphate glasses and fi bers for medical applications", *Journal of Non-Crystalline Solids*, vol 425, pp. 52–60.

Massera, J, Hupa, L, Kokkari. A., Narhi, T. (2015b). "The influence of SrO and CaO in silicate and phosphate bioactive glasses on human gingival fibroblasts", *Journal of Materials Science: Materials in Medicine* , vol 26, pp. 196.

Massera, J, Mayran, M, Rocherulle, J, and Hupa, L. (2015) "Crystallization behavior of phosphate glasses and its impact on the glasses ' bioactivity," *Journal of Material Science.*, vol. 50, pp. 3091–3102.

McAndrew, J, Efrimescu , C, Sheehan, E, Niall, D. (2013). "Through the looking glass ; bioactive glass S53P4 (BonAlive Ò) in the treatment of chronic osteomyelitis", *Irish Journal of Medicine*, vol 4, pp. 509–511.

Micro-Computed Tomography (26 September 2016): Retrieved from http: www.b-cube.ch/index.php?option=com_content&view=article&id=21&Itemid=19.

Neel, E. A. A., Pickup, D. M., Valappil, S. P., Newport, J., & Knowles, J. C. (2009). "Bioactive functional materials : a perspective on phosphate-based glasses", *Journal of Materials Chemistry*, vol 19, pp. 690–701.

O'Brien, F. J. (2011). "Biomaterials & scaffolds for tissue engineering", *Materials Today*, vol 14(3), pp. 88–95.

O'Donnell, MD, Watts, SJ, Law, R. V. (2009). "The effect of phosphate content on the bioactivity of soda-lime-phosphosilicate glasses", *Journal of Materials Science: Materials in Medicine,*vol 20, pp. 1611–1618.

Ohji, T., Fukushima, M. (2012). "Macro-porous ceramics : processing and properties", *International Materials Reviews*, vol *57*(2), pp. 115-131.

Operating Instructions Planetary Mono Mill pulverisette6 (26 September 2016): Retrieved from

http:www.johnmorris.com.au/files/product/attachments/11583/26687_manual_instr.pdf

Peltola, M., Aitasalo, K., Suonpa, J., Varpula, M., & Yli-urpo, A. (2006). "Bioactive glass S53P4 in frontal sinus obliteration : a long-term clinical experience", *Wiley Interscience*, vol 28(9), pp. 834–841.

Qin, L., Genant, H.K., Griffith, J. F. & Leung, K.S. (2007). "Advanced bioimaging technologies in assessment of quality bone and scaffold materials", Heilmann, U Ed. Berlin Heidelberg.

Rahaman, M.N., Day, D.E., Bal, S., Fu,Q.,Jung, S.B., Bonewald,L.F.,Tomsia,A.P. (2011). "Bioactive glass in tissue engineering", *Acta Biomaterilia*, vol 7(6), pp. 2355–2373.

Rahaman, M. N., Brown, R. F., Bal, B. S., & Day, D. E. (2006). "Bioactive Glasses for Nonbearing Applications in Total Joint Replacement", *Seminars in Artthroplasty*, vol 17, pp. 102–112.

Rawlings, R. D. (1993). "Bioactive Glasses and Glass-Ceramics", *Clinical Materials* vol 14, pp. 155–179.

Ray, C. S., & Day, D. E. (1997). "An Analysis of Nucleation-Rate Type of Curves in Glass as Determined by Differential Thermal Analysis", *Journal of American Ceramic Society*, vol 108(12), pp. 3100–3108.

Rezwan, K., Chen, Q. Z., Blaker, J. J., & Boccaccini, A.R (2006). "Biodegradable and bioactive porous polymer / inorganic composite scaffolds for bone tissue engineering", *Biomaterials*, vol 27, pp. 3413–3431.

Richard,M.N.C. (2000). "Bioactive behaviour of a borate glass", M.S Thesis, University of Missouri-Rolla.

Sabree, I., Gough, J. E., & Derby, B. (2015). "Mechanical properties of porous ceramic scaffolds: Influence of internal dimensions", *Ceramics International*, vol 41, pp. 8425–8432.

Salgado, J., Coutinho, O. P., & Reis, R. L. (2004). "Bone Tissue Engineering : State of the Art and Future Trends", *Macromolecular Bioscience*, vol 4, pp. 743–765.

Santocildes-romero, M. E., Crawford, A., Hatton, P. V, Goodchild, R. L., Reaney, I. M., & Miller, C. A. (2015). "The osteogenic response of mesenchymal stromal cells to strontium-substituted bioactive glasses", *Journal of Tissue Enginnering and Regenerative Medicine*, vol 9, pp. 619–631.

Sepulveda, Pilar, Jones, J. R., Jones, J. R., & Hench, L. L. (2002). "Bioactive Sol – Gel Foams for Tissue Repair Bioactive sol-gel foams for tissue repair", *Journal of Biomedical Materials Research*, vol 59(2), pp. 340- 348.

Song, H., Islam, S., & Lee, B. (2008). "A Novel Method to Fabricate Unidirectional Porous Hydroxyapatite", *Journal of Americam Ceramic Society*, vol 91 (9), pp. 3125–3127.

Sriranganathan, D., Kanwal, N., Hing, K. A., & Hill, R. G. (2016). "Strontium substituted bioactive glasses for tissue engineered scaffolds : the importance of octacalcium phosphate", *Journal of Materials Science: Materials in Medicine*, vol 27(2), pp. 39.

Studart, R., Gonzenbach, U. T., Tervoort, E., & Gauckler, L. J. (2006). "Processing Routes to Macroporous Ceramics: A Review", *Journal of American Ceramic Society*, vol 89(6) , pp. 1771-1789.

Fagerlund,S., Hupa, L. (2010). "Crystallization of 45S5 during Isothermal Heat Treatment", *Ceramic Materials*, vol 62(3), pp. 349–354.

Thomson, R. C., Yaszemski, M. J., Powers, J. M., & Mikos, A. G. (1998). "Hydroxyapatite fiber reinforced poly (-hydroxy ester) foams for bone regeneration", *Biomaterials*, vol 19, pp. 1935–1937.

Tilocca.A. (2009). "Structural models of bioactive glasses from molecular dynamics simulations", *Proceedings of the Royal Society A*, vol 465, pp. 1003–1027.

Tisdel,C.L, Goldberg, V.M, Parr, J.A, Bensusan,J.S, Staikoff,L.S, Stevenson, S. (1994). "The influence of a hydroxyapatite and Tri-Calcium phosphate coating on bone growth into titanium fiber-metal implants", *The Journal of Bone and Joint Surgery. American Volume*, vol 76A(2), pp.159-171 .

Tomford, W. W. (1995). "Transmission of disease through transplantation of

musculoskeletal allografts", *The Journal of Bone and Joint Surgery. American Volume*, vol *77*(11), pp. 1742–1754.

Valentini, P., & Paoli, C. P. (2000). "Sinus Grafting with Porous Bone Mineral (Bio-Oss) for Implant Placement : A 5-Year Study on 15 Patients", *The International Journal of Periodontics and Restorative Dentistry*, vol 20(3), pp. 245-253.

Vallet-regí, M., & Balas, F. (2008). "Silica Materials for Medical Applications", *The Open Biomedical Engineering Journal*, vol 2, pp. 1–9.

Vaughan, J. (1981). "The physiology of bone", Oxford University Press.

Wang, M. (2003). "Developing bioactive composite materials for tissue replacement" *Biomaterials*, vol 24, pp. 2133–2151.

Watts, S. J., Hill, R. G., Donnell, M. D. O., & Law, R. V. (2010). "Influence of magnesia on the structure and properties of bioactive glasses", *Journal of Non-Crystalline Solids*, vol 356(9–10), pp. 517–524.

Westermarek, S. (2000) "Use of mercury porosimetry and nitrogen adsorption in characterization of the pore structure of mannitol and microcrystalline cellulose powders, granules and tables", Academic Dissertation, University of Helsinki.

Williams, D. F. (1989). "A model for biocompatibility", *Journal of Biomedical Engineering*, vol 11, pp. 185–191.

Wu, Z. Y., Hill, R. G., Yue, S., Nightingale, D., Lee, P. D., & Jones, J. R. (2011). "Acta Biomaterialia Melt-derived bioactive glass scaffolds produced by a gel-cast foaming technique",*Acta Biomaterialia*, vol 7(4), pp. 1807–1816.

Xynos, I. D., Edgar, A. J., Buttery, L. D. K., Hench, L. L., & Polak, J. M. (2000). "Gene-expression profiling of human osteoblasts following treatment with the ionic products of Bioglass® 45S5 dissolution", *Journal of Biomedical Materials Research*, vol 55(2), pp. 151-157

Yang, X. B., Roach, H. I., Clarke, N. M. P., Howdle, S. M., Quirk, R., Shakesheff, K. M., & Oreffo, R. O. C. (2001). "Human Osteoprogenitor Growth and Differentiation on Synthetic Biodegradable Structures After Surface Modification", *Bone*, vol 29(6), pp. 523–531.

Yao, A, Wang , D, Day, D. E. (2007). "In Vitro Bioactive Characteristics of Borate-Based Glasses with Controllable Degradation Behavior", *Journal of American Ceramic Society*, vol 90(1) , pp. 303–306.

Yamamuro, T.(2004). "Bioceramics", Poitut, D.G. Ed. Biomechanics and biomaterials in orthopedics, Publisher: Springer London.

Yamamuro,T., Hench,L.L., Wilson,L., Ed. (1990)." Handbook of bioactive ceramics, vol 1, Florida: CrC Press, Boca Raton.

Zachariasen,W.H. (1932). "The atomic arrangement in glass", *Journal of American Ceramic Society*, vol 54(1), pp. 3841–3851.

Zhang, D., Hupa, M., & Hupa, L. (2008). "In situ pH within particle beds of bioactive glasses", *Acta Biomaterialia*, vol 4, pp. 1498–1505.

Zheng, Q., Potuzak, M., Mauro, J. C., Smedskjaer, M. M., Youngman, R. E., & Yue, Y. (2012). "Composition-structure-property relationships in boroaluminosilicate glasses", *Journal of Non-Crystalline Solids*, vol 358(6–7), pp. 993–1002.